

8-2016

Design of Bistable Composite Laminates for Shape Morphing Applications

Subramanian Annamalai

Clemson University, sannama@clemson.edu

Follow this and additional works at: https://tigerprints.clemson.edu/all_theses

Recommended Citation

Annamalai, Subramanian, "Design of Bistable Composite Laminates for Shape Morphing Applications" (2016). *All Theses*. 2491.
https://tigerprints.clemson.edu/all_theses/2491

This Thesis is brought to you for free and open access by the Theses at TigerPrints. It has been accepted for inclusion in All Theses by an authorized administrator of TigerPrints. For more information, please contact kokeefe@clemson.edu.

DESIGN OF BISTABLE COMPOSITE LAMINATES FOR
SHAPE MORPHING APPLICATIONS

A Thesis
Presented to
the Graduate School of
Clemson University

In Partial Fulfillment
of the Requirements for the Degree
Master of Science
Mechanical Engineering

by
Subramanian Annamalai
August 2016

Accepted by:
Dr. Oliver Myers, Committee Chair
Dr. Georges Fadel, Committee Co-Chair
Dr. Srikanth Pilla

ABSTRACT

Composite materials, specifically Laminated Fibre Reinforced Polymers / Plastics (FRP), are versatile material systems which have become a part of everyday life. These are no longer considered “space age” materials, but are also being used in aircraft/military, automotive/transportation and construction/civil infrastructure applications. The major reasons behind these materials gaining prominence are that they are light weight, they have high strength to weight ratio and tailored properties. In the recent past, 35 years back, an entirely new research area in the field of composite materials had begun called “Bistable Composites”. These composites, as the name suggests, have two stable shapes and a snap through / snap back phenomenon between these two shapes, which makes them suitable materials for use in “Adaptive Structures”. Bistable composites are unsymmetric laminated FRPs that exhibit bistability because of the unsymmetric laminate stacking sequence about the middle surface.

In this research, the possibility of obtaining desired shapes in both stable states of any given geometry is explored using Finite Element (FE) simulations and experimental validation. The methodology followed is as follows: the given geometry is tessellated and several iterations are carried out to find the combination of symmetric and unsymmetric laminates for which the desired shapes are achievable. To decide on the proper tessellation and carry out the iterations efficiently, two major topics are addressed initially. They are the behavior of individual unsymmetric laminates and the behavior of the combination of symmetric and unsymmetric laminates. In the individual unsymmetric laminates, the effects of geometry and fibre orientation on the snap through and snap back loads are

studied, to identify the parameters that controls the critical load at which the shape changes. In the combination of symmetric and unsymmetric laminates, various standard geometries are split into smaller geometries, each of those are made into symmetric or unsymmetric laminates and different combinations of those symmetric and unsymmetric laminates are studied to find the various bistable shapes that are possible in each standard geometry. An experimental setup is built to measure the snap through and snap back loads of the individual rectangular unsymmetric laminates. The simulation results obtained are validated by fabricating those laminates and conducting experiments to confirm the data obtained numerically.

DEDICATION

To my parents and grandparents, and to my family and friends.

ACKNOWLEDGMENTS

I would like to express my sincere gratitude to my Advisor Dr. Oliver J. Myers, and my Co-Advisor Dr. Georges M. Fadel, for their dynamic guidance and valuable technical input which helped me immensely in the progress of this research, without them this work would not have been possible. I would like to thank Dr. Srikanth Pilla, who was instrumental in providing me with innumerable tips and for his active role in this research.

I am thankful to the staff members of the Mechanical Engineering Machine Shop for making it possible for me to use the shop facilities and being kind enough to help me with anything I needed in the shop.

I also acknowledge my family and friends for their constant encouragement and support throughout the course of my graduate studies and masters thesis.

TABLE OF CONTENTS

	Page
TITLE PAGE	i
ABSTRACT	ii
DEDICATION	iv
ACKNOWLEDGMENTS	v
LIST OF TABLES	viii
LIST OF FIGURES	x
CHAPTER	
I. INTRODUCTION	1
Composites.....	3
Fibre Reinforced Polymer Composites	4
Laminated FRP	5
Special Cases of Laminates	19
Thesis Outline	22
II. LITERATURE REVIEW	23
Basic Foundation	23
Variations in Composite Structure	48
Application of Bistable Composites	53
Optimization of Bistable Composites	62
Multistable Composites	69
Concluding Remarks.....	72
III. SIMULATIONS AND EXPERIMENTS	73
Research Objectives and Methodology	74
Problem Formulation in FEA.....	74
Preliminary Simulation and Inference	81
Fabrication of the Unsymmetric Laminates.....	85
Experimental Setup.....	89

Table of Contents (Continued)

	Page
IV. RESULTS AND DISCUSSION	94
Effect of Geometry on the Snap Through and Snap Back Loads of an Individual Unsymmetric Laminate	94
Effect of Fibre Orientation on the Snap Through and Snap Back Loads of an Individual Unsymmetric Laminate	112
Square Geometry	117
Rectangle Geometry.....	121
Circle Geometry.....	124
Ellipse Geometry	127
Headrest Application	129
Spoiler Application	131
Fabrication Results.....	133
Experimental Setup Results	136
V. CONCLUSION AND FUTURE WORK	138
Conclusion	138
Future Work	147
APPENDICES	150
A: Simulation Procedure in ABAQUS	151
B: Part Drawings and Bill of Material of the Experimental Setup.....	153
REFERENCES	158

LIST OF TABLES

Table		Page
1.1	Tensor versus contracted notation for stresses and strains	8
2.1	Representation of the analysis steps	34
2.2	Comparison of measured versus FE calculated critical loads.....	35
2.3	Comparison between FE analysis and experimental results	38
2.4	Optima for deflection constrained optimization with geometry variables	69
3.1	Moduli comparison of two different prepregs	76
3.2	Material properties of the AS4 – 8552 prepregs	76
4.1	Rectangle – I snap through and snap back load trend.....	98
4.2	Rectangle – II snap through and snap back load trend	100
4.3	Trapezoid – I snap through and snap back load trend	102
4.4	Trapezoid – II snap through and snap back load trend	104
4.5	Triangle – I snap through and snap back load trend	106
4.6	Triangle – II snap through and snap back load trend.....	108
4.7	Post fab and post load shapes of different types of triangle	110
4.8	Post fab and post load shapes of different fibre orientation in rectangles	113
4.9	Post fab and post load shapes of different fibre orientation in triangles	115
4.10	Post fab and post load shapes of different combination of four squares.....	119

List of Tables (Continued)

Table		Page
4.11	Post fab and post load shapes of different combination of nine squares - I.....	120
4.12	Post fab and post load shapes of different combination of nine squares - II	121
4.13	Post fab and post load shapes of different combination of three triangles forming rectangle	123
4.14	Post fab shapes of different polygon approximations.....	126
4.15	LSS and post fab shapes of ellipse and its variations	128
4.16	Post fab and post load shapes of two variations of plus structure.....	130
4.17	Post fab and Post load shapes of three structures for spoiler application	132
4.18	Changes in number of plies.....	134
4.19	Snap through and snap back loads from experiments.....	136
4.20	Snap through and snap back loads from simulation	137

LIST OF FIGURES

Figure	Page
1.1 Requirement triangle of adaptive structures	2
1.2 Lamina with unidirectional fibres	5
1.3 Unbonded view of laminate construction	6
1.4 Basic form of micromechanics of lamina	6
1.5 Stresses on an element	8
1.6 Unidirectionally reinforced lamina	11
1.7 Coordinate transformations.....	13
1.8 Geometry of deformation in the x-z plane.....	15
1.9 In-plane forces on a flat laminate.....	17
1.10 Moments on a flat laminate.....	17
1.11 Geometry of an N-layered laminate.....	17
1.12 Unbonded view of (a) symmetric laminate; (b) unsymmetric laminate	21
2.1 Laminate shapes (a) at elevated curing temperature, and at room temperature, (b) saddle shape (c) first cylindrical shape (d) second cylindrical shape	24
2.2 Room-temperature shapes of thin $[0_2/90_2]$ and thick $[0_4/90_4]$ square laminates	25
2.3 Temperature-curvature relations for the $[-\Theta_4/\Theta_4]$ laminates	26
2.4 Temperature-curvature relations for the $[(90-\Theta)_4/\Theta_4]$ laminates.....	27
2.5 Temperature-curvature relations for the $[(\Theta-90)_4/\Theta_4]$ laminates.....	27

List of Figures (Continued)

Figure	Page
2.6 Comparisons of the proposed theory with the Jun & Hong theory and finite element analysis: temperature-curvature relations for a $[0_2/30_2]$ laminate.....	28
2.7 Non-dimensional curvatures a^* and b^* predicted by Abaqus and by the Rayleigh-Ritz model (square plates).....	30
2.8 Curvature-temperature relationship (Rayleigh-Ritz and Abaqus model, $L^* > L^*_{cr}$).....	30
2.9 Non-dimensional curvatures a^* and b^* predicted by Abaqus and Rayleigh- Ritz model for square plates with thickness ratio $t_0/t_{90} = 0.93$	31
2.10 Non-dimensional curvatures a^* and b^* predicted by Abaqus and by the Rayleigh-Ritz model for plates with $AR = 2$	31
2.11 Non-dimensional curvatures a^* and b^* predicted by Abaqus and by the Rayleigh-Ritz model for plates with $AR = 3$	32
2.12 Non-dimensional curvatures a^* and b^* predicted by Abaqus and by the Rayleigh-Ritz model for plates with $AR = 10$	32
2.13 FE model boundary conditions	33
2.14 Applied force versus step time. Laminate is in the dry state	35
2.15 Applied load to attain snap-through.....	37
2.16 Room temperature shapes of square $[0_2/90_2]_T$	37
2.17 $P-\delta$ curve for a square 150 mm X 150 mm laminate	38
2.18 Stacking sequence for the bi-stable panel.....	39
2.19 Numerical equilibrium shapes	40
2.20 Equilibrium configurations	40
2.21 Stabilized load-displacement diagrams versus reaction forces.....	41

List of Figures (Continued)

Figure	Page
2.22 Equilibrium shapes obtained with the analytical model (a) 1st equilibrium shape (b) 2nd equilibrium shape	43
2.23 Analytical vs FE shape for the 4-layer plate (a) flat configuration (b) curled configuration.....	44
2.24 Analytical vs FE shape for the 8-layer plate (a) flat configuration (b) curled configuration.....	44
2.25 Load measurement apparatus.....	45
2.26 Boundary conditions of straight edge specimens.....	46
2.27 Non-dimensional snap-through and snap-back results for square specimens.....	47
2.28 Non-dimensional snap-through and snap-back results for rectangular specimens	47
2.29 Non-dimensional snap-through/back results of the triangular-A and -B group.....	47
2.30 Lay-up of a 4-ply laminate.....	48
2.31 As cured curvatures exhibited by laminate (approx. to scale).....	49
2.32 Schematic geometry of the three different deformation modes.....	49
2.33 Construction of 2 central plies & Edge profiles showing multiple stable states.....	49
2.34 Layup of laminate with an array of multiple discrete transverse strips.....	50
2.35 Manufactured laminates.....	52
2.36 Bifurcation diagrams for (a) steel laminates, $\mu=0.2$, and (b) aluminum laminates, $\mu=0.5$	52

List of Figures (Continued)

Figure	Page
2.37 Variable wing sweep structure idealization & swept configuration	54
2.38 Geometric characteristics of the shell	54
2.39 Stacking sequence regions for the spar structure	54
2.40 Boundary conditions	55
2.41 Swept configuration: Experimental & FE model.....	55
2.42 NACA 23012 airfoil	56
2.43 Assembly for camber change.....	57
2.44 Lateral view of the stable shapes for camber change of airfoil section	57
2.45 Loads relationship with displacements at actuation points.....	57
2.46 Assembly for chord length change	58
2.47 Lateral view for chord length change (a) 1 st stable shape (b) 2 nd stable shape.....	58
2.48 (a) Experimental apparatus, (b) Configuration of the piezoelectric patches	59
2.49 Experimental velocity-to-base acceleration FRFs for small oscillations around state 1 & 2.....	60
2.50 Experimental frequency response diagrams with initial condition at state 2 for a forcing level of 2g and forward sweep. Peak –to-peak (a) velocity (b) piezoelectric voltage.....	61
2.51 Average power vs forcing frequency, load resistance 98.5 kΩ	61
2.52 Lay-up of CFRP and GFRP cross-ply laminates with 0° and 90° layer orientation resulting in maximum curvatures.....	63

List of Figures (Continued)

Figure	Page
2.53	Curvatures of a CFRP laminate with variable layer ratio 64
2.54	Failure modes and strength coefficients 65
2.55	Schematic of n-ply laminate ensuring curvatures of equal magnitude and opposite directions in the two cylindrical shapes 67
2.56	Deflection constrained design space 68
2.57	Actuation procedure for coupled bistable composite shells 70
2.58	Two different approaches of attaching a biasing strip on a single shell 71
2.59	Finite element predictions of the stable configurations of three connected bistable plates and the transitions between these states resulting from actuation 72
3.1	(a) Individual laminate, (b) Multiple connected laminates 75
3.2	Angle convention in FEA simulations 77
3.3	(a) Mesh of individual laminate, (b) Mesh of multiple connected laminate 78
3.4	Laminate shapes (a) at elevated curing temperature, and at room temperature, (b) saddle shape, (c) first cylindrical shape, (d) second cylindrical shape 79
3.5	Loading and boundary conditions for snap through and snap back simulations 79
3.6	Load vs displacement plot at the load application point 81
3.7	Rectangular laminate (a) Geometrical model, (b) Quadrilateral mesh 82
3.8	(a) First stable shape, (b) Second stable shape 83

List of Figures (Continued)

Figure	Page
3.9 Combined load vs displacement plot of snap through and snap back.....	83
3.10 Exploded view of the older mold.....	86
3.11 Isometric and front view of the older mold	86
3.12 Isometric and sectional front view of the corrected mold.....	87
3.13 Isometric, front and side views of the experimental setup.....	90
3.14 Slotted weight hanger system	90
3.15 Laminate portion in the experimental setup.....	91
3.16 (a) Snap through loading position, (b) Snap back loading position.....	93
4.1 Variation in geometry based on ‘c’ dimension	95
4.2 Snap through / longer fibre interaction chart	96
4.3 Snap back / shorter fibre interaction chart	96
4.4 Rectangle – I (Increasing ‘a’, keeping ‘b’ constant).....	97
4.5 Rectangle – I FEA plots	99
4.6 Rectangle – II (Increasing ‘b’, keeping ‘a’ constant)	100
4.7 Rectangle – II FEA plots.....	101
4.8 Trapezoid – I (Increasing ‘a’, keeping ‘b’ constant).....	101
4.9 Trapezoid – I FEA plots.....	102
4.10 Trapezoid – II (Increasing ‘b’, keeping ‘a’ constant)	103
4.11 Trapezoid – II FEA plots	104

List of Figures (Continued)

Figure	Page
4.12 Triangle – I (Increasing ‘a’, keeping ‘b’ constant)	105
4.13 Triangle – I FEA plots	106
4.14 Triangle – II (Increasing ‘b’, keeping ‘a’ constant).....	107
4.15 Triangle – II FEA plots	108
4.16 (a) Triangle notation, (b) Representation of triangle types.....	109
4.17 Types of triangle FEA plots.....	111
4.18 Rectangle – fiber orientation FEA plots.....	113
4.19 40°-60°-80° triangle	115
4.20 (a) Four squares split-up (b) Nine squares split-up.....	117
4.21 Split-up of rectangle geometry into three triangles.....	122
4.22 (a) Circle approximation – 10 sided polygon, (b) LSS representation	125
4.23 Tessellation of ellipse and its two variations	127
4.24 Blown up view of the tessellated lower portion of first ellipse variation.....	128
4.25 Flat type and protruded type headrest with plus shaped understructure	130
4.26 Rectangular unsymmetric laminate [0/90] _T	133
4.27 After curing (a) without trimming edges, (b) with trimmed edges.....	134
4.28 Two ply samples (a) sample 2, (b) sample 3	135
5.1 Bistable laminate with boundary symmetric laminate.....	149

CHAPTER ONE

INTRODUCTION

In engineering, the term ‘adaptive structure’ has come to mean any structure which can alter either its geometric form or material properties. The terms ‘smart’, ‘intelligent’ and ‘active’ have all been applied to describe both materials and structures which exhibit these properties [1, 2, 3]. Increasingly, the ability to adapt to a performance demand or environmental conditions has become a key design criterion for a range of structural and mechanical systems. It is precisely this type of requirement which has become a key driver in the development of adaptive structure technology. There are many examples of adaptive structures from a broad range of engineering applications, but much of the driving force for development has come from the aeronautical and space research fields. The need for a high level of material performance in terms of strength, flexibility and minimal weight, has led to some of the most advanced adaptive structures currently in existence [4].

Conciliating the conflicting requirements of load-carrying capacity, deformability and light weight is the dominant issue in the mechanical design of shape-adaptable systems. While established technologies and disciplines that successfully deal with the fulfilment of just two out of the three requirements are presently available as shown in Fig.1.1, the simultaneous accomplishment of all three of them represents a real challenge.

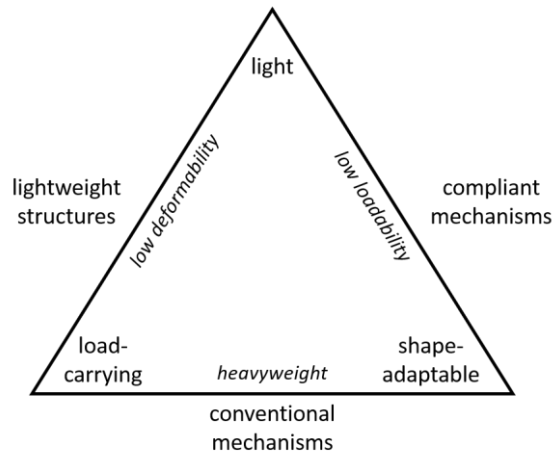


Figure 1.1: Requirement triangle of adaptive structures [4]

As shown in Fig 1.1, there are three disciplines, each of which satisfy two of the three requirements. The first discipline is lightweight design (design of structures with a high strength-to-weight ratio). Lightweight structures, however, are typically provided with a low degree of deformability. Because in most of the structural optimization procedures, the criterion often used is minimizing weight while maximizing stiffness. The second discipline is conventional mechanisms. They are highly deformable and able to carry high loads, but, far from being lightweight optimized. Finally, the third discipline is compliant mechanisms (systems designed to reach a given level of deformability by exploiting structural strain). They offer an excellent combination of deformability and low weight, but are limited – at the present state of the art – in their load-carrying capacity.

With the advent of a new discipline bistable composites, the challenge of satisfying all three requirements of an adaptive structure may be overcome to an extent. That is, even though they are light weight and have good load carrying capacity, they are capable of having only two stable shapes. Hence, such a structure cannot be called an ideal adaptive

structure, but still it can be effectively used for structural applications where shape change between only two defined shapes are required.

Bistable Composites are a common type of unsymmetric laminate fibre reinforced polymer composites. Detailed explanations of what is a composite; what is a fibre reinforced polymer composite; what is an unsymmetric laminate; followed by the research objectives are provided in this chapter.

Composites

A composite material (generally referred to as composite) is formed by the combination of two or more distinct materials that results in a new material with enhanced properties. The oldest composites are natural, “Wood” consists of cellulose fibres reinforced in lignin matrix, while manmade composites date back to the use of “Straw-reinforced clay” for bricks and pottery [5]. One of the basic example to understand the benefits of composites is “Concrete”. Rocks are combined with cement to make concrete, which is as strong as the rocks it contains, but can be shaped more easily than carving rock. While the enhanced properties of concrete are strength and ease of fabrication, in general, most physical, chemical, and processing-related properties can be enhanced by a suitable combination of materials.

Sometimes, composites use more than one type of reinforcement material, in which case they are called hybrids. For example, consider reinforced concrete, a particle-reinforced composite (concrete) that is further fibre reinforced with steel rods. Sometimes different materials are layered to form an enhanced product, as in the case of sandwich construction where a light core material is sandwiched between two faces of stiff and strong

materials. Modern composites use metal, ceramic, or polymer binders / matrix reinforced with a variety of fibres or particles. For example, fibreglass boats are made of a polyester resin reinforced with glass fibres. Based on the matrix, the modern day composites can be classified into Metal composites, Ceramic composites and Polymer composites. Similarly based on the reinforcement, they can be classified into Fibre reinforced composites and Particle / Whisker reinforced composites [6].

The major application of the modern day composites are in the aerospace, automotive, marine and construction industries. In most of these applications, the widely used type of composites is Fibre reinforced polymer composite. The advantages of the composites are light weight, high specific strength, high specific stiffness, tailored properties, good damping etc. The disadvantages of the composites are high cost, lack of well proven design rules, manufacturing difficulties, joining, and thermal limits [7].

Fibre Reinforced Polymer Composites

In the fibre reinforced polymer composites (FRP), the matrix is made of polymers (mostly thermoset polymers) like epoxy, unsaturated polyesters, vinyl esters, phenolics etc. and the fibre is made of either synthetic fibres like carbon, glass, aramid etc. or natural fibres like sisal, jute, coir etc. The matrix is the continuous phase in a composite and its principal role is to give shape to the structure. The reinforcement is the discontinuous phase in the composite and its principal role is to provide strength, stiffness, and other mechanical properties to the composite. Matrix covers and surrounds the reinforcement, hence it is the component of the composite that is directly exposed to the environment.

Based on the fibre arrangement in the matrix, the fibre reinforced polymer composites can be classified into Fibrous composites and Laminated composites. If the fibres are just mixed with the polymer matrix, this forms Fibrous composites and if the fibres and matrix are in a layered construction, they form Laminated composites. Based on the fibre itself, the Laminated composites can be further classified into Continuous long fibre laminated composites and Discontinuous fibre laminated composites. Continuous long fibres are available in three different forms, uni-directionally oriented, bi-directionally oriented (woven, stitched mat etc.) and randomly oriented (continuous strand mat). Discontinuous fibres are available in two different forms, randomly oriented (chopped strand mat) and preferentially oriented (oriented strand board) [5]. This research mainly concentrates on “Laminated Fibre Reinforced Polymer Composite” with continuous long uni-directionally oriented fibres [8].

Laminated FRP

Lamina / Individual Ply is a flat arrangement of continuous long or discontinuous fibres in a matrix. Two or more lamina stacked together forms a Laminate. A lamina with unidirectional fibres is shown in Fig.1.2 and a laminate formed by stacking five unidirectional lamina is shown in Fig.1.3.

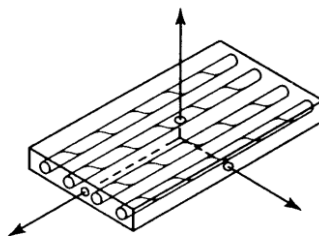


Figure 1.2: Lamina with unidirectional fibres [8]

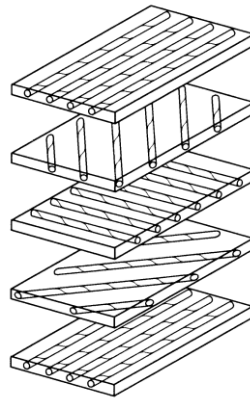


Figure 1.3: Unbonded view of laminate construction [8]

A major purpose of lamination is to tailor the directional dependence of strength and stiffness of a composite to match the loading environment of the structural element. The elastic constants (stiffness and compliance) of a laminated FRP can be found in three steps as follows,

1. Micromechanical behavior of a lamina
2. Macromechanical behavior of a lamina
3. Macromechanical behavior of a laminate

Micromechanical behavior of a lamina

The micromechanical behavior of a lamina deals with the calculation of the homogenized engineering constants of a lamina given the engineering constants for each individual constituent that makes up the lamina as depicted in Fig.1.4.

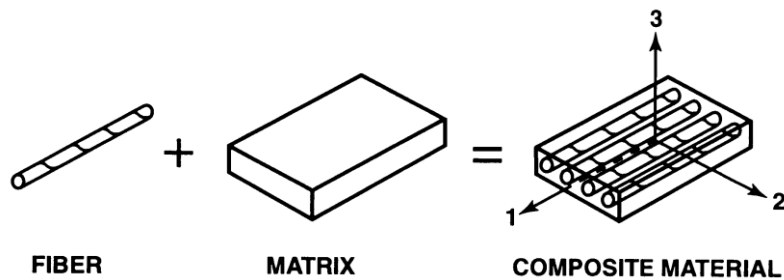


Figure 1.4: Basic form of micromechanics of lamina [8]

The major assumptions of this theory are: the lamina is linearly elastic, macroscopically homogeneous, and transversely isotropic; the fibres are linearly elastic, macroscopically homogeneous, transversely isotropic or isotropic, regularly spaced, perfectly aligned, and perfectly bonded to the matrix; the matrix is linearly elastic, macroscopically homogeneous, isotropic, and void free. Based on these assumptions, for a unidirectional composite lamina, the engineering constants E_1 , E_2 , ν_{12} , G_{12} are calculated from the engineering constants of fibre & matrix E_f , E_m , ν_f , ν_m , G_f , G_m and volume fractions of fibre & matrix V_f , V_m using the rule of mixtures formulae given below [7],

$$E_1 = E_f V_f + E_m V_m \quad (1.1)$$

$$E_2 = \frac{E_f E_m}{E_f V_m + E_m V_f} \quad (1.2)$$

$$\nu_{12} = \nu_f V_f + \nu_m V_m \quad (1.3)$$

$$G_{12} = \frac{G_f G_m}{G_f V_m + G_m V_f} \quad (1.4)$$

where E , ν and G terms are the modulus of elasticity, poisson's ratio and modulus of rigidity of a material.

Macromechanical behavior of a lamina

The macromechanical behavior of a lamina helps in developing the stiffness and compliance matrix of a lamina in terms of its engineering constants that are found from the micromechanical behavior of a lamina. The starting point of the macromechanical behavior of a lamina is the stress-strain relationship of an anisotropic (without isotropy – no plane of symmetry) material. The generalized Hooke's law relating stresses to strains can be written in contracted notation as,

$$\sigma_i = C_{ij}\varepsilon_j \quad i, j = 1, \dots, 6 \quad (1.5)$$

where σ_i are the stress components shown on a three-dimensional cube in x, y and z coordinates in Fig.1.5. C_{ij} is the stiffness matrix, and ε_j are the strain components.

The contracted notation for three-dimensional stresses and strains is defined in comparison to the usual tensor notation in Table 1.1.

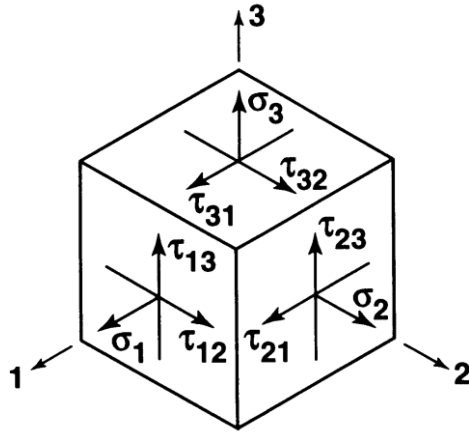


Figure 1.5: Stresses on an element [8]

Stresses		Strains	
Tensor Notation	Contracted Notation	Tensor Notation	Contracted Notation
σ_{11} (σ_1)	σ_1	ε_{11} (ε_1)	ε_1
σ_{22} (σ_2)	σ_2	ε_{22} (ε_2)	ε_2
σ_{33} (σ_3)	σ_3	ε_{33} (ε_3)	ε_3
$\tau_{23} = \sigma_{23}$	σ_4	$\gamma_{23} = 2\varepsilon_{23}$	ε_4
$\tau_{31} = \sigma_{31}$	σ_5	$\gamma_{31} = 2\varepsilon_{31}$	ε_5
$\tau_{12} = \sigma_{12}$	σ_6	$\gamma_{12} = 2\varepsilon_{12}$	ε_6

Table 1.1: Tensor versus contracted notation for stresses and strains [8]

The engineering shear strain γ_{ij} is equal to two times of the tensor shear strain ε_{ij} . The stiffness matrix C_{ij} has 36 constants as per the contracted notation. When important characteristics of the strain energy are considered, it can be shown that $C_{ij} = C_{ji}$, which makes the stiffness matrix symmetric. So, only 21 of the constants are independent. Also

the inverse of the stress-strain relation is called the strain-stress relation and can be written as,

$$\varepsilon_i = S_{ij}\sigma_j \quad i, j = 1, \dots, 6 \quad (1.6)$$

where S_{ij} is the compliance matrix. With foregoing reductions from 36 to 21 independent constants, the stress-strain relations in matrix form are,

$$\begin{bmatrix} \sigma_1 \\ \sigma_2 \\ \sigma_3 \\ \tau_{23} \\ \tau_{31} \\ \tau_{12} \end{bmatrix} = \begin{bmatrix} C_{11} & C_{12} & C_{13} & C_{14} & C_{15} & C_{16} \\ C_{12} & C_{22} & C_{23} & C_{24} & C_{25} & C_{26} \\ C_{13} & C_{23} & C_{33} & C_{34} & C_{35} & C_{36} \\ C_{14} & C_{24} & C_{34} & C_{44} & C_{45} & C_{46} \\ C_{15} & C_{25} & C_{35} & C_{45} & C_{55} & C_{56} \\ C_{16} & C_{26} & C_{36} & C_{46} & C_{56} & C_{66} \end{bmatrix} \begin{bmatrix} \varepsilon_1 \\ \varepsilon_2 \\ \varepsilon_3 \\ \gamma_{23} \\ \gamma_{31} \\ \gamma_{12} \end{bmatrix} \quad (1.7)$$

This relation characterizes anisotropic materials. If there are two orthogonal planes of material property symmetry for a material, symmetry will exist relative to a third mutually orthogonal plane. The stress-strain relations in such a case are,

$$\begin{bmatrix} \sigma_1 \\ \sigma_2 \\ \sigma_3 \\ \tau_{23} \\ \tau_{31} \\ \tau_{12} \end{bmatrix} = \begin{bmatrix} C_{11} & C_{12} & C_{13} & 0 & 0 & 0 \\ C_{12} & C_{22} & C_{23} & 0 & 0 & 0 \\ C_{13} & C_{23} & C_{33} & 0 & 0 & 0 \\ 0 & 0 & 0 & C_{44} & 0 & 0 \\ 0 & 0 & 0 & 0 & C_{55} & 0 \\ 0 & 0 & 0 & 0 & 0 & C_{66} \end{bmatrix} \begin{bmatrix} \varepsilon_1 \\ \varepsilon_2 \\ \varepsilon_3 \\ \gamma_{23} \\ \gamma_{31} \\ \gamma_{12} \end{bmatrix} \quad (1.8)$$

This relation characterizes orthotropic materials. There are only nine independent constants in the stiffness matrix. If at every point of a material there is one plane in which the mechanical properties are equal in all directions, then the material is called transversely isotropic. If, for example, the 2-3 plane is the plane of isotropy, then the 2 and 3 subscripts on the stiffnesses are interchangeable. Then stress-strain relations have only five independent constants,

$$\begin{bmatrix} \sigma_1 \\ \sigma_2 \\ \sigma_3 \\ \tau_{23} \\ \tau_{31} \\ \tau_{12} \end{bmatrix} = \begin{bmatrix} C_{11} & C_{12} & C_{12} & 0 & 0 & 0 \\ C_{12} & C_{22} & C_{23} & 0 & 0 & 0 \\ C_{12} & C_{23} & C_{22} & 0 & 0 & 0 \\ 0 & 0 & 0 & (C_{22} - C_{23})/2 & 0 & 0 \\ 0 & 0 & 0 & 0 & C_{66} & 0 \\ 0 & 0 & 0 & 0 & 0 & C_{66} \end{bmatrix} \begin{bmatrix} \varepsilon_1 \\ \varepsilon_2 \\ \varepsilon_3 \\ \gamma_{23} \\ \gamma_{31} \\ \gamma_{12} \end{bmatrix} \quad (1.9)$$

A unidirectional composite lamina is a transversely isotropic material. The strain-stress relations for a transversely isotropic material are,

$$\begin{bmatrix} \varepsilon_1 \\ \varepsilon_2 \\ \varepsilon_3 \\ \gamma_{23} \\ \gamma_{31} \\ \gamma_{12} \end{bmatrix} = \begin{bmatrix} S_{11} & S_{12} & S_{12} & 0 & 0 & 0 \\ S_{12} & S_{22} & S_{23} & 0 & 0 & 0 \\ S_{12} & S_{23} & S_{22} & 0 & 0 & 0 \\ 0 & 0 & 0 & 2(S_{22} - S_{23}) & 0 & 0 \\ 0 & 0 & 0 & 0 & S_{66} & 0 \\ 0 & 0 & 0 & 0 & 0 & S_{66} \end{bmatrix} \begin{bmatrix} \sigma_1 \\ \sigma_2 \\ \sigma_3 \\ \tau_{23} \\ \tau_{31} \\ \tau_{12} \end{bmatrix} \quad (1.10)$$

where in the 2-3 plane is a symmetry plane in which the compliances are isotropic and in the 1-direction (transverse to the symmetry plane), the compliances are different. The engineering constants are generally slope of a stress-strain curve (e.g., $E = \sigma/\varepsilon$) or the slope of a strain-strain curve (e.g., $\nu = -\varepsilon_y/\varepsilon_x$). Thus, the components of the compliance (S_{ij}) matrix are determined more directly than those of the stiffness (C_{ij}) matrix. For an orthotropic material, the compliance matrix components in terms of engineering constants are,

$$[S_{ij}] = \begin{bmatrix} \frac{1}{E_1} & -\frac{\nu_{21}}{E_2} & -\frac{\nu_{31}}{E_3} & 0 & 0 & 0 \\ -\frac{\nu_{12}}{E_1} & \frac{1}{E_2} & -\frac{\nu_{32}}{E_3} & 0 & 0 & 0 \\ -\frac{\nu_{13}}{E_3} & -\frac{\nu_{23}}{E_2} & \frac{1}{E_3} & 0 & 0 & 0 \\ 0 & 0 & 0 & \frac{1}{G_{23}} & 0 & 0 \\ 0 & 0 & 0 & 0 & \frac{1}{G_{31}} & 0 \\ 0 & 0 & 0 & 0 & 0 & \frac{1}{G_{12}} \end{bmatrix} \quad (1.11)$$

For a unidirectionally reinforced lamina in the 1-2 plane as shown in Fig.1.6, a plane stress state is defined by setting,

$$\sigma_3 = 0 \quad \tau_{23} = 0 \quad \tau_{31} = 0$$

A plane stress state in a lamina is not merely an idealization of reality, but instead is a practical and achievable objective of how a lamina must be used with fibres in its plane. Also, it is expected, a lamina is only loaded in plane stress because carrying in-plane stresses is its fundamental capability.

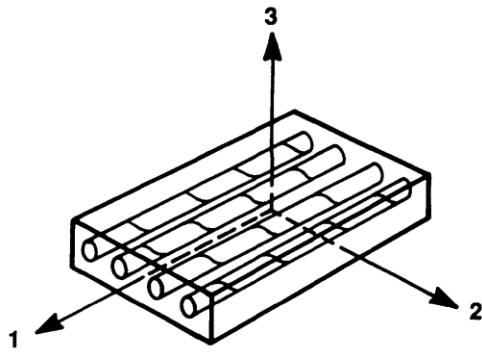


Figure 1.6: Unidirectionally reinforced lamina [8]

For transversely isotropic materials, imposing a state of plane stress reduces the strain-stress relations to,

$$\begin{bmatrix} \varepsilon_1 \\ \varepsilon_2 \\ \gamma_{12} \end{bmatrix} = \begin{bmatrix} \frac{1}{E_1} & -\frac{\nu_{21}}{E_2} & 0 \\ -\frac{\nu_{12}}{E_1} & \frac{1}{E_2} & 0 \\ 0 & 0 & \frac{1}{G_{12}} \end{bmatrix} \begin{bmatrix} \sigma_1 \\ \sigma_2 \\ \tau_{12} \end{bmatrix} \quad (1.12)$$

The stress-strain relations is obtained by inverting the above shown strain-stress relations,

$$\begin{bmatrix} \sigma_1 \\ \sigma_2 \\ \tau_{12} \end{bmatrix} = \begin{bmatrix} Q_{11} & Q_{12} & 0 \\ Q_{12} & Q_{22} & 0 \\ 0 & 0 & Q_{66} \end{bmatrix} \begin{bmatrix} \varepsilon_1 \\ \varepsilon_2 \\ \gamma_{12} \end{bmatrix} \quad (1.13)$$

where the Q_{ij} are the so-called reduced stiffnesses for a plane stress state in the 1-2 plane which are determined as the components of the inverted compliance matrix. The Q_{ij} are given by,

$$Q_{11} = \frac{E_1}{1 - \nu_{12}\nu_{21}} \quad (1.14)$$

$$Q_{22} = \frac{E_2}{1 - \nu_{12}\nu_{21}} \quad (1.15)$$

$$Q_{12} = \frac{\nu_{12}E_2}{1 - \nu_{12}\nu_{21}} = \frac{\nu_{21}E_1}{1 - \nu_{12}\nu_{21}} \quad (1.16)$$

$$Q_{66} = G_{12} \quad (1.17)$$

Thus, the reduced stiffnesses are calculated from the four independent material properties, E_1 , E_2 , ν_{12} and G_{12} calculated from the micromechanical behavior of lamina, in addition to the reciprocal relation $\nu_{12}/E_1 = \nu_{21}/E_2$.

So far, all the stiffnesses and compliances have been calculated in the local coordinate system (1, 2, 3). Hence, before moving to the macromechanical behavior of a laminate, these properties should be transformed to the global coordinate system (x, y, z), as the laminate has a set of lamina with various fibre orientations that are bonded together. Consider a lamina under plane stress condition, with local coordinates (1, 2) oriented at an angle θ with respect to the global coordinates (x, y) as shown in Fig.1.7.

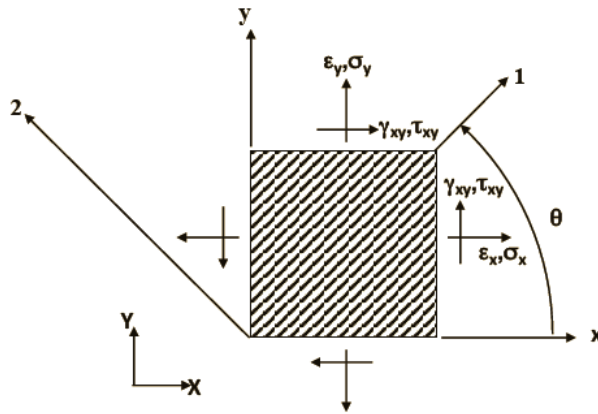


Figure 1.7: Coordinate transformations [7]

The stresses and strains are transformed from local to global coordinates using the inverse of the transformation matrix ($[T]^{-1}$) as shown below,

$$[T]^{-1} = \begin{bmatrix} \cos^2 \theta & \sin^2 \theta & -2 \cos \theta \sin \theta \\ \sin^2 \theta & \cos^2 \theta & 2 \cos \theta \sin \theta \\ \cos \theta \sin \theta & -\cos \theta \sin \theta & \cos^2 \theta - \sin^2 \theta \end{bmatrix} \quad (1.18)$$

The stresses and strains in the global coordinates can be related by using the transformed reduced stiffness matrix $[\bar{Q}]$ as shown below,

$$\begin{bmatrix} \sigma_x \\ \sigma_y \\ \tau_{xy} \end{bmatrix} = \begin{bmatrix} \bar{Q}_{11} & \bar{Q}_{12} & \bar{Q}_{16} \\ \bar{Q}_{12} & \bar{Q}_{22} & \bar{Q}_{26} \\ \bar{Q}_{16} & \bar{Q}_{26} & \bar{Q}_{66} \end{bmatrix} \begin{bmatrix} \varepsilon_x \\ \varepsilon_y \\ \gamma_{xy} \end{bmatrix} \quad (1.19)$$

The $[\bar{Q}]$ matrix is obtained from the $[Q]$ matrix, it is computed as,

$$[\bar{Q}] = [T]^{-1}[Q][T]^{-T} \quad (1.20)$$

where $[T]^{-T}$ denotes the transpose of the inverse of $[T]$. The coefficients \bar{Q}_{16} and \bar{Q}_{26} are non-zero, which implies if the global axis does not coincide with the local axis, when shear stress is applied, not only shear strain but also normal strains are produced.

Macromechanical behavior of a laminate

The macromechanical behavior of a laminate helps in finding the response of a laminate under loading i.e., imposed forces and moments. The stiffnesses and strengths of a laminate are obtained from the properties of the constituent laminae by the classical lamination theory (CLT). The relation of the laminate forces and moments to the strains and curvatures is found using CLT, where the laminate stiffnesses are the link from the forces and moments to the strains and curvature. The stress-strain relations derived in the macromechanical behavior of a lamina can be thought of as stress-strain relations of the k^{th} layer in a multilayered laminate.

$$\{\sigma\}_k = [\bar{Q}]_k \{\varepsilon\}_k \quad (1.21)$$

The three major assumptions made in the CLT are,

1. The laminate is presumed to consist of perfectly bonded laminae. Moreover, the bond are presumed to be infinitesimally thin as well as non-shear-deformable. That is, the displacements are continuous across lamina boundaries so that no lamina can slip relative to another.
2. A line originally straight and perpendicular to the middle surface of the laminate (normal to the middle surface), is assumed to remain straight and perpendicular to the middle

surface when the laminate is deformed. This is equivalent to ignoring the shearing strains in planes perpendicular to the middle surface ($\gamma_{xz} = \gamma_{yz} = 0$), where z is the direction of the normal to the middle surface in Fig.1.8.

3. The normal are presumed to have a constant length so that the strain perpendicular to the middle surface is also ignored ($\epsilon_z = 0$).

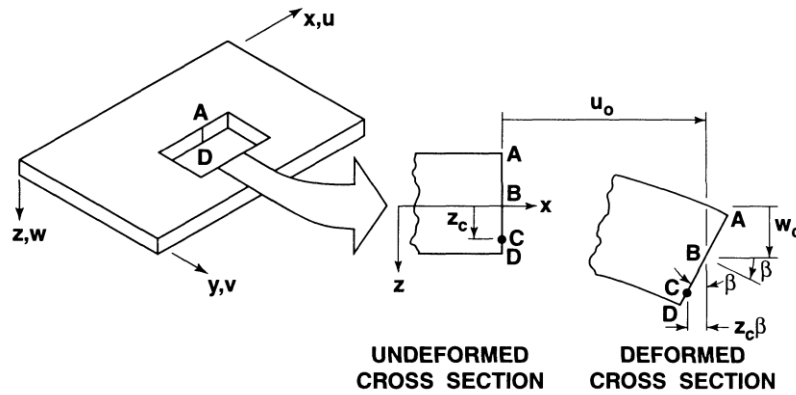


Figure 1.8: Geometry of deformation in the x-z plane [8]

The implications of these assumptions on the laminate displacements u , v , and w in the x -, y -, and z -directions are derived by use of the laminate cross section in the x - z plane shown in Fig.1.8. The displacements u and v , at any point z through the laminate thickness are,

$$u = u_0 - z \frac{\partial w_0}{\partial x} \quad (1.22)$$

$$v = v_0 - z \frac{\partial w_0}{\partial y} \quad (1.23)$$

The small strains (linear elasticity) are defined in terms of displacements as,

$$\begin{bmatrix} \varepsilon_x \\ \varepsilon_y \\ \gamma_{xy} \end{bmatrix} = \begin{bmatrix} \frac{\partial u}{\partial x} \\ \frac{\partial v}{\partial y} \\ \frac{\partial u}{\partial y} + \frac{\partial v}{\partial x} \end{bmatrix} \quad (1.24)$$

Thus for the derived displacements u and v, the strains are,

$$\begin{bmatrix} \varepsilon_x \\ \varepsilon_y \\ \gamma_{xy} \end{bmatrix} = \begin{bmatrix} \varepsilon_x^0 \\ \varepsilon_y^0 \\ \gamma_{xy}^0 \end{bmatrix} + z \begin{bmatrix} \kappa_x \\ \kappa_y \\ \kappa_{xy} \end{bmatrix} \quad (1.25)$$

where $\varepsilon_x^0, \varepsilon_y^0, \gamma_{xy}^0$ are called as the middle-surface strains; κ_x, κ_y are the curvatures of the plate due to bending and κ_{xy} is the curvature due to twisting. By substitution of the strain variation through the thickness, in the stress-strain relations, the stresses in the kth layer can be expressed in terms of the laminate middle-surface strains and curvatures as,

$$\begin{bmatrix} \sigma_x \\ \sigma_y \\ \tau_{xy} \end{bmatrix}_k = \begin{bmatrix} \bar{Q}_{11} & \bar{Q}_{12} & \bar{Q}_{16} \\ \bar{Q}_{12} & \bar{Q}_{22} & \bar{Q}_{26} \\ \bar{Q}_{16} & \bar{Q}_{26} & \bar{Q}_{66} \end{bmatrix}_k \left[\begin{bmatrix} \varepsilon_x^0 \\ \varepsilon_y^0 \\ \gamma_{xy}^0 \end{bmatrix} + z \begin{bmatrix} \kappa_x \\ \kappa_y \\ \kappa_{xy} \end{bmatrix} \right] \quad (1.26)$$

The resultant forces and moments acting on a laminate are obtained by integration of the stresses in each lamina through the laminate thickness. The entire collection of force and moment resultants for an n-layered laminate are depicted in Fig.1.9 and 1.10 and are defined as,

$$\begin{bmatrix} N_x \\ N_y \\ N_{xy} \end{bmatrix} = \sum_{k=1}^n \int_{z_{k-1}}^{z_k} \begin{bmatrix} \sigma_x \\ \sigma_y \\ \tau_{xy} \end{bmatrix}_k dz \quad (1.27)$$

$$\begin{bmatrix} M_x \\ M_y \\ M_{xy} \end{bmatrix} = \sum_{k=1}^n \int_{z_{k-1}}^{z_k} \begin{bmatrix} \sigma_x \\ \sigma_y \\ \tau_{xy} \end{bmatrix}_k dz \quad (1.28)$$

where z_k and z_{k-1} are defined in the basic laminate geometry shown in Fig.1.11.

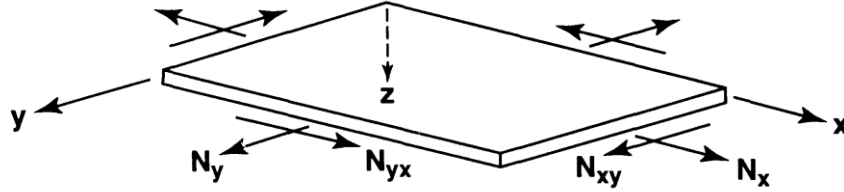


Figure 1.9: In-plane forces on a flat laminate [8]

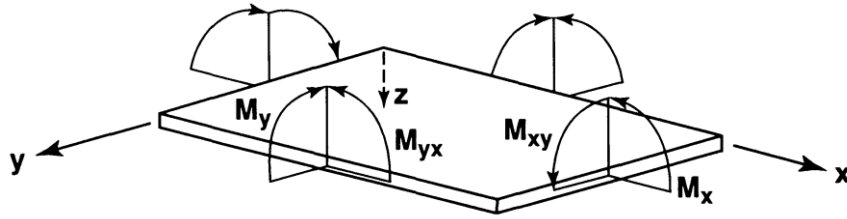


Figure 1.10: Moments on a flat laminate [8]

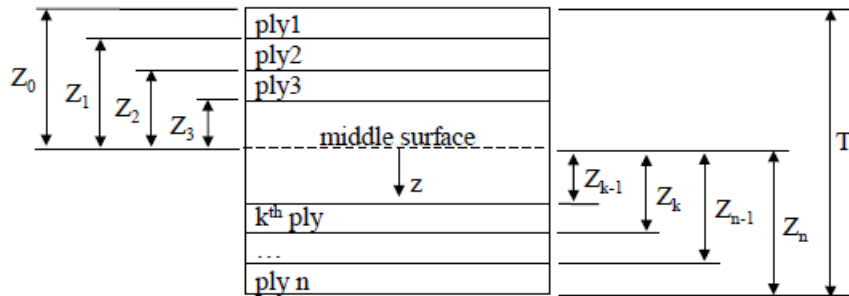


Figure 1.11: Geometry of an N-layered laminate [7]

When the lamina stress-strain relations, are substituted, the forces and moments become,

$$\begin{bmatrix} N_x \\ N_y \\ N_{xy} \end{bmatrix} = \sum_{k=1}^n \begin{bmatrix} \bar{Q}_{11} & \bar{Q}_{12} & \bar{Q}_{16} \\ \bar{Q}_{12} & \bar{Q}_{22} & \bar{Q}_{26} \\ \bar{Q}_{16} & \bar{Q}_{26} & \bar{Q}_{66} \end{bmatrix}_k \left[\int_{z_{k-1}}^{z_k} \begin{bmatrix} \epsilon_x^0 \\ \epsilon_y^0 \\ \gamma_{xy}^0 \end{bmatrix} dz + \int_{z_{k-1}}^{z_k} \begin{bmatrix} \kappa_x \\ \kappa_y \\ \kappa_{xy} \end{bmatrix} z dz \right] \quad (1.29)$$

$$\begin{bmatrix} M_x \\ M_y \\ M_{xy} \end{bmatrix} = \sum_{k=1}^n \begin{bmatrix} \bar{Q}_{11} & \bar{Q}_{12} & \bar{Q}_{16} \\ \bar{Q}_{12} & \bar{Q}_{22} & \bar{Q}_{26} \\ \bar{Q}_{16} & \bar{Q}_{26} & \bar{Q}_{66} \end{bmatrix}_k \left[\int_{z_{k-1}}^{z_k} \begin{bmatrix} \varepsilon_x^0 \\ \varepsilon_y^0 \\ \gamma_{xy}^0 \end{bmatrix} z dz + \int_{z_{k-1}}^{z_k} \begin{bmatrix} \kappa_x \\ \kappa_y \\ \kappa_{xy} \end{bmatrix} z^2 dz \right] \quad (1.30)$$

As ε_x^0 , ε_y^0 , γ_{xy}^0 , κ_x , κ_y and κ_{xy} are not functions of z , but are middle surface values and curvatures, they can be removed from within the summation signs.

$$\begin{bmatrix} N_x \\ N_y \\ N_{xy} \end{bmatrix} = \begin{bmatrix} A_{11} & A_{12} & A_{16} \\ A_{12} & A_{22} & A_{26} \\ A_{16} & A_{26} & A_{66} \end{bmatrix} \begin{bmatrix} \varepsilon_x^0 \\ \varepsilon_y^0 \\ \gamma_{xy}^0 \end{bmatrix} + \begin{bmatrix} B_{11} & B_{12} & B_{16} \\ B_{12} & B_{22} & B_{26} \\ B_{16} & B_{26} & B_{66} \end{bmatrix} \begin{bmatrix} \kappa_x \\ \kappa_y \\ \kappa_{xy} \end{bmatrix} \quad (1.31)$$

$$\begin{bmatrix} M_x \\ M_y \\ M_{xy} \end{bmatrix} = \begin{bmatrix} B_{11} & B_{12} & B_{16} \\ B_{12} & B_{22} & B_{26} \\ B_{16} & B_{26} & B_{66} \end{bmatrix} \begin{bmatrix} \varepsilon_x^0 \\ \varepsilon_y^0 \\ \gamma_{xy}^0 \end{bmatrix} + \begin{bmatrix} D_{11} & D_{12} & D_{16} \\ D_{12} & D_{22} & D_{26} \\ D_{16} & D_{26} & D_{66} \end{bmatrix} \begin{bmatrix} \kappa_x \\ \kappa_y \\ \kappa_{xy} \end{bmatrix} \quad (1.32)$$

$$\begin{aligned} A_{ij} &= \sum_{k=1}^n (\bar{Q}_{ij})_k (z_k - z_{k-1}) \\ B_{ij} &= \frac{1}{2} \sum_{k=1}^n (\bar{Q}_{ij})_k (z_k^2 - z_{k-1}^2) \\ D_{ij} &= \frac{1}{3} \sum_{k=1}^n (\bar{Q}_{ij})_k (z_k^3 - z_{k-1}^3) \end{aligned} \quad (1.33)$$

The A_{ij} are extensional stiffnesses, the B_{ij} are bending-extension coupling stiffnesses, and the D_{ij} are bending stiffnesses. The mere presence of the B_{ij} implies coupling between bending and extension of a laminate, because both forces and curvatures as well as moments and strains simultaneously exist. If both the force and moment matrices are combined, it gives the ABD matrix which links the forces and moments to the strains and curvatures and this matrix is called as the stiffness matrix of a laminate.

$$\begin{bmatrix} N_x \\ N_y \\ N_{xy} \\ M_x \\ M_y \\ M_{xy} \end{bmatrix} = \begin{bmatrix} A_{11} & A_{12} & A_{16} & B_{11} & B_{12} & B_{16} \\ A_{12} & A_{22} & A_{26} & B_{12} & B_{22} & B_{26} \\ A_{16} & A_{26} & A_{66} & B_{16} & B_{26} & B_{66} \\ B_{11} & B_{12} & B_{16} & D_{11} & D_{12} & D_{16} \\ B_{12} & B_{22} & B_{26} & D_{12} & D_{22} & D_{26} \\ B_{16} & B_{26} & B_{66} & D_{16} & D_{26} & D_{66} \end{bmatrix} \begin{bmatrix} \varepsilon_x^0 \\ \varepsilon_y^0 \\ \varepsilon_{xy}^0 \\ \kappa_x \\ \kappa_y \\ \kappa_{xy} \end{bmatrix} \quad (1.34)$$

Thus using the three steps provided here, the elastic constants of a laminated FRP can be found from the engineering constants of the basic constituents of the composite - fibre and matrix.

Special Cases of Laminates

Before proceeding to the special cases of laminates, it is better to understand the manner in which the laminate lay-up is specified, i.e., stacking sequence notation. For regular (equal thickness layers) laminates, a listing of the layers and their orientations suffices, for example, [0/90/45]. If multiple laminae occur at the same angle, then subscripts are used to designate the number of such multiple layers, for example, [0/0/0/90/90] = [0₃/90₂]. If sequences of laminae are repeated, then those sequences are grouped with a subscript to indicate the number of sequence repetitions, for example, [0/90/45/0/90/45] = [0/90/45]₂. If the laminae are located symmetrically with respect to the middle surface of the laminate, they are called as symmetric laminates, the simplest representation of such a laminate, for example, [0/90/45/45/90/0] = [0/90/45]_s. Finally, if all the laminae are specified in the stacking sequence and no implications of repeated sequences, symmetry are desired, then a subscript T is used to indicate complete or total specification for emphasis, for example, [0/90/45/-45/0/90]_T.

For some special cases of laminates, the stiffnesses take on certain simplified values as opposed to the general form. There are many different special cases of laminates such as symmetric, unsymmetric, anti-symmetric, balanced, cross-ply, angle-ply etc., but here the explanation is provided only for symmetric and unsymmetric laminates.

Symmetric laminates

For symmetric laminates, the general stiffness equations simplify considerably. The symmetry has the form such that for each pair of equal thickness laminae,

1. Both laminae are of the same material properties and fibre orientations, i.e., both laminae have the same $(\bar{Q}_{ij})_k$.
2. If one lamina is a certain distance above the middle surface, then the other lamina is the same distance below the middle surface.

Because of the symmetry of the $(\bar{Q}_{ij})_k$ and the thicknesses t_k , all the bending-extension coupling stiffnesses B_{ij} can be shown to be zero. A symmetric laminate $[0/90]_s$, that satisfies all the conditions of symmetry is as shown in Fig.1.12 (a), where all the laminae are of equal thickness and made of same material.

Unsymmetric laminates

Unsymmetric laminates are the most general class of laminates. Any laminate that is not symmetric about the middle surface is called an unsymmetric laminate. For example, a simple cross-ply unsymmetric laminate $[0_2/90_2]_T$ is as shown in Fig.1.12 (b).

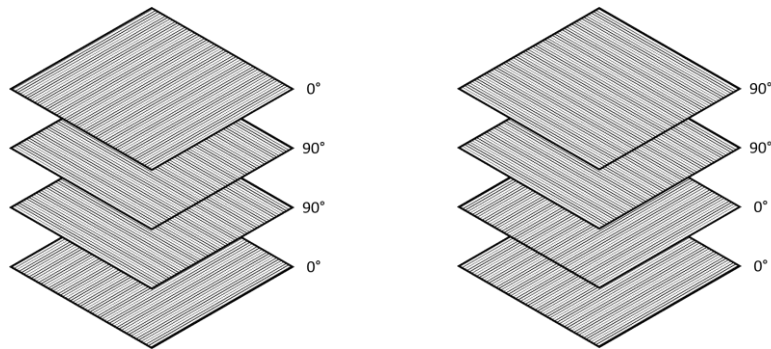


Figure 1.12: Unbonded view of (a) symmetric laminate; (b) unsymmetric laminate

Most high performance composites are cured at elevated temperature to fully activate the matrix that holds the fibres together and ensure a strong final structure. When the structure is kept at the curing temperature in the oven, it is at a high ‘stress free’ state. But when the structure is cooled back to room temperature, a large temperature change is introduced with respect to its “stress free” state. This temperature differential, causes thermally induced stresses within the structure and these stresses cause the structure to deform. The way it deforms is dictated by the stiffness matrix (ABD matrix), which in turn is defined by the laminate stacking sequence. If the laminate is made symmetric, the coupling between bending and extension gets eliminated ($B_{ij} = 0$) and hence the laminate does not bend or twist during the process of cooling down from the curing temperature. This is the primary reason, the commercial composite structures are almost always designed as symmetric laminates.

If the laminate is made unsymmetric, then it deforms. During the initial stages of composite research, those deformations were regarded as undesirable, but later they were considered to be quite useful and even desirable in certain structural applications. That is, sometimes there might be a need for the laminate to have a certain curvature or twist rather

than just being flat. The CLT predicted the cured shape of unsymmetric laminates to be saddle shaped (the curvatures are $\kappa_x = -\kappa_y$ or $-\kappa_x = \kappa_y$). But in the year 1981, M. W. Hyer [1] in his research found out the cured shape to be cylindrical ($+\kappa_x, \kappa_y = 0$) and the availability of a second stable cylindrical shape ($\kappa_x = 0, -\kappa_y$) as well. This is when the unsymmetric laminated FRP were started being called as bistable composites. He also identified a snap through & snap back phenomenon between the two stable shapes, which helped in the utilization of these laminates in shape morphing applications. Thus, his paper formed the beginning of an entirely new research area in the field of composite materials named “Bistable Composites”.

Thesis Outline

In Chapter 2, the literature review is presented. It gives a detailed summary of the research that happened in the past and happening currently in the field of bistable composites. In Chapter 3, based on the literature review, the research objectives that has been formulated, the methodology proposed and the step by step procedure of this research which includes both simulations and experiments are presented. In Chapter 4, the results obtained from the various simulations and experiments done along with the discussions and findings of this research are presented. In the last, Chapter 5 presents the summary of the work done and the future works possible that can propel this research forward.

CHAPTER TWO

LITERATURE REVIEW

From the inception of this concept in the year 1981 by M. W. Hyer [9], there has been continuous research in the field of Bistable Composites in a wide variety of areas like analytical & numerical simulation of bistable composites, snap through actuation using piezoelectric & shape memory alloys, dynamic analysis & morphing control and design of multistable composites. The literature reviewed for this research is classified into the following major topics,

- i. Basic foundation
- ii. Variations in composite structure
- iii. Application of bistable composites
- iv. Optimization of bistable composites
- v. Multistable composites

Basic Foundation

The very first paper on bistable composites was written by Hyer [9], as he was the first person to identify the bistable behaviour of unsymmetric laminates. In his work, he explains the inability of Classical Lamination Theory to predict correctly the room temperature shapes of thin unsymmetric laminates. The problem with the Classical lamination theory is that it predicts the room temperature shapes of all unsymmetric laminates to be saddle shape with unique curvature characteristics. However, this is true only with thicker laminates and Hyer showed that the thinner laminates have two room

temperature shapes (two cylindrical shapes) and they exhibit a snap through or oil canning phenomenon between the two shapes. Hyer carried out a non-linear extension of the theory, to arrive at the two room temperature shapes and explained the snap through phenomenon. The solutions obtained are one term Galerkin or Rayleigh-Ritz solutions. He also experimentally validated the results. Cross ply $[0_n/90_n]$ $n=1,2,\dots$ family of laminates were used for the study, as some of the A_{ij} , B_{ij} & D_{ij} terms for this family are zero and the associated algebra is simpler to compute. A cured laminate is flat at the curing temperature. As it cools, it is assumed to be free of any mechanical load which can produce net work and it is assumed that the out of plane deflections developed are only because of the differences in thermal expansion properties of the individual lamina.

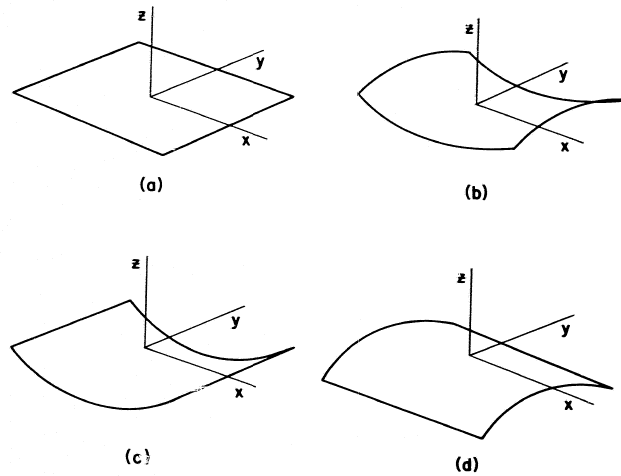


Figure 2.1: Laminate shapes (a) at elevated curing temperature, and at room temperature, (b) saddle shape (c) first cylindrical shape (d) second cylindrical shape [9]

As the laminate cools down from the curing temperature, it takes any one of the three shapes shown in Fig.1 (b), (c) & (d), depending on whichever shape has the minimum total potential energy. Square laminates ($L_x = L_y = L$) made of T300/5208

graphite-epoxy in side length range of 0-150 mm were considered in two thickness variations $[0_2/90_2]$ & $[0_4/90_4]$.

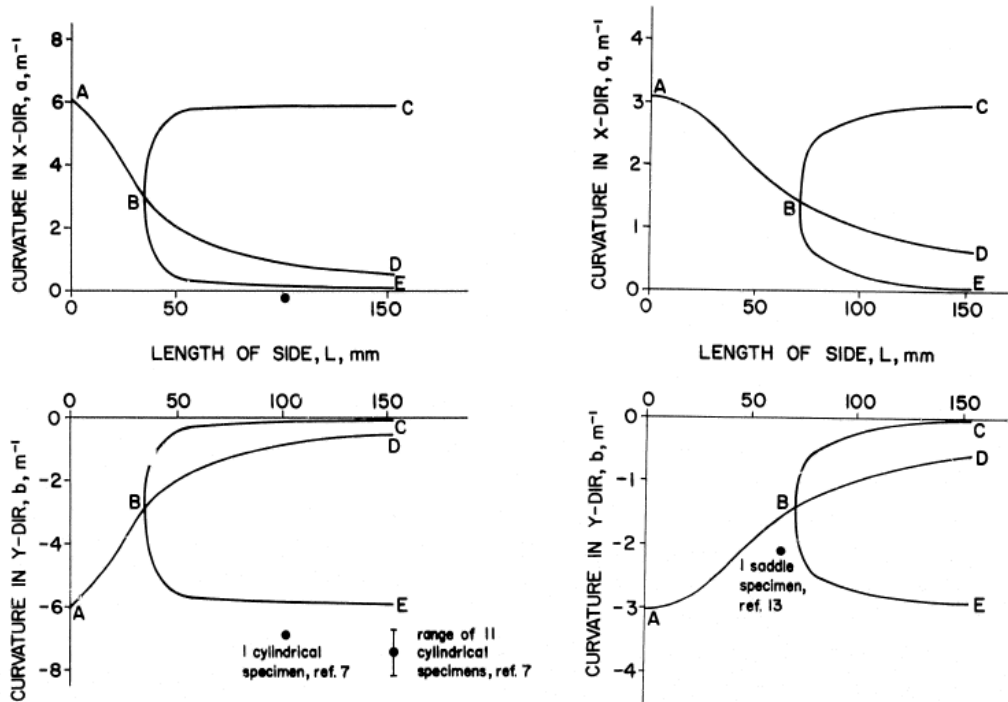


Figure 2.2: Room-temperature shapes of thin $[0_2/90_2]$ and thick $[0_4/90_4]$ square laminates [9]

Fig. 2.2 illustrates the effect of the length of side (L) on the room temperature shapes and shows the characteristics of the predicted room temperature shapes for two different thickness laminates. The critical length of the side is found to be 35 mm for thinner laminates and 71 mm for thicker laminates until which only the saddle shape exists. Beyond the bifurcation point 'B', the two cylindrical shapes come into existence. Although there was a paucity of experimental data to compare with the entire numerical prediction, the results reported were encouraging and formed a good starting point for the entire field of bistable composites.

Dano & Hyer [10] developed a theory based on the Rayleigh-Ritz minimization of total potential energy to predict the deformation behaviour of general unsymmetric laminates that are flat at their elevated curing temperature and are cooled to room temperature. They also compared their theory with the previously proposed Jun & Hong theory [11] and Finite Element Analysis results. Curvatures of three families of unsymmetric laminates $[-\Theta_4/\Theta_4]$, $[(90-\Theta)_4/\Theta_4]$, and $[(\Theta-90)_4/\Theta_4]$, where Θ is any angle from 0° to 90° were predicted using the proposed theory. All three families exhibited two stable shapes as shown in Fig. 2.3-2.5. Because there are multiple equilibrium configurations, once the bifurcation point is reached, the Abaqus model must be coaxed to continue on a particular path to obtain the different shapes at room temperature. Without any imperfection, Abaqus usually converged to the unstable shape. Thus for each path, one separate set of finite element calculations are carried out resulting in three sets for each model.

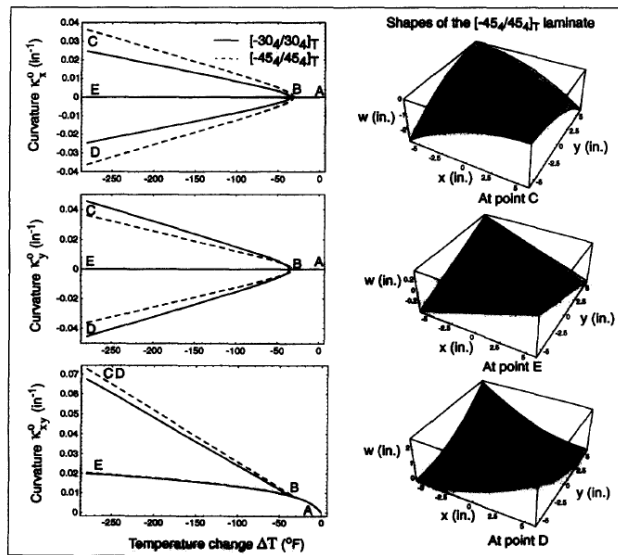


Figure 2.3: Temperature-curvature relations for the $[-\Theta_4/\Theta_4]$ laminates [10]

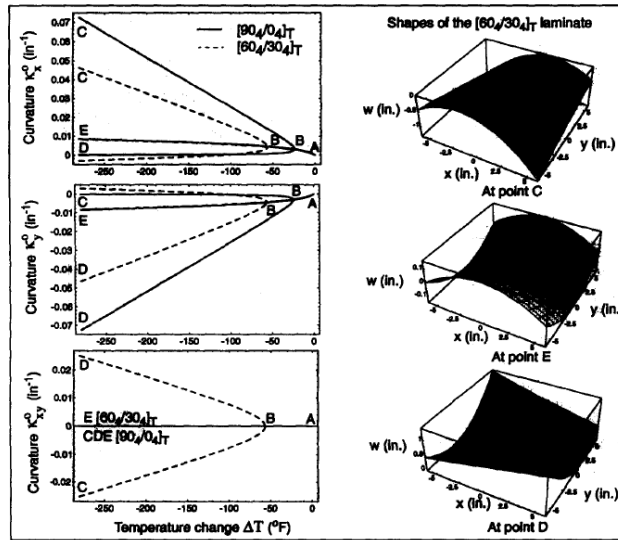


Figure 2.4: Temperature-curvature relations for the $[(90-\Theta)_4/\Theta_4]$ laminates [10]

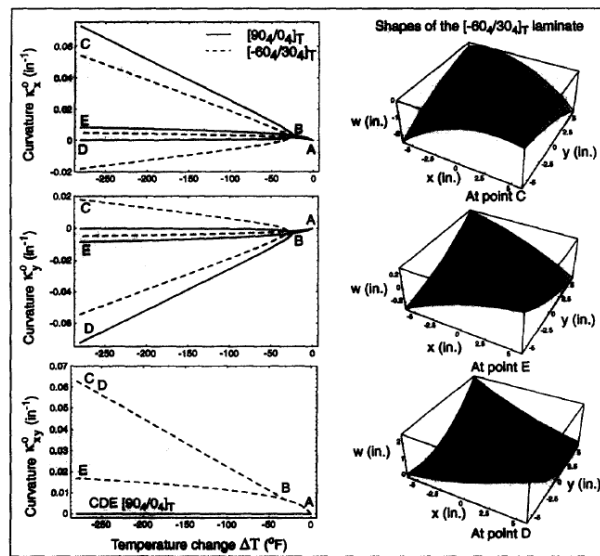


Figure 2.5: Temperature-curvature relations for the $[(\Theta-90)_4/\Theta_4]$ laminates [10]

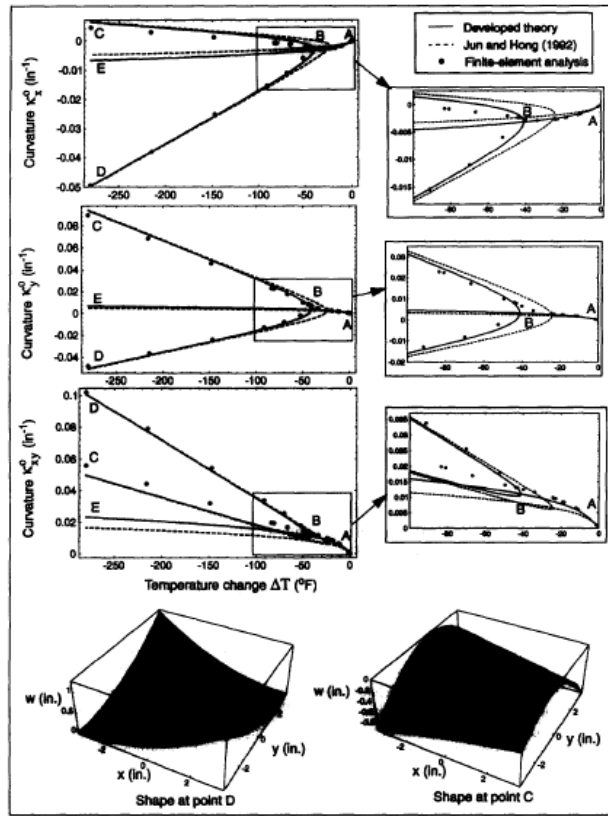


Figure 2.6: Comparisons of the proposed theory with the Jun & Hong theory and finite element analysis: temperature-curvature relations for a $[0_2/30_2]$ laminate [10]

Fig. 2.6 shows the comparison between the proposed theory, Jun & Hong theory and finite element analysis. From the comparison it is seen that there is a difference in the bifurcation temperature predicted by the two theories, however for the two stable shapes at room temperature the two theories match. Thus adding more variables in the strains as done in the proposed theory, influences the predicted bifurcation temperature as well as the curvature of the unstable shape. The finite element analysis performed shows that for temperatures near cure, the proposed theory seems to give more accurate results than the Jun and Hong theory. But as the temperature is decreased to room temperature, the predictions from both the Jun and Hong theory and the proposed theory come closer to the finite element results.

Gigliotti et al. [12] studied the loss of bifurcation in square laminates due to asymmetric thickness and the change in aspect ratio of rectangular laminates on the existence and stability of the cylindrical shapes. They developed a finite element solution (Abaqus) and compared it with Rayleigh-Ritz solution. The non-dimensional curvatures and lengths considered for the study were,

$$a^* = aL^2/t \quad (2.1)$$

$$b^* = bL^2/t \quad (2.2)$$

$$L^* = (L^2/t^2)\alpha\Delta T \quad (2.3)$$

where a & b are the curvature along x -direction & y -direction respectively, L is the length of the plate, t is the thickness of the plate, α is the difference between the transverse and the longitudinal coefficients of thermal expansion and ΔT is the temperature differential. S4R elements, 4-node general purpose reduced integration shell elements which allow shear deformation were used. Geometrically nonlinear algorithms (NLGEOM) was used to obtain the different stable shapes in Abaqus. A perfectly modelled square always yields an unstable saddle shape in Abaqus for whatever may be the length, so an imperfection was introduced in the form of a quasi-square (e.g. 100 mm X 99 mm in place of 100 mm X 100 mm) to get the stable cylindrical shapes in the static step.

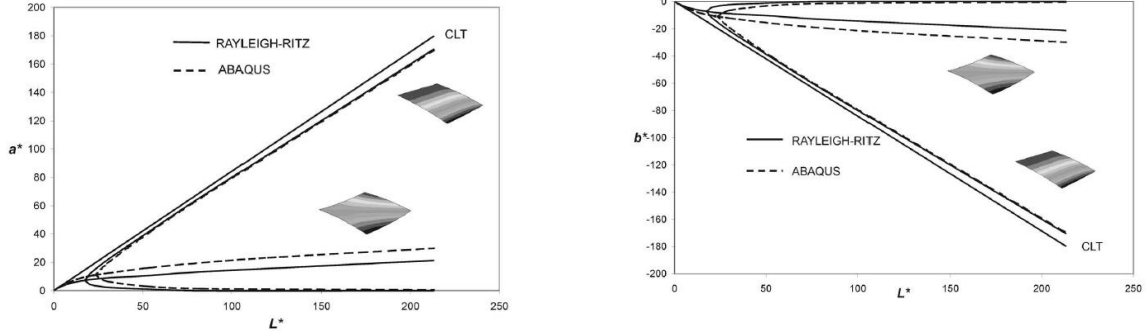


Figure 2.7: Non-dimensional curvatures a^* and b^* predicted by Abaqus and by the Rayleigh-Ritz model (square plates) [12]

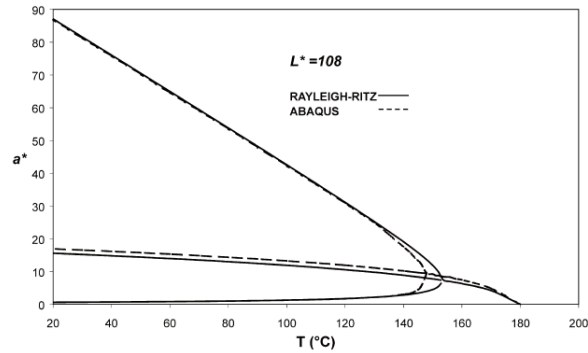


Figure 2.8: Curvature-temperature relationship (Rayleigh-Ritz and Abaqus model, $L^* > L^*_{cr}$) [12]

Abaqus predicted the value of the critical length of the side L^*_{cr} to be 24 as shown in Fig. 2.7, and for a length L^* greater than L^*_{cr} , it predicted the value of the critical temperature T_{cr} to be 147°C as shown in Fig. 2.8. The Rayleigh-Ritz and Abaqus solutions for the non-dimensional curvature a^* , appears to be shifted for values of temperature between 130°C and 180°C . The discrepancies were due to the fact that the in-plane shear strain γ_{xy} has been neglected in the Rayleigh-Ritz model. To avoid this discrepancy, the Abaqus non-linear solution was forced to develop negligible in-plane shear strain and the two solutions were matched.

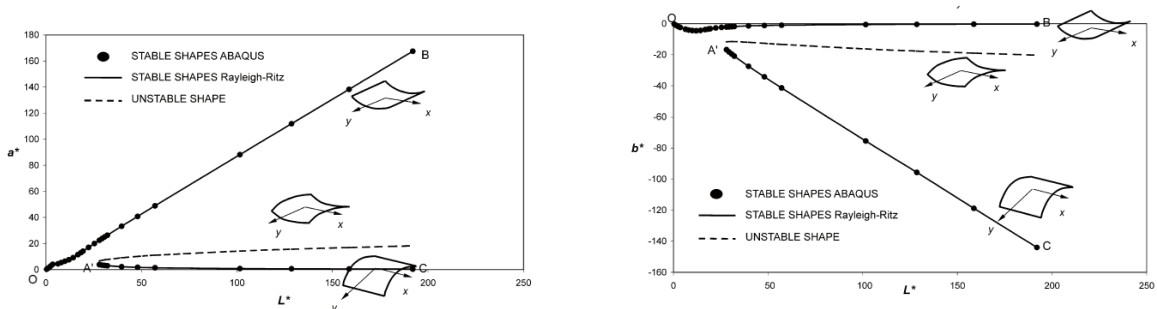


Figure 2.9: Non-dimensional curvatures a^* and b^* predicted by Abaqus and Rayleigh-Ritz model for square plates with thickness ratio $t_0/t_{90} = 0.93$ [12]

Fig. 2.9 shows the curvature predicted by Abaqus and the Rayleigh–Ritz model for a square plate with thickness ratio $t_0/t_{90}=0.93$ within a range of non-dimensional lengths between 0 and 210. The two solutions were practically coincident, discrepancies were negligible. It must be noted that before point A' and its corresponding value of non-dimensional length, $L^*_{A'}$, only one solution was found. Thus not all values of non-dimensional length allow multiple shapes. Also, as the t_0/t_{90} ratio diminished, the point A' at which multiple solutions became observable progressively shifted towards high values of non-dimensional length.

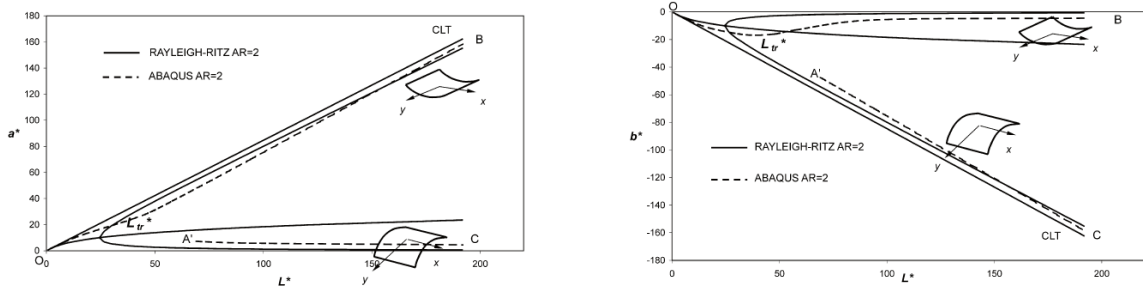


Figure 2.10: Non-dimensional curvatures a^* and b^* predicted by Abaqus and by the Rayleigh-Ritz model for plates with $AR = 2$ [12]

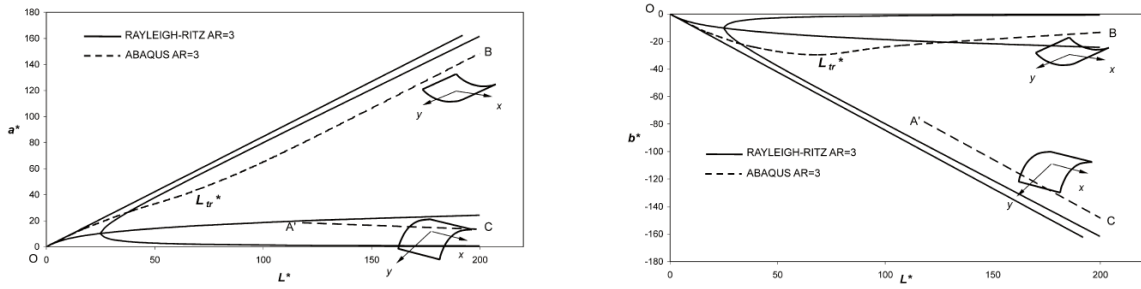


Figure 2.11: Non-dimensional curvatures a^* and b^* predicted by Abaqus and by the Rayleigh-Ritz model for plates with $AR = 3$ [12]

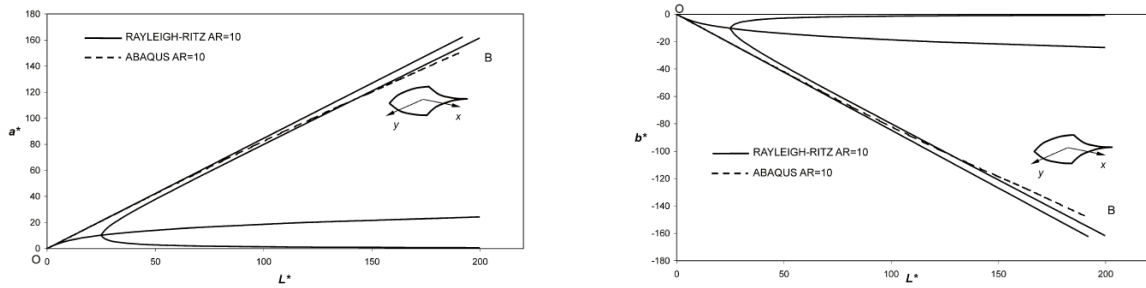


Figure 2.12: Non-dimensional curvatures a^* and b^* predicted by Abaqus and by the Rayleigh-Ritz model for plates with $AR = 10$ [12]

Fig. 2.10-2.12 shows the results for plates with aspect ratio, $AR=2$, $AR=3$ and $AR=10$ within a range of non-dimensional lengths between 0 and 190. Saddle-like configurations and cylindrical configurations were separated by smooth transition values of non-dimensional length indicated as L^*_{tr} . Major effects observed while increasing the aspect ratio,

1. Increase in the values of L^*_{tr} and reduction in the range of existence of multiple solutions, L^*_{tr} was about 40 for $AR=2$ and 70 for $AR=3$.
2. Increase in the magnitude of the b^* curvatures, indicating a progressive dominance of saddle-like solutions.
3. Diminishing effect of nonlinearities on the a^* curvatures.

For $AR=10$, L^*_{tr} disappeared from the range of non-dimensional lengths considered in the study and within this range the resulting shapes were quasi-saddles. It is evident from Fig. 2.10-2.12 that the loss of bifurcation, the existence of multiple shapes and the transition from cylindrical to saddle shapes can be characterised by two parameters, the aspect ratio AR and the non-dimensional length L^* .

Portela et al. [13] studied a novel morphing structure concept made of bistable unsymmetric laminates actuated by a piezoelectric Macro Fibre Composite (MFC). They also included the environmental effects like moisture absorption in their analysis. Non-linear Finite Element (FE) Analysis had been used to reproduce the cured shapes of the unsymmetric laminate and to simulate the combined laminate / actuator system. The plate geometry and boundary conditions are as depicted in Fig. 2.13.

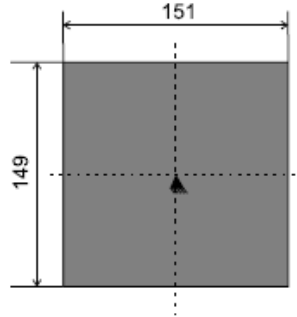


Figure 2.13: FE model boundary conditions [13]

Using perfectly square plates in the FE model will make the analysis converge to unstable saddle shapes instead of stable cylindrical ones. Hence, geometric imperfections were included in all the models. Two materials used for the initial tests and the analysis were AS4-8552 and T800-2020 carbon fibre / epoxy prepreg. General purpose shell elements were used (type SR4 in Abaqus). Large deformation theory was used

(*NLGEOM) to calculate the plate's deformation due to a temperature change of $\Delta T = -160^\circ\text{C}$ as shown in Table 2.1.

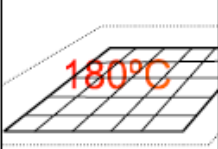
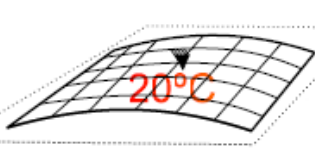
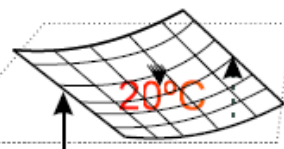
Step name:	0,Initial	$\xrightarrow{\Delta T}$	1.Cooling	$\xrightarrow{\quad}$	2.Snap
Solver type:			Static w/ NLGEOM		Static, Riks w/ NLGEOM
Geometry at end of step:					

Table 2.1: Representation of the analysis steps [13]

Composite materials absorb moisture from the atmosphere in which they are immersed. In this application, the effect of hygroscopic stress field is to relax the existing residual stress field and thus reduce the plates' curvature. A modification of the thermal expansion coefficients is required to account for the hygroscopic effects. Assuming plane stress conditions and neglecting the mechanical strains,

$$\{\varepsilon\}^k = \{\alpha\}^k \Delta T + \{\beta\}^k \Delta M = \{\alpha^*\}^k \Delta T \quad (2.4)$$

where $\{\alpha\}^k$ and $\{\beta\}^k$ are the coefficient of thermal expansion and moisture expansion in the ply coordinate system respectively; $\{\alpha^*\}^k$ is the equivalent moisture expansion coefficient accounting for the effect of both thermal and hygroscopic residual strains; ΔT is the applied temperature field and ΔM is the percent weight gained through moisture absorption. With this data inserted into the FE model, the change in curvature due to moisture absorption was determined by calculating the curvature of the moist material.

To model the snap through, the load was applied in the middle of the plate which was supported on a rigid table. The FE curves were obtained for a plate in a dry state and

in a moistened state. The moisture content was considered to be 0.2%. Fig. 2.14 shows the variation of the applied load with the step time. The critical force was measured experimentally and compared with the ones found in the FE models as given in Table 2.2.

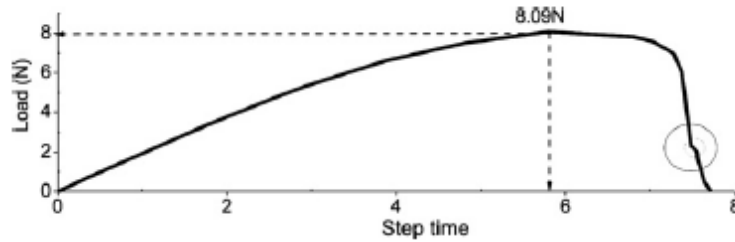


Figure 2.14: Applied force versus step time. Laminate is in the dry state [13]

	FE (N)	Measurement (N)	Error (%)
150 mm, [0/90], AS4	8.1	7.9	2.2
150 mm, [0/90], T800	2.9	2.4	20.4
200 mm, [0/90], T800	2.3	2.3	2.8
300 mm, [0/90], T800	3.0	3.1	2.3
120 mm, [0/45], T800	1.2	1.9	37.3

Table 2.2: Comparison of measured versus FE calculated critical loads [13]

The development of the FE models resulted in better understanding of the behaviour of the laminate with a thick piezoelectric patch bonded to its surface. The snap through loads correlated well with experimental results even when the environmental effects were included.

Tawfik et al. [14] investigated the stability of the cylindrical laminates. They reported the critical force required for the snap through behaviour and the critical aspect ratio where snap through will cease to occur. The motivation of their study was to formulate a methodology that handles the geometrical nonlinearity of this problem to be implemented in a commercial Finite Element Analysis (FEA) software like Abaqus. The

following methodology was used to obtain the cured shape and the snap through behaviour:

1. Set the boundary conditions by fixing the middle point of the panel.
2. A geometrically non-linear STATIC, STABILIZE procedure was used to model the curing shape of the imperfect laminate.
3. Reset the boundary conditions such that the corner points were restrained from movement in the z-direction while the middle point was restricted from movement in both x- and y-directions.
4. The cured shape obtained was subjected to a concentrated load, in the z-direction, at the middle point of the panel (Fig. 2.15(a)). The applied load was normally higher than the snap-through load, and hence the panel would deform past the other equilibrium position.
5. The applied load was removed in order to make sure that the laminate would retain a stable equilibrium position that was different from the one obtained at the end of the curing cycle.
6. Again a concentrated load at the middle point of the plate, was applied in the opposite direction (Fig. 2.15(b)). The applied load was selected such that the panel will deform past the original cured shape.
7. The applied load was removed, and the resulting curved shape of the plate was verified against the one obtained after curing.

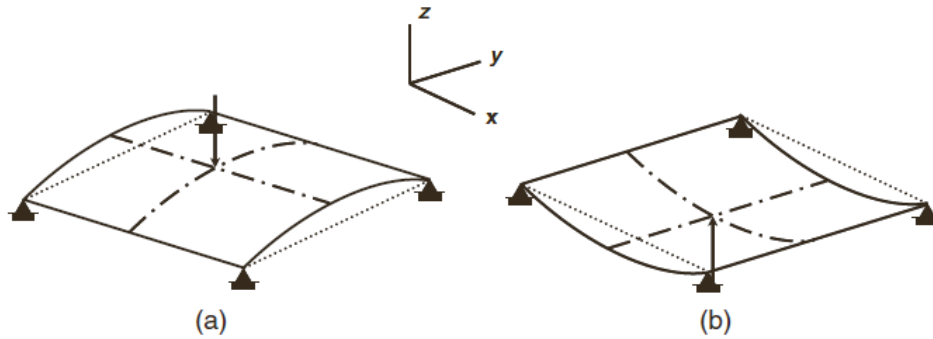


Figure 2.15: Applied load to attain snap-through [14]

The laminates were manufactured from T300/5208 graphite-epoxy. The obtained curvature of the cured shape, κ was calculated using the approximation,

$$\kappa = \frac{1}{R} = \frac{8d}{C^2 + 4d^2} \quad (2.5)$$

where R is the radius of the curvature, d is the out-of-plane deformation, and C is the side length. Fig. 2.16 shows a comparison of the Abaqus results with Hyer's [9] extended CLT and the experimentally measured curvatures from Hyer [15] for square laminates of various side lengths. Fig. 2.17 shows the P - δ curve extracted from Abaqus for a cross-ply unsymmetric 150 mm X 150 mm square laminate with $[0_2/90_2]_T$ stacking sequence. A point load of 2.55 N was needed for this square cylindrical panel to snap through.

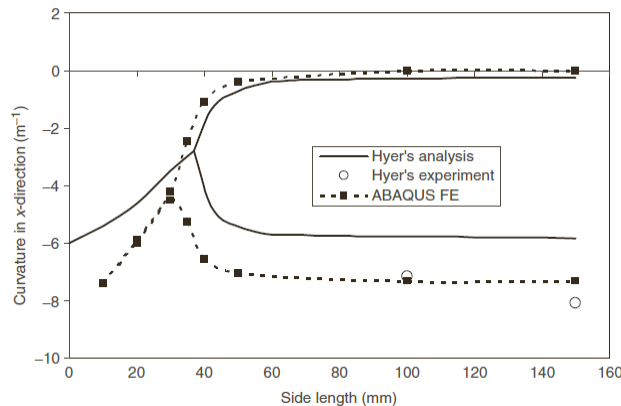


Figure 2.16: Room temperature shapes of square $[0_2/90_2]_T$ [14]

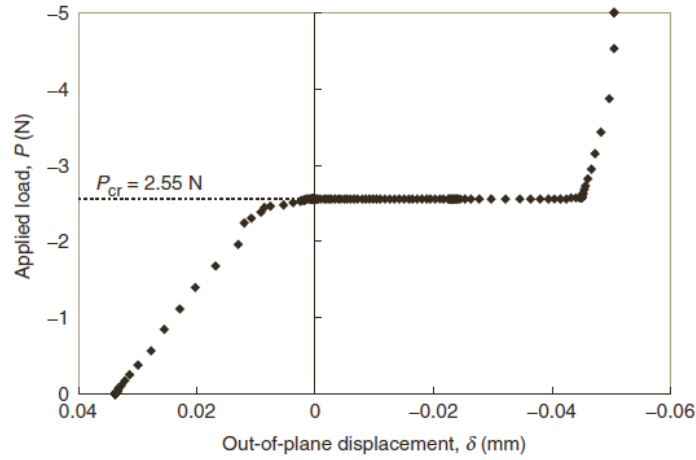


Figure 2.17: P- δ curve for a square 150 mm X 150 mm laminate [14]

Maintaining one side at 150 mm in length and changing the other side, the aspect ratio AR was varied from 1 to 8. As shown in Table 2.3, the trend of snap through load and snap back load with increasing AR was captured by the Abaqus predictions. The difference in the results could have been due to a number of reasons, such as modeling the boundary conditions or the applied loading.

Aspect ratio, AR	Snap-through load (N)			Snap-back load (N)		
	Experiment	ABAQUS [®]	% Difference	Experiment	ABAQUS [®]	% Difference
1.0	2.37	2.55	7.59	2.37	2.55	7.59
1.2	1.96	2.03	3.78	2.41	3.13	30.06
1.5	1.27	1.49	16.75	2.45	3.03	23.86
2.0	0.86	1.04	21.13	2.69	2.97	10.74
3.0	0.46	0.67	46.20	2.18	2.79	27.86
6.0	0.28	0.29	5.78	–	0.56	–
8.0	–	–	–	–	–	–

Table 2.3: Comparison between FE analysis and experimental results [14]

It was significant that tests of laminates with AR=8 did not snap through as predicted analytically. Thus, this work proposed an efficient methodology in order to predict the anticlastic behavior in composites using a commercial finite element code.

Mattioni et al. [16] developed a new methodology to overcome the problem of coaxing the numerical analysis to converge into one or the other branch of solution, as unsymmetric laminate bifurcates at a given value of temperature when they cool down. There are various strategies for dealing with this issue, in particular, for snap-through problems an explicit dynamic scheme (e.g. Abaqus/Explicit) is the most reliable because it accounts for the inertia effects but it can be very expensive from the computational point of view. For this reason, they employed a different strategy, based on modified static simulation in their methodology.

The laminate structure considered for analysis was a rectangular plate made of both symmetric and unsymmetric laminates; the stacking sequence is as shown in Fig. 2.18. T300/914 carbon fibre laminates were used for the analysis. The panel was modelled using 800 four nodes shell elements (S4R) in Abaqus. Equilibrium configurations were predicted with two separate analyses: a “*Static” step and a “*Static, stabilize” step.

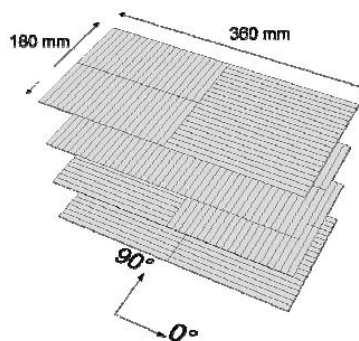


Figure 2.18: Stacking sequence for the bi-stable panel [16]

Using the “*Static” analysis, the solution always converged to the first equilibrium shape and “negative eigenvalue warnings” were issued by the solver. To

capture the second equilibrium shape, a separate analysis made use of the “stabilize” option. An alternative way to obtain the second equilibrium shape was loading one of the two computed equilibrium configurations with a concentrated force. The structure will first deform elastically, then if the force is large enough, it will bifurcate. This procedure required attention in the choice of the load and the boundary conditions, but provided the full load-displacement diagram that characterises the extreme non-linear behavior of the structure.

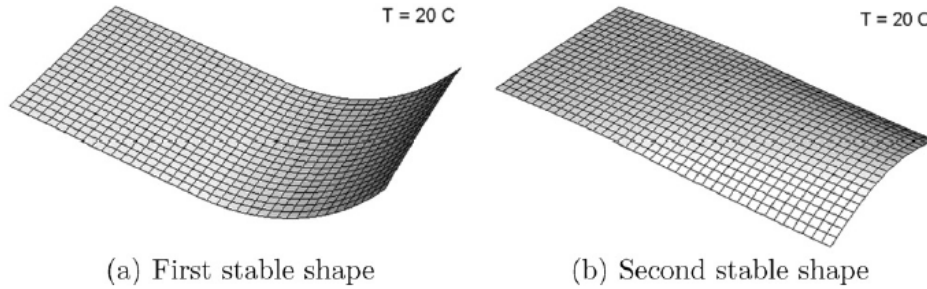


Figure 2.19: Numerical equilibrium shapes [16]

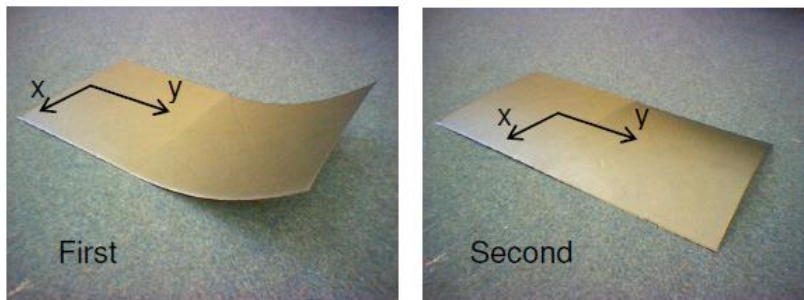


Figure 2.20: Equilibrium configurations [16]

The predicted equilibrium configurations at room temperature (Fig. 2.19), show good agreement with the experimental shapes shown in Fig. 2.20. The aim of this analysis was to compute the maximum out-of-plane load that the panel can withstand before changing configuration.

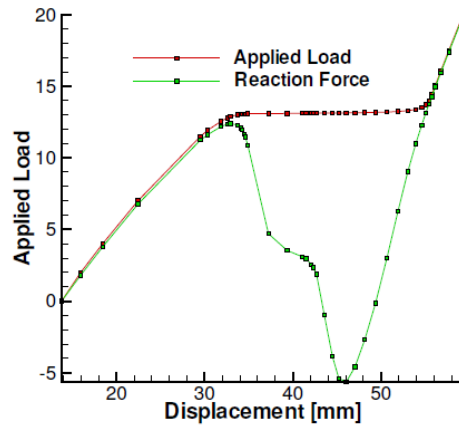


Figure 2.21: Stabilized load-displacement diagrams versus reaction forces [16]

Fig. 2.21 shows a comparison between the applied load and the sum of the reaction forces at the four corner nodes. The two curves were identical till the limit load is reached, after which the structure becomes unstable and while the red curve continues horizontally due to stabilisation, the green one follows the unstable equilibrium path. Eventually the curves met again in the new stable portion of the diagram. This methodology is computationally effective and produces similar results and converges to the same shape as the explicit dynamic analysis.

Mattioni et al. [17] modelled the non-linear out of plane displacements of partially unsymmetric laminates using both finite element analysis and an analytical method. They extended the previous analytical models to account for boundary conditions different from the free-free type so far used, as it was essential to study the interactions of bistable structures as components of larger structures and this was also required to model different geometries with analytical techniques. To model boundary conditions that are not simply free edges, the hypothesis of constant curvature had to be removed, since it was too restrictive. To allow the curvature to vary across the domain, a fourth order displacement

function was chosen as a basis to extend the model. The previous approximation function chosen by Dano & Hyer [18], which assumed the curvature to be constant throughout the domain was,

$$w(x, y) = -\frac{1}{2}(w_{20}x^2 + w_{02}y^2 + w_{11}xy) \quad (2.6)$$

where w_{20} , w_{02} & w_{11} are unknown coefficients which represent, respectively, the negative of the curvatures in the x and y directions and the negative of the twist curvature,

$$w_{20} = -\frac{\partial^2 w^0}{\partial x^2}; w_{02} = -\frac{\partial^2 w^0}{\partial y^2}; w_{11} = -2\frac{\partial^2 w^0}{\partial x \partial y} \quad (2.7)$$

The out of plane displacement function chosen by Mattioni et al, is the result of the product of two parabolas along the principal directions,

$$w(x, y) = P(x).G(y) \quad (2.8)$$

$$P(x) = p_0 + p_1x + p_2x^2 \quad (2.9)$$

$$G(y) = g_0 + g_1y + g_2y^2$$

To simplify the computation of derivatives and integrals, this expression is rearranged as,

$$w(x, y) = w_{00} + w_{10}x + w_{01}y + w_{20}x^2 + w_{02}y^2 + w_{11}xy + w_{12}xy^2 + w_{21}x^2y + w_{22}x^2y^2 \quad (2.10)$$

Within this notation, the first subscript refers to the order of the x -variable while the second one refers to the order of the y -variable. First they applied this modified model to a square plate before applying it to more complex type of structures. The total potential energy was assembled and minimized with the help of the software Maple 9.5, and the

results were compared to Hyer's model and FEA. The modified model predicted a quadratic curvature while the Hyer's model had a constant value throughout the domain.

Once the approach proved to be effective with the results of square laminates, the theory was applied for panels with piecewise variation of the laminate in planform. The same stacking sequence of the bistable panel from Mattioni et al [16] with symmetric layup $[0_2/90_2]_S$ on the left hand side of the plate and unsymmetric layup $[0_4/90_4]_T$ on the right hand side of the plate was used for this analysis.

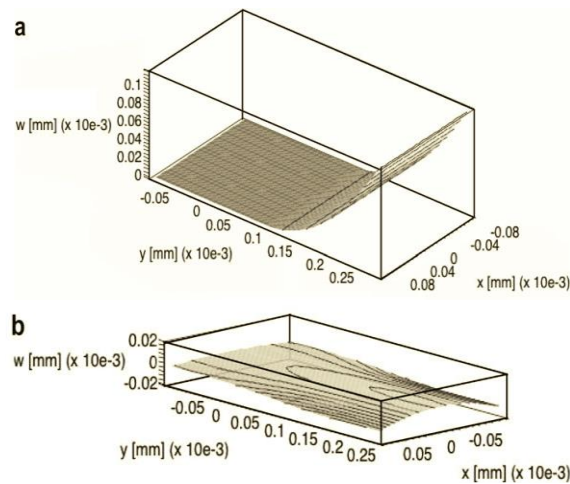


Figure 2.22: Equilibrium shapes obtained with the analytical model (a) 1st equilibrium shape (b) 2nd equilibrium shape [17]

The analytical model successfully captured the behaviour of bistable structure as shown in Fig. 2.22. Also they pointed out, their entire analysis is on macroscopic / laminate level and to understand the behaviour at ply / lamina level, a different approach needs to be taken. As the fibre and matrix continuity at ply level can only be obtained for those layers with fibres at 0° (i.e., parallel to the y-axis), for those layers at 90° , such continuity relies entirely on the matrix since the fibres are parallel to the boundary. Hence

for engineering modelling purposes, the assumption of structural continuity at laminate level was considered acceptable.

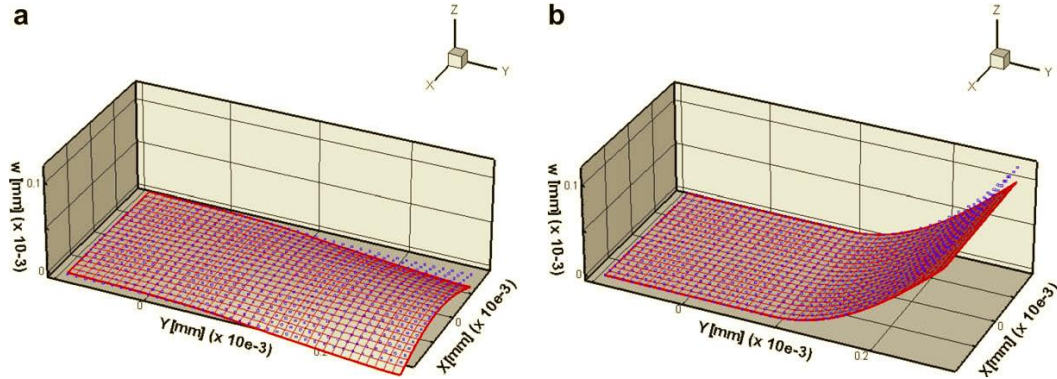


Figure 2.23: Analytical vs FE shape for the 4-layer plate (a) flat configuration (b) curled configuration [17]

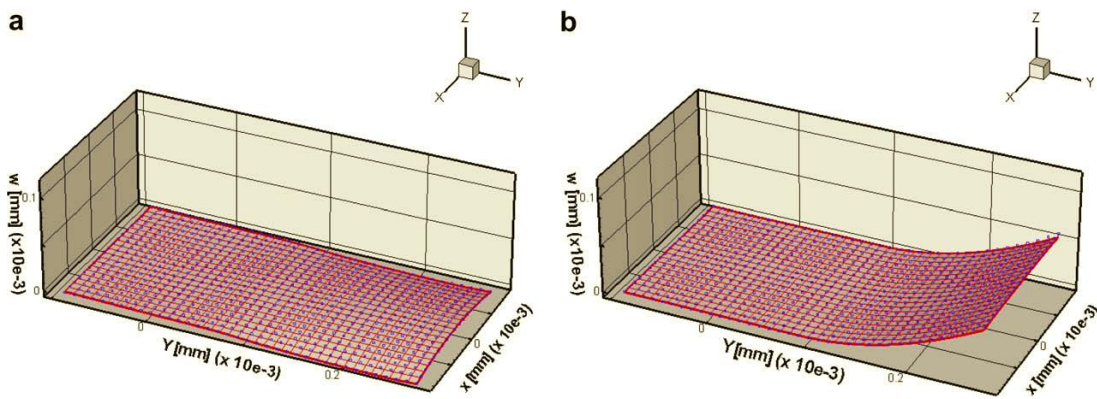


Figure 2.24: Analytical vs FE shape for the 8-layer plate (a) flat configuration (b) curled configuration [17]

In Fig. 2.23 & 2.24, the markers represent the analytical data and the mesh represents the FEA results. The analytical model, because of its reduced number of degrees of freedom, is in a sense stiffer and therefore it better captured the reduced displacements of the 8-layered panel compared to 4-layered panel. Also comparison with experimental data, showed that FEA is also stiffer due to the mesh size selected to get a compromise between accuracy and computational efficiency.

Tawfik et al. [19] examined the bistable characteristics with focus on the change in geometry for a subset of configurations, namely, rectangular, trapezoidal and triangular using both FEA and Experimental Validation. These geometries were systematically investigated leading to a set of non-dimensional parameters establishing the values required for bistable behavior. The experimental setup included a number of components: air bearings, pin supports, air compressor, air filters, and load cell. The selection of these components was made based on the compressed air source quality and load requirements to trigger snap through behavior in the tested panel. A schematic of the load measurement apparatus used by them is provided in Fig. 2.25.

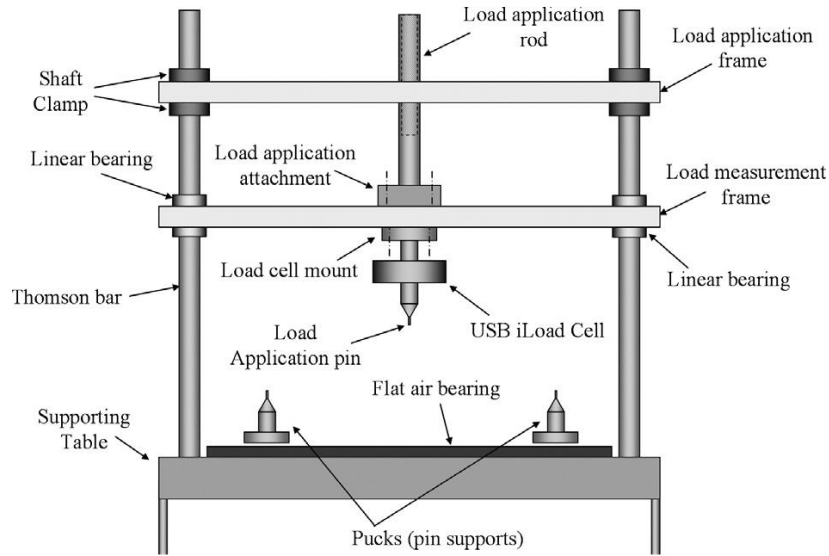


Figure 2.25: Load measurement apparatus [19]

All panels were manufactured from Hexcel IM7/8551-7 Graphite/Epoxy prepreg with stacking sequence $[0_2/90_2]_T$ resulting in a total nominal thickness of $555 \mu\text{m}$. The boundary conditions applied for the six different geometries are as shown in Fig. 2.26. Within the square specimen group, the side length of the square was decreased from 150 mm to 50 mm in steps of 25 mm. Within the rectangular specimen group, the length was

held constant at 150 mm and the width was decreased. Within the trapezoidal-A specimen group, the lower base and the height of the trapezoid were held constant at 150 mm, and the top base was decreased. Within the trapezoidal-B specimen group, the lower base was held constant at 150 mm, the top base was held constant at 25 mm and the height was decreased. Within the triangular-A specimen group, the height of the triangle was held constant at 150 mm and the base was decreased. Within the triangular-B specimen group, the base was held constant at 150 mm and the height was decreased.

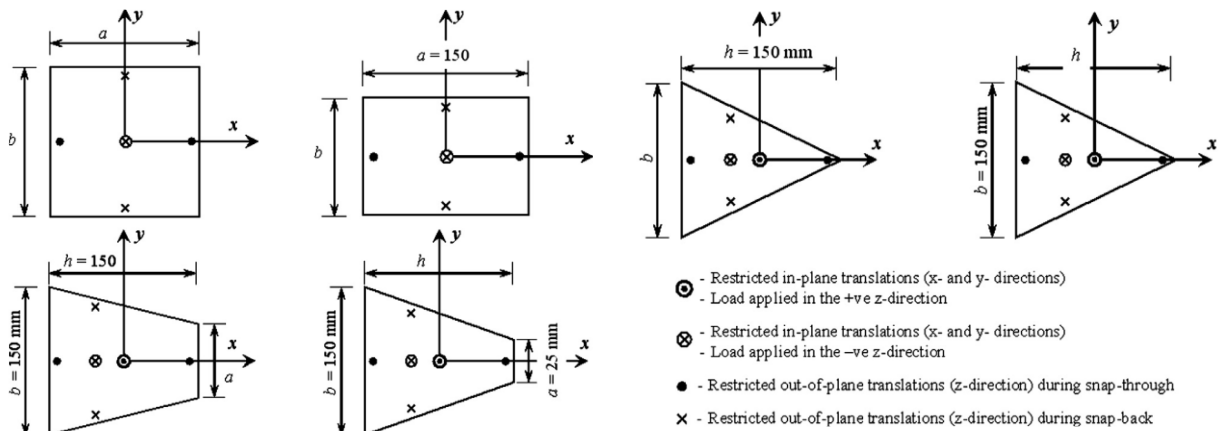


Figure 2.26: Boundary conditions of straight edge specimens [19]

The non-dimensional force, P^* ($P^* = P_i / P_{\text{Square} \#1}$), as a function of the sidelength, L^* of a square can be described by a monotonically decreasing quadratic expression as illustrated in Fig. 2.27. This monotonically decreasing quadratic trend, associated to both snap-through and snap-back, had been referred to as the “shape scaling effect”. Non-dimensional loads, P^* , at corresponding non-dimensional width, b^* , of a rectangle are provided in Fig. 2.28. The critical loads show 30–40% increase reaching a peak at b^* close to 200 before rapidly decreasing, this phenomenon was termed as “transverse-side stiffening effect”. Non-dimensional loads, P^* , at corresponding non-dimensional base b^*

of triangular-A specimens and non-dimensional height h^* of triangular-B specimens are provided in Fig. 2.29 for snap-through and snap-back. The analytical predictions were in agreement with test data for both snap-through and snap-back cases.

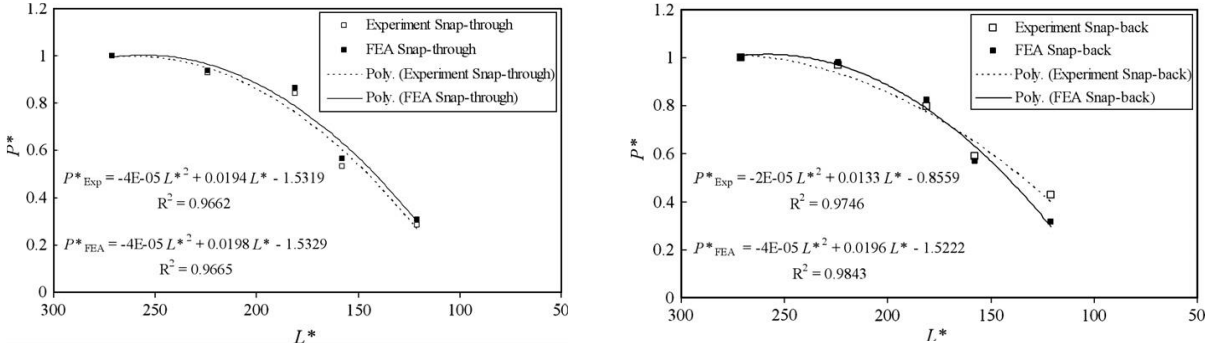


Figure 2.27: Non-dimensional snap-through and snap-back results for square specimens [19]

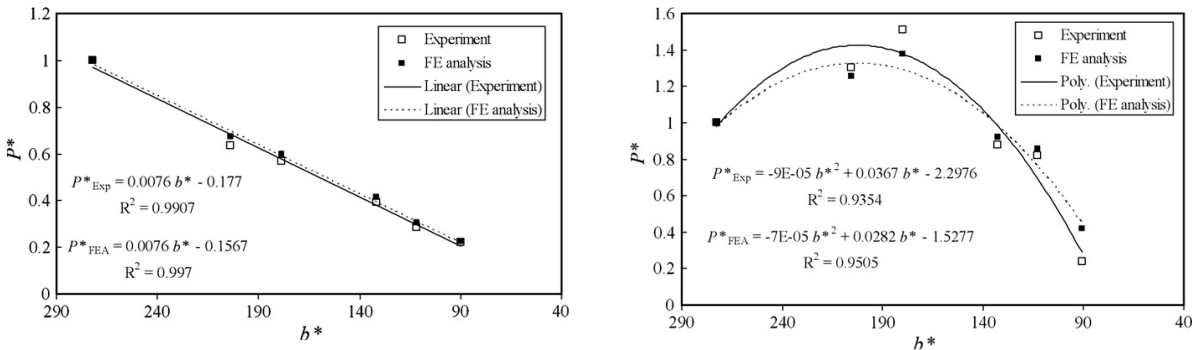


Figure 2.28: Non-dimensional snap-through and snap-back results for rectangular specimens [19]

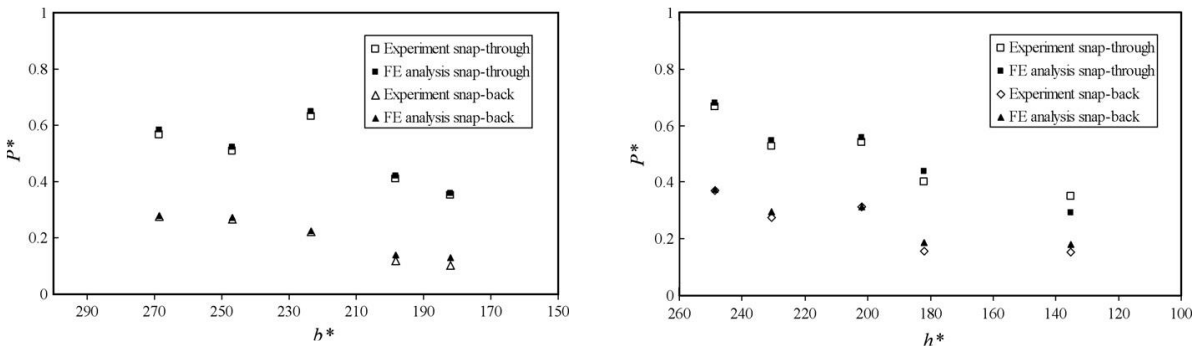


Figure 2.29: Non-dimensional snap-through/back results of the triangular-A and -B group [19]

The apparatus and test minimized friction effects via an air cushion design. The developed Abaqus finite element methodology predictions were in agreement with the test data. The effect of changing one shape parameter at a time was investigated and stability trends were obtained for snap-through and snap-back.

Variations in Composite Structure

Potter et al. [20] showed that the number of stable geometries can be controlled by the details of the lay-up from the minimum of two to, in principle, an unlimited number. They presented a very preliminary experimental investigation of the design space available for such composite laminates. They tested a 4-ply laminate made up of the lay-up as shown in Fig. 2.30, where W and L_1 were both 240 mm and L_2 was 120 mm. The prepreg used was AS4/8552 from Hexcel and had a nominal cured ply thickness of 0.25 mm.

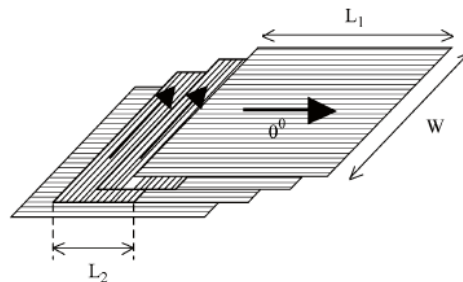


Figure 2.30: Lay-up of a 4-ply laminate [20]

At any point on the laminate, the lay-up is symmetrical about the center plane of the lay-up. As cured the laminate exhibited two stable states with a snap-through between them. The two states had the form of a simple bowing in the width direction as shown in

Fig. 2.31. As L_2 was continuously reduced, the shape kept changing from simple bow to twisted and compound bow as shown in Fig. 2.32.

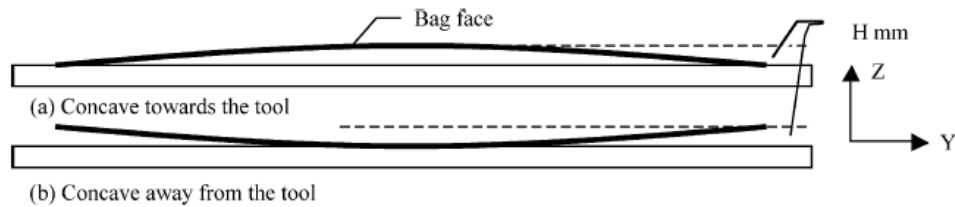


Figure 2.31: As cured curvatures exhibited by laminate (approx. to scale) [20]

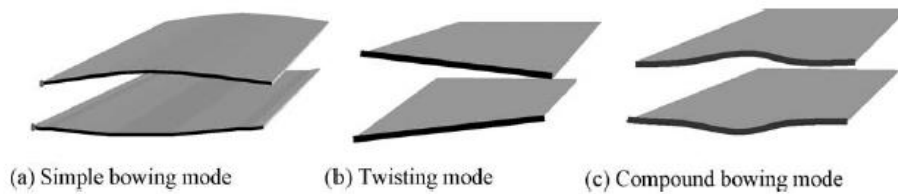


Figure 2.32: Schematic geometry of the three different deformation modes [20]

When they tested multiple strips of transverse material in more than one direction, made from a thinner prepreg of 0.125 mm nominal thickness, they obtained multiple stable states. The layup of central plies & results obtained are as shown in Fig. 2.33.

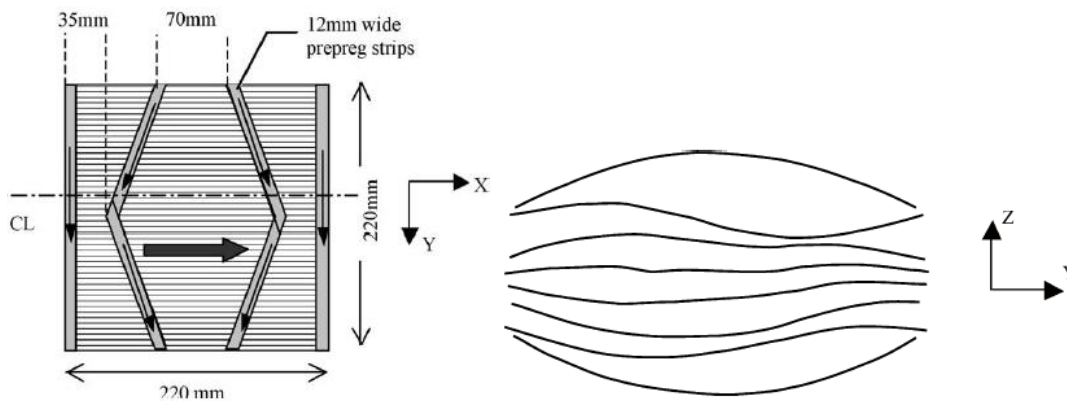


Figure 2.33: Construction of 2 central plies & Edge profiles showing multiple stable states [20]

When they tested multiple discrete strips of transverse material applied in an array of local reinforcements as shown in Fig. 2.34, they obtained an array of surface dimples

corresponding to the discrete strips of transverse material. Each surface dimple exhibited a snap-through into a second state. However, none of the second states were truly stable, in each case requiring a small load to maintain it in that state.

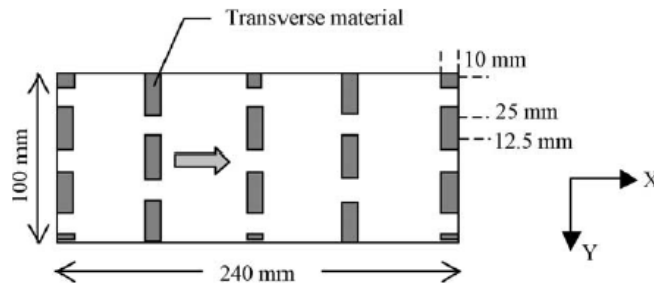


Figure 2.34: Layup of laminate with an array of multiple discrete transverse strips [20]

Clearly, a large number of design freedoms were available such as the relative proportion of the plan area, width, material, direction, shape and ply count of the constraining material. Additional design freedoms were obtained by manipulating the residual stress levels in the main unidirectional reinforcement and by allowing some or all of the constraining material to be arranged unsymmetrically with respect to the mid-plane of the laminate. Thicker plates do not suit well for these cases and also the material & manufacturing variability should be kept within limits to achieve all these possible states. Lastly, since these kinds of laminates were symmetric & balanced about the mid plane of the laminate, and they still exhibited bistable features, these classes of composites were termed separately as “Locally Asymmetric Plates or Shells”.

Daynes & Weaver [21] studied unsymmetric laminates which had an inner isotropic metallic layer. They found that the curvatures of the hybrid laminates can be doubled compared to pure unsymmetric CFRP (Carbon Fibre Reinforced Plastic) laminates. In this work they had calculated the hybrid laminate out-of-plane deformations

by minimizing the potential energy of the extended stress-displacement relations in combination with the Rayleigh-Ritz method. The shear interaction due to thermal expansion mismatches between the prepreg plies and metal layer prior to curing was included in the analytical techniques and shown to be significant. The Hexcel 8552/IM7 CFRP prepreg with both steel and aluminum inner layers were studied. Slippage effects were modelled by the modification of the coefficient of thermal expansion from α_i to $\bar{\alpha}_i$ as per the following equation,

$$\bar{\alpha} = \begin{cases} \mu \varepsilon_m^{cure} / 2\Delta T & (k = f) \\ \varepsilon_m^{cure} / 2\Delta T & (k = m) \\ \alpha_{22} & (k = r) \end{cases} \quad (2.11)$$

where f, m and r are fibre direction, metal layer and transverse respectively, k is the ply, μ is the slip coefficient, ε_m^{cure} is the mid-plane strains at cure in the metal layer. A quarter of the laminate was modelled due to the double symmetry. The laminate selected for the convergence study in FE program had dimensions 200 X 200 X 1 mm, a 0.25 mm steel inner layer and a $[0_3/St/90_3]_T$ layup. By gradually decreasing the plan-form area of the FE models it was possible to both assess the effect of plan-form area on snap through loads and to find the critical edge length at which a laminate was no longer bistable. Five 200 X 200 X 1 mm laminates were manufactured with layups $[0_3/Al/90_3]_T$ (0.25 mm Aluminum), $[0_2/Al/90_2]_T$ (0.50 mm Aluminum), $[0_3/St/90_3]_T$ (0.25 mm Steel), $[0_2/St/90_2]_T$ (0.50 mm Steel) and $[0_4/90_4]_T$ as shown in Fig. 2.35. Data from analytical expressions and FE models for curvature vs. edge length for the five manufactured laminates are as shown in Fig. 2.36.

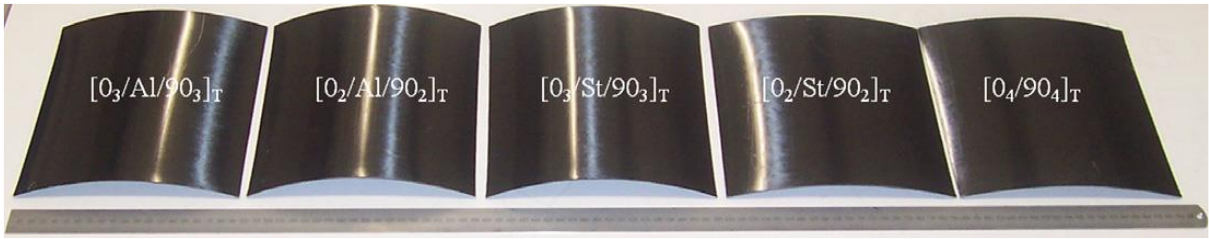


Figure 2.35: Manufactured laminates [21]

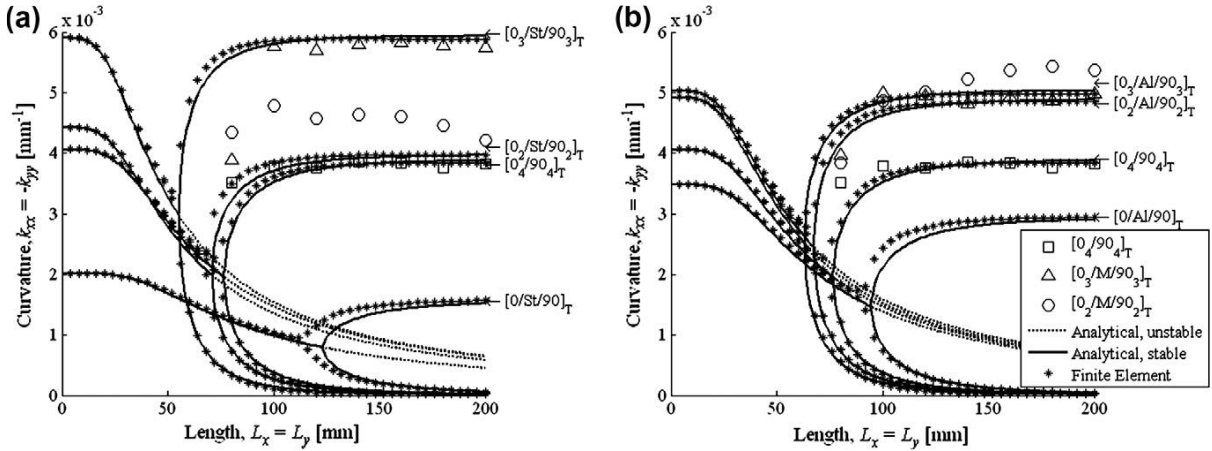


Figure 2.36: Bifurcation diagrams for (a) steel laminates, $\mu=0.2$, and (b) aluminum laminates, $\mu=0.5$ [21]

A steel layer thickness of 0.25 mm increased the curvatures of the laminate by 51% compared to the $[0_4/90_4]_T$ laminate. The best aluminium thickness was 0.50 mm which increased the curvatures by 41% compared to the $[0_4/90_4]_T$ laminate. The $[0_3/St/90_3]_T$ laminate had the largest snap through energy of all the manufactured samples. Increased metal–fibre slippage prior to cure, resulted in increased stable curvatures and snap-through energies. They proposed that the residual stress fields which occur during the manufacture of multi-layered fibre reinforced hybrid composites can be used to design hybridized unsymmetric laminates with controlled deformation states and curvatures.

Application of Bistable Composites

Mattioni et al. [22] have used the increased transverse curvature of the spar obtained from using a shell structure laminated with unsymmetric stack sequence in the variable sweep wings application. The effect of this increased curvature was twofold: to increase the moment of inertia to withstand bending stresses and, under certain loading conditions, to behave like an elastic hinge to allow the sweep angle of the wing to change. The variable sweep wing structure proposed by them, consists of two spars with an interconnected truss-rib structure as shown in Fig. 2.37. The particular choice of the truss-ribs was due to the kinematics of the structure, where the ribs must not constrain the spars during the sweeping. The magnitude of the load to induce bifurcation in the structure and the radius r of the folded region, depends mainly on the material properties and the transverse curvature of the shell.

$$M_y = \frac{D_{22}}{R} \quad (2.12)$$

$$r = \sqrt{\frac{D_{11}^*}{D_{22}^*}} R \quad (2.13)$$

where D_{22} is a component of the flexural matrix, M_y is the moment that has to be applied to a flat plate to produce the curvature $k_y = 1/R$, D_{ii}^* are the components of the reduced flexural matrix of the laminate, R and r are the undeformed transverse curvature radius and the deformed longitudinal curvature radius of the shell respectively as shown in Fig. 2.38.

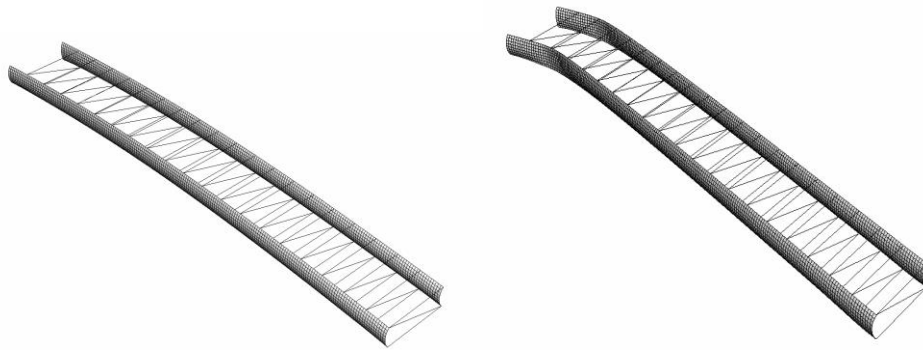


Figure 2.37: Variable wing sweep structure idealization & swept configuration [22]

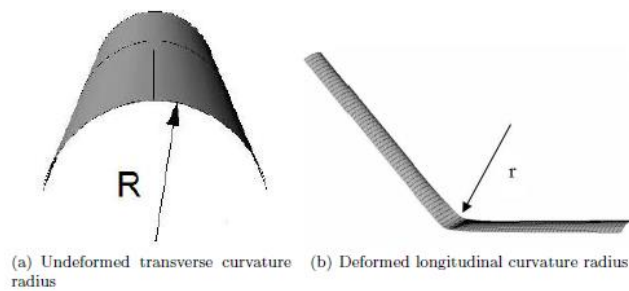


Figure 2.38: Geometric characteristics of the shell [22]

The stacking sequence was as shown in Fig. 2.39. The green area (the web) consists of an unsymmetric laminate $[0^\circ/90^\circ]_T$ while the red area (the spar-caps) had the same base laminate $[0^\circ/90^\circ]_T$ plus a reinforcement of five layers of 0° unidirectional fibres.

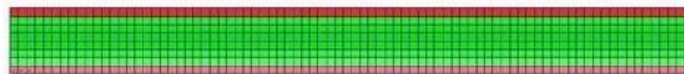


Figure 2.39: Stacking sequence regions for the spar structure [22]

To model the spar structure ‘S4R’ shell elements were used, while for the truss-rib structure ‘T3D2’ rod elements were chosen. The spar was manufactured using

unidirectional prepreg carbon fibres, cured on an aluminum tool with a curvature radius of 53.5 mm and a length of 1000 mm. Loads and boundary conditions were as shown in Fig. 2.40. The spar successfully snapped from the straight to the swept back configuration under its own weight plus an additional load of 5 N at 220 mm from the root section.

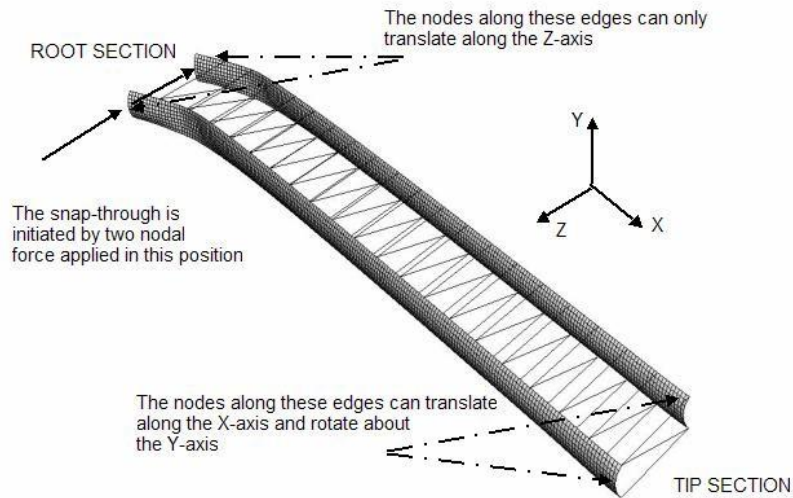


Figure 2.40: Boundary conditions [22]

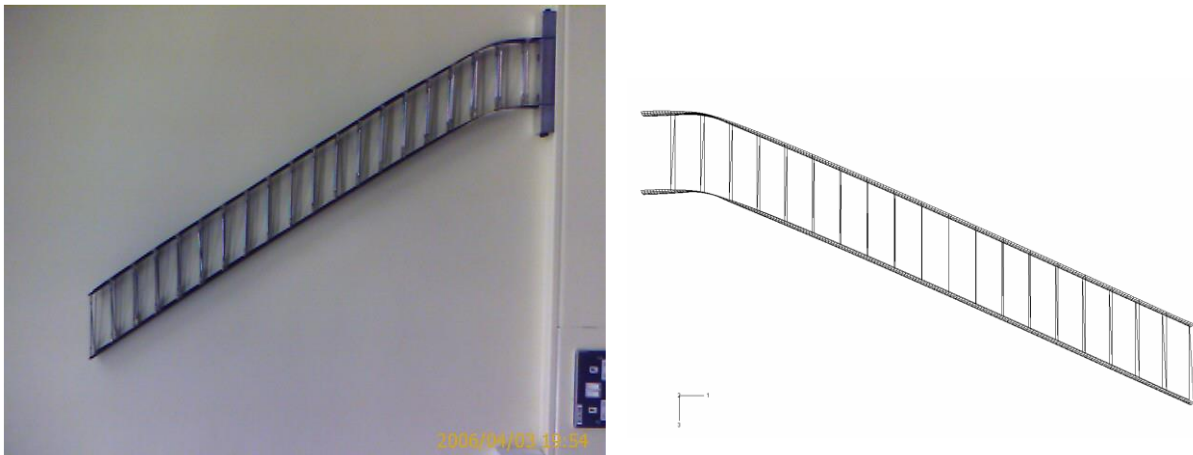


Figure 2.41: Swept configuration: Experimental & FE model [22]

Experimental & FE results showed good agreement as seen in Fig. 2.41. Thus the possibility of tailoring the deformations caused by residual stress fields in unsymmetric laminates, was considered as a way to add morphing capabilities to the structure.

Diaconu et al. [18] investigated the potential of using bistable laminated composite structures for morphing an airfoil section. They evaluated the magnitude of loads required to actuate the airfoil section between the stable shapes. NACA 23012 airfoil as shown in Fig. 2.42 with two stiffening spars and a chord of 680 mm was taken as the sample structure for analysis. As the structure to be morphed was relatively flexible, aerodynamic pressure on it would require a detailed aeroelastic analysis and hence was ignored in their study. Abaqus was used for the finite element analysis and they used the bistable laminated composite made of graphite/epoxy with a lamina thickness of 0.125 mm.

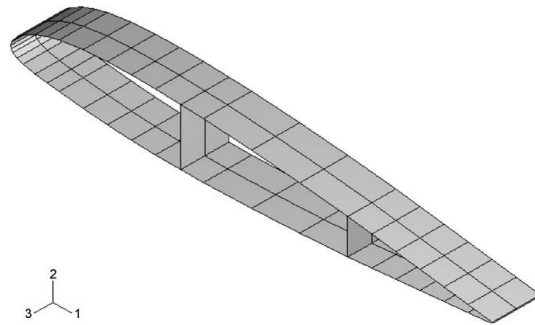


Figure 2.42: NACA 23012 airfoil [23]

For morphing the airfoil section, attention was paid to changing the camber of the airfoil section and to changing the length of its chord. The camber change for the airfoil section was realised by inserting a square bistable composite plate of dimensions 234 X 234 mm in horizontal position along its chord as shown in Fig. 2.43.

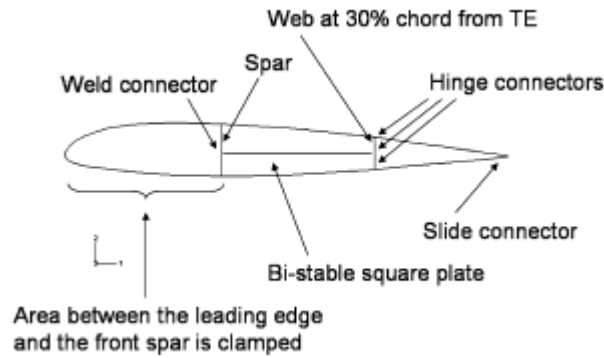


Figure 2.43: Assembly for camber change [23]



Figure 2.44: Lateral view of the stable shapes for camber change of airfoil section [23]

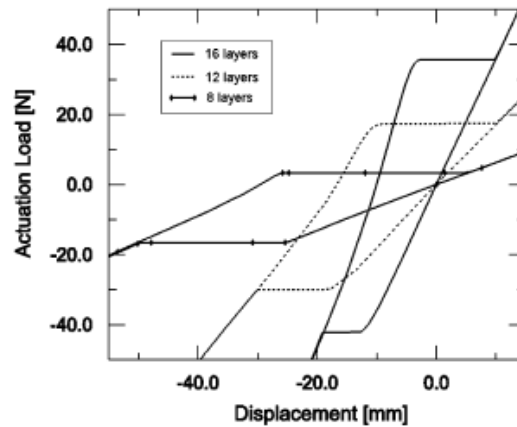


Figure 2.45: Loads relationship with displacements at actuation points [23]

For the bistable part, three unsymmetric cross-ply laminate configurations, $[90_4/0_4]_T$, $[90_6/0_6]_T$, and $[90_8/0_8]_T$, were chosen. The two stable shapes are as shown in Fig. 2.44 for the $[90_8/0_8]_T$ configuration. The first stable shape was the original airfoil with the bistable plate inserted along the chord. The second stable shape had the top and bottom skins bent above and below the bistable plate and the web behind the bistable plate slightly moved from its original vertical position. Fig. 2.45 shows the relationship

between the actuation loads and the vertical displacements for the two corners of the bistable plate obtained from FEA for each of the three laminate configurations.

The chord length change for the airfoil section was realized by inserting a rectangular bi-stable plate into the airfoil section in vertical position along its main spar as shown in Fig. 2.46. The bistable plate had the length $L = 300$ mm, the width $W = 70$ mm and was connected at its corners to the spar.

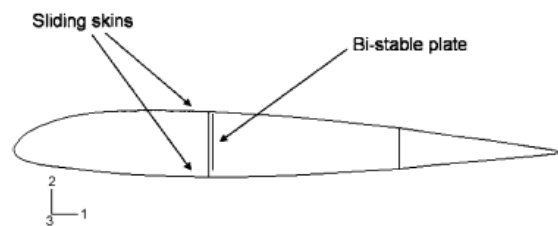


Figure 2.46: Assembly for chord length change [23]

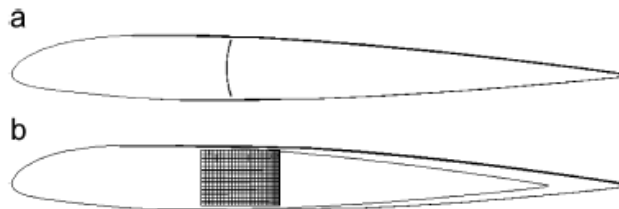
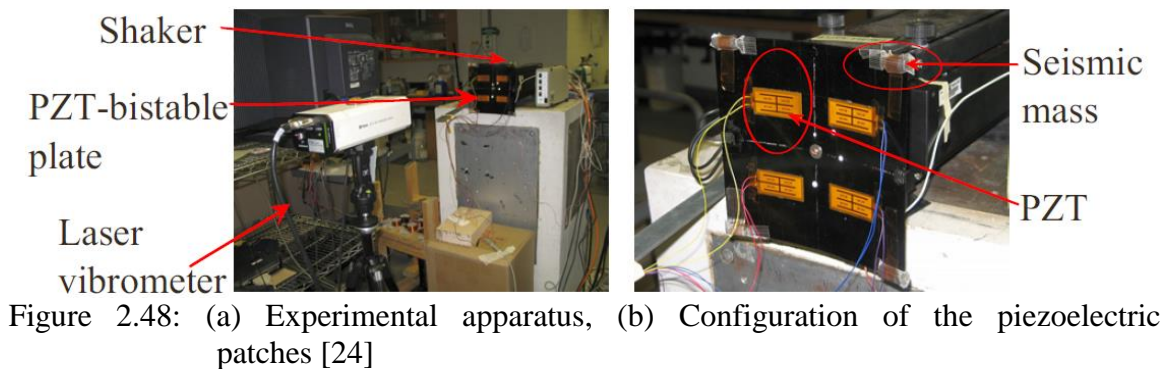


Figure 2.47: Lateral view for chord length change (a) 1st stable shape (b) 2nd stable shape [23]

Two cross-ply unsymmetric laminate configurations, $[90_2/0_2]_T$ and $[90_3/0_3]_T$ were considered for the bistable plate. The two stable shapes of the structure are shown for the $[90_2/0_2]_T$ configuration in Fig. 2.47. The increase in chord length is clearly seen in the second stable shape and also the bistable plate had a new role, it acted as an internal stiffener for the airfoil section because half of its fibres were perpendicular to the chord and in the direction of the aerodynamic forces. However this method was regarded to be aerodynamically less efficient than changing the camber of the airfoil. Overall, the

morphing function would increase aerodynamic performance and these methods showed sufficient merit that the next stage of design can be addressed.

Arrieta et al. [24] proposed to exploit the rich nonlinear behaviour of a bistable composite plate with bonded piezoelectric patches for broadband nonlinear energy harvesting. The piezoelectric bistable composite plates does not require strong external magnets which may be obtrusive for the powered electrical components, as well as for the circuitry of harvester itself. Furthermore, in the absence of magnets bistable plates can be designed to occupy smaller volumes than bistable cantilevers. A $[90_2/0_2]_T$ 200 X 200 mm carbon fibre epoxy bistable composite plate with seismic masses attached to each corner to obtain a more flexible structure was employed as experimental specimen. The plate was mounted from its center to an electromechanical shaker, as shown in Fig. 2.48(a). Four PZT-5A flexible piezoelectric patches were bonded to the surface of the bistable plate using a high shear strain epoxy, as shown in Fig. 2.48(b).



The dynamic response of the plate as shown in Fig. 2.49 was first studied confined to each stable state using frequency response functions (FRF) for a very low forcing amplitude of 0.05g to minimize nonlinear effects. Two modes had been observed

on each stable state, ω_1^{s1} and ω_2^{s1} at 10.9 and 15.8 Hz for stable state 1, and ω_1^{s2} and ω_2^{s2} at 9.4 and 12.9 Hz for stable state 2. For a linear response, a single amplitude value was sampled for consecutive periods for a given forcing frequency. Conversely several points for a given frequency indicated the presence of multiple harmonics in the response signalling nonlinear oscillations.

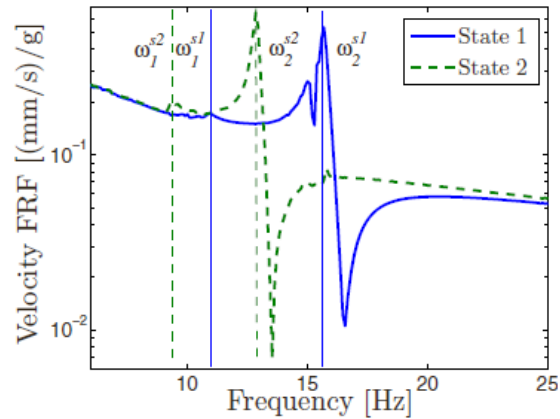


Figure 2.49: Experimental velocity-to-base acceleration FRFs for small oscillations around state 1 & 2 [24]

Frequency response diagrams for velocity and piezoelectric voltage with initial condition at stable state 2 stepping up the frequency from 6 Hz for a forcing amplitude of 2g are shown in Fig. 2.50. Subharmonic oscillations were confined to a stable state, whereas chaotic and large amplitude LCO for this configuration and control parameters involved snap-through between stable states.

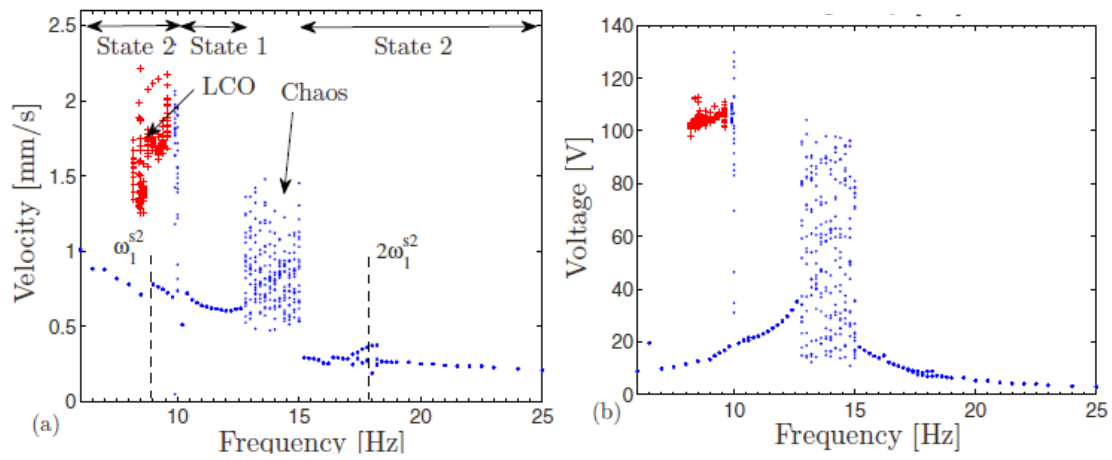


Figure 2.50: Experimental frequency response diagrams with initial condition at state 2 for a forcing level of 2g and forward sweep. Peak –to-peak (a) velocity (b) piezoelectric voltage [24]

Fig. 2.51 presents the average power as a function of the forcing frequency for oscillations with initial condition at stable state 2 for a load of 98.5 k Ω . Even for this non-optimal load, large average power is harvested over a wide range of frequencies showing the broadband characteristic of the proposed device.

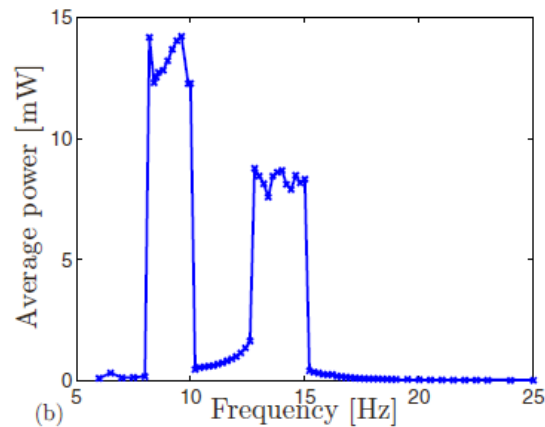


Figure 2.51: Average power vs forcing frequency, load resistance 98.5 k Ω [24]

Optimization of Bistable Composites

Hufenbach et al. [25] developed a genetic algorithm in combination with a nonlinear calculation method which can purposefully adapt the laminate lay-up, depending on the loading and process parameters. To begin with the optimization problem to realize a defined laminate curvature, the fitness function considered was a multimodal function. It was not given in a closed analytical form due to the application of a numerical energy principle. Thus, the conventional optimization methods, like the gradient method were not suitable for finding an optimum, because either the derivatives of the function were missing or the methods were likely to get stuck in a local optimum. For the best adjustment of the residual stresses, the genetic algorithms offered special advantages and allowed one to find the optimal combination of the fibre/matrix combination, number of layers, layer orientation, and hygrothermal process and load conditions. The method had been successfully verified on unsymmetric glass fibre (GFRP) & carbon fibre (CFRP) reinforced plastics. The theory applied was based on the principle of total minimum potential energy, which is given by

$$\Pi = \int_V \left(\frac{1}{2} \bar{Q}_{ij} \varepsilon_i \varepsilon_j - \eta_{T_i} \varepsilon_i \Delta T - \eta_{M_i} \varepsilon_i \Delta M - \eta_{S_i} \varepsilon_i \right) dV \quad (2.14)$$

where \bar{Q}_{ij} are the reduced transformed stiffnesses with $i, j = 1, 2, 6$, ΔT & ΔM are the differences in temperature and relative media concentration, and η_{T_i} , η_{M_i} and η_{S_i} are related to the thermal-expansion coefficients α_j , swelling coefficients β_j and shrinkage coefficients s_j respectively. The GFRP composite had a higher curvature than the CFRP laminate. But no general statement about the curvature magnitudes for laminates made of

different materials had been given because of the significant influence of many different material parameters. These algorithms were applied to determine the optimum laminate lay-up either in order to maximize the laminate curvature or to adjust the curvature to the defined limits, by changing the number of layers, layer thickness, layer orientation, layer material, fibre volume content, laminate size, and process parameters. It was found that, depending on the laminate material, the maximum curvature had to be realized by different lay-ups.

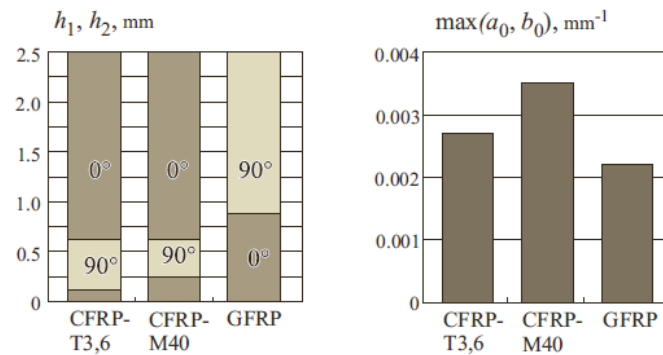


Figure 2.52: Lay-up of CFRP and GFRP cross-ply laminates with 0° and 90° layer orientation resulting in maximum curvatures [25]

The left bar graph in Figure 2.52 shows the optimum single-layer thicknesses h_1 and h_2 and the layer arrangement in the investigated composites with a global height of 2.5 mm. Furthermore, it was observed that, regardless of the global height of the laminates, the ratios of the single-layer thicknesses which result in the maximum curvature were the same. So, once the optimum lay-up ratio is found for a special material, it can be transferred to any laminate of the same material with a varying total thickness. This approach can be utilised for near net-shape technology and also the added benefit is, it helps to reduce the production costs by replacing complex-shaped tools by plane ones.

Hufenbach and Gude [26] developed a dimensioning tool consisting of an advanced stability and failure analysis in combination with a novel optimisation procedure in order to adjust the deformations of unsymmetric laminates to technical requirements. The different states of stability due to residual stresses in a cross-ply laminate $[0/90]$ of dimension $300 \times 300 \times 1$ mm was considered for the optimization problem. Starting from a purely 0° Unidirectional (UD) laminate (ratio $h_1/h = 0$, h_1 is height of 90° layer and h is the total height), which is plane, firstly a monostable cylindrical shape occurred as soon as the thickness of the 90° layer increases as shown in Fig. 2.53. For small ratios, also a second unstable state was calculated. The associated unstable equilibrium state turns into a stable equilibrium for a thickness ratio $h_1/h = 0.3$. For a ratio between 0.3 and 0.7, two stable cylindrical shapes with generally different curvatures existed.

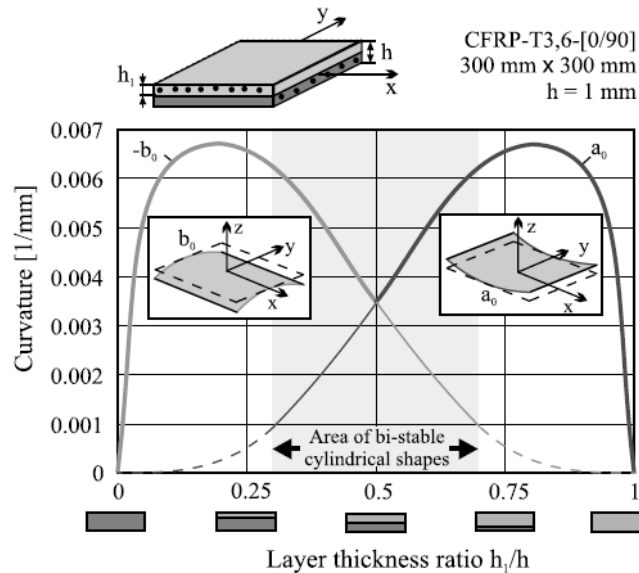


Figure 2.53: Curvatures of a CFRP laminate with variable layer ratio [26]

The realistic description of the failure of the UD-layer, which is the basic element of technical composites, is of special interest for the structural design of composite structures. For this type of laminate, it had to be distinguished between the basic failure modes, fibre failure (FF) and inter-fibre failure (IFF), with its sub-modes tensile, compressive and shear failure. Each of these modes were assigned one strength coefficient as shown in Fig. 2.54. Physically based failure mode concept (FMC) was applied, as it features an easier mathematical formulation using invariants. The invariants were given by,

$$\begin{aligned}
 I_1 &= \sigma_1 \\
 I_2 &= \sigma_2 + \sigma_3 \\
 I_3 &= \tau_{31}^2 + \tau_{21}^2 \\
 I_4 &= (\sigma_2 - \sigma_3)^2 + 4\tau_{23}^2 \\
 I_5 &= (\sigma_2 - \sigma_3)(\tau_{31}^2 - \tau_{21}^2) - 4\tau_{23}\tau_{31}\tau_{21}
 \end{aligned} \tag{2.15}$$

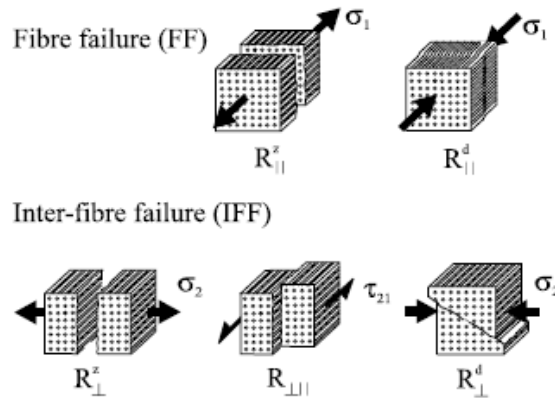


Figure 2.54: Failure modes and strength coefficients [26]

From the invariants, the failure conditions and in turn the reserve factors were derived and then the resultant reserve factor was determined. This factor was used in the

optimization algorithm. Hence this new optimization procedure enable the efficient design of multi-layered composites and the adjustment of curvature to technical demands with stability and failure criteria built into the algorithm.

Betts et al. [27] presented an optimization technique for the design of bistable laminates enabled by an analytical solution for an unsymmetric laminate design. The optimization formulation maximizes the bending stiffness in the direction of known loading condition while the bending stiffness in the direction of snap-through was minimized. A minimum deflection requirement was applied as a constraint. The structural requirement to resist normal operating loads and a low energy requirement for actuation were conflicting, leading to constrained optimization of the laminate design. The out-of-plane displacement in the z direction, ‘w’ was assumed to be of the form,

$$w(x,y) = 0.5(ax^2 + by^2 + cxy) \quad (2.16)$$

where a, b and c are the curvatures. A laminate of arbitrary orthogonal layup with two stable shapes of equal and opposite curvature was considered by applying the following design rules,

1. Even number of plies with pair of plies about the laminate midplane 90° apart.
2. Square edge length L.
3. Equal ply thicknesses about the laminate midplane t1, t2 . . . tn.
4. Each ply is made from the same material.

The stacking sequence, illustrated in Fig. 2.55, was selected as it provided scope for tailoring the directional stiffness properties, while the orthogonal alignment of plies and the square laminate profile enabled maximum useful deflection between states.

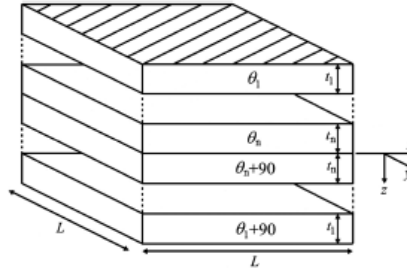


Figure 2.55: Schematic of n-ply laminate ensuring curvatures of equal magnitude and opposite directions in the two cylindrical shapes [27]

The objective function optimized the ratio of bending stiffness between two specified orientations, θ_1 and θ_2 as shown in the equation,

$$\text{Objective Function} = \frac{\delta a_{\theta_2}}{\delta M_{x\theta_2}} / \frac{\delta a_{\theta_1}}{\delta M_{x\theta_1}} \quad (2.17)$$

They characterized the bending stiffness at θ by the change of major shape coefficient a_{θ} with respect to a moment applied in that direction $M_{x\theta}$. For a deflection constraint, the out-of-plane displacement at a corner between states I and II was used. The corner deflection between states w_{def} at $x=y=L/2$ can be expressed by,

$$w_{\text{def}} = w_1 - w_2 = 0.125(a_1 + b_1 + c_1)L^2 - 0.125(a_2 + b_2 + c_2)L^2 \quad (2.18)$$

The curvatures a, b and c can be expressed in terms of the first state alone, as the two states were having curvatures of equal and opposite magnitude. Therefore the equation had been rewritten in terms of only a_1 and b_1 by,

$$w_{\text{def}} = 0.25(a_1 + b_1)L^2 \quad (2.19)$$

This equation was used to define the constraint on minimum deflection. The optimization problem was solved using MATLAB's sequential quadratic programming minimizer, `fmincon`. Due to the multimodal nature of the design space, multiple starting points were used to capture all local optima. In the deflection constrained optimization,

the ply orientation was the only variable and results obtained are as shown in Fig. 2.56. The dots represent all optima, while the grey area depicts the infeasible regions, the darker areas are the monostable regions and the lighter areas have deflection between states less than the minimum deflection constraint.

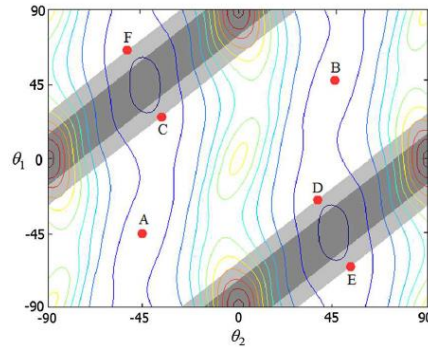


Figure 2.56: Deflection constrained design space [27]

This problem had six optimum solutions. The two cross-ply solutions $[-45_2/45_2]_T$ and $[45_2/-45_2]_T$, points A and B are unconstrained optima where the gradients were zero. The other four solutions, points C-F, were on the deflection constraint boundaries and are global optima. In the constrained optimization, in addition to ply orientations, geometric design variables were also included. Table 2.4 shows all eight optimum solutions. As with previous example, the cross-ply designs of $[-45_2/45_2]_T$ and $[45_2/-45_2]_T$, A and B, were local optima. Also there were four optimal solutions along the deflection constraint boundaries. The geometric variables of these solutions all reach either the upper or lower bounds in order to maximize the laminate deflection.

	First ply angle, θ deg	Second ply angle, θ deg	First ply thickness, mm	Second ply thickness, mm	Laminate edge length, m	Deflection, mm	Objective function
A	-45.0	-45.0	0.05-0.75	0.05-0.75	0.22-0.5	100-515	0.319
B	45.0	45.0	0.05-0.75	0.05-0.75	0.22-0.5	100-515	0.319
C	-49.9	52.8	0.05	0.15	0.5	100	0.220
D	49.9	-52.8	0.05	0.15	0.5	100	0.220
E	-40.1	37.2	0.05	0.15	0.5	100	0.220
F	40.1	-37.2	0.05	0.15	0.5	100	0.220
G	-45.0	45.0	0.094	0.106	0.5	100	0.191
H	45.0	-45.0	0.094	0.106	0.5	100	0.191

Table 2.4: Optima for deflection constrained optimization with geometry variables [27]

There is a further pair of optima, G and H, these solutions were $[\mp 45_2]_T$ and $[\pm 45_2]_T$ which had the lowest objective function value but violated the deflection constraints in the previous example, as the limits on the edge length and thicknesses did not allow sufficient deflection. This approach demonstrated that appreciable difference in bending stiffnesses could be achieved while ensuring that the specified deflection constraint was satisfied.

Multistable Composites

Cui & Santer [28] presented a novel continuous composite surface which possessed a high degree of multistability. They first showed how two identical bistable composite shells with tailored asymmetric bistability may be connected to form a continuous quadstable surface. The concept was then extended to surfaces composed of three and by extension more identical bistable shells connected in series in order to achieve additional stable states. If 'n' bistable components are connected, the resulting system may exhibit up to 2^n discrete stable configurations. The composite shells investigated in this paper were made of Hexcel IM7/8552 Graphite/Epoxy Prepreg and the stacking sequence was $[0/90]$. Finite Element Analysis (FEA) was exclusively used as the simulation method in this research.

For a coupled bistable shell structure, a maximum of four stable states may be present. The key to achieving highly multistable surfaces was the stability of intermediate states. The actuation process was implemented by applying a controlled displacement to the driving shell until the shell snaps through to another stable state. Also, the central point and two free vertices of the driven shell had to be fixed for avoiding rotation (Fig. 2.57(a)). The deformation got transmitted to the driven shell through the common edge. After the actuation, the fixed vertices were released and if the driven shell did not snap to a new stable configuration and the driving shell maintained its new shape (Fig. 2.57(b)), the intermediate state was deemed stable and the connected shells determined to have four stable states. The coupled bistable shell structure remained bistable (Fig. 2.57(c)).

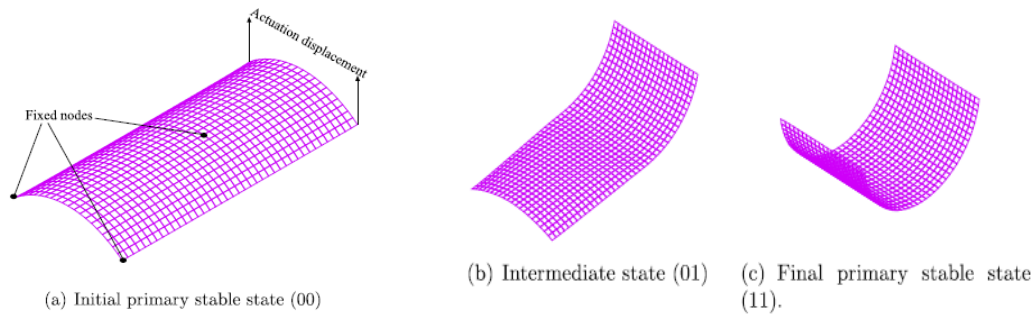


Figure 2.57: Actuation procedure for coupled bistable composite shells [28]

The degree of bistable asymmetry influenced the multistable behaviour of the coupled composite shells, thus biasing strips made of symmetric [0/0] laminates were attached to the center of bistable composite shells to vary its asymmetric bistability. To investigate the influence of attaching biasing strips on the bistability of composite shells, the strips were attached parallel or perpendicular to the linking edges as shown in Fig. 2.58. The degree of asymmetric bistability of the single shell increased in both cases and the stable state possessing lower potential energy became the preferred stable state.

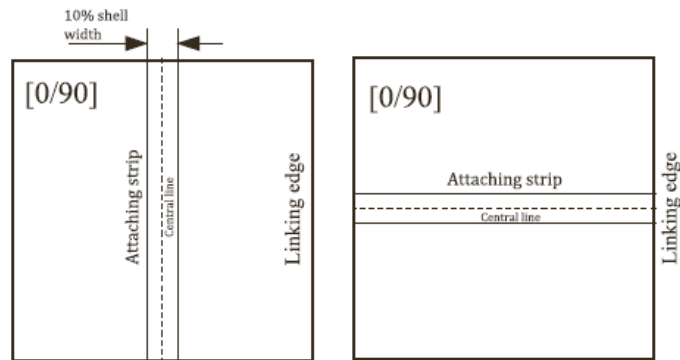


Figure 2.58: Two different approaches of attaching a biasing strip on a single shell [28]

The coupled bistable shells with perpendicular biasing strips demonstrated two potential energy minima which represent two primary stable states, whereas the coupled bistable shells with parallel biasing strips demonstrated three potential energy minima. Hence, besides the two primary stable states, this surface can achieve two stable intermediate states and possesses quadstability.

For a three connected square bistable shells with parallel biasing strips, in addition to the two primary stable states 000 and 111, this surface had up to a six intermediate stable states. Four actuation steps were applied to verify the stability of these intermediate states, specifically:

- step A: actuate from state 000 to state 100;
- step B: actuate from state 100 to state 110;
- step C: actuate from state 110 to state 010;
- step D: actuate from state 100 to state 101.

In each actuation step, a controlled displacement was only applied to the driving shell as the actuation load and the other two driven shells were unconstrained. Fig. 2.59

illustrates the configuration transitions in these steps. Due to symmetry, the shapes of state 001 and state 011 were not illustrated.

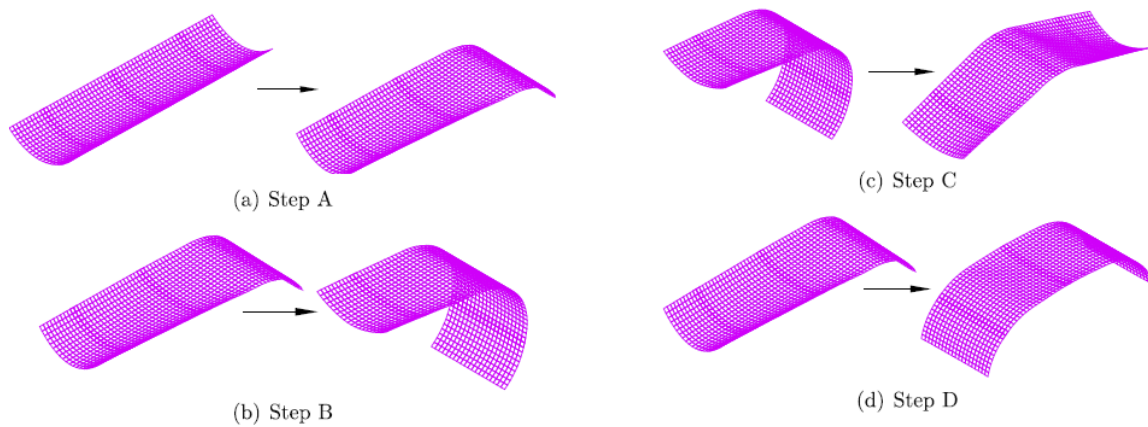


Figure 2.59: Finite element predictions of the stable configurations of three connected bistable plates and the transitions between these states resulting from actuation [28]

To ensure the shells have continuous, robust and smooth connections, the compound shells were fabricated directly as a whole rectangular shell. The physical composite surface showed the same number of stable states as expected. A highly multistable surface fabricated without conventional fixation and presenting smooth curvature changes had been successfully demonstrated.

Concluding Remarks

There is much interest in bistable composites as evidenced by the amount of papers and variability of topics presented. This literature review is the basis for the understanding of the problem and for the setting of the research questions which are posed in the next chapter.

CHAPTER THREE

SIMULATIONS AND EXPERIMENTS

Research Objectives and Methodology

The ultimate objective of this research is to achieve desired shapes in both stable states of any given geometry, by using a combination of symmetric and unsymmetric laminates. The three step methodology proposed to achieve this objective is as follows,

1. Any given geometry is converted into a tessellated geometry, i.e., subdivided into multiple connected triangles using the concept of tessellation.
2. The fibre orientation and laminate stacking sequence of each individual triangle composite laminate is varied, to obtain different combinations of symmetric and unsymmetric laminates.
3. Each combination of symmetric and unsymmetric laminates will have unique bistable shapes. Continuous iterations are carried out, till the desired bistable shapes are achieved.

The triangular composite laminates behave in a specific way when they are present in its individual form and in an entirely different way, when they are present in a multiple connected triangle form (tessellated geometry). Because of this reason, and to reduce the number of iterations needed to arrive at the final combination of symmetric and unsymmetric laminates, there are two major topics that need to be addressed. They are, Behavior of Individual Unsymmetric Laminates and Behavior of Combination of Symmetric and Unsymmetric Laminates. Each of these topics are dealt in detail in this research, in order to create a pathway to achieve the ultimate objective.

The overall research can be broadly divided into two sections: Simulations and Experiments. Among these topics, simulations constitute the major part of the research. Simulations are carried out for both individual unsymmetric laminates and combined symmetric & unsymmetric laminates. Experiments are done only on individual unsymmetric laminates. First, the unsymmetric laminates are fabricated, and second the snap through and snap back loads are measured using the experimental setup developed in this research.

PART-I: SIMULATIONS

ABAQUS finite element analysis software is used for the simulations. In this section, the problem formulation and the step by step procedure to run the simulations are provided. The description of a preliminary simulation that was carried out and inferences from that simulation result are also provided. Even though, each simulation of the combined symmetric and unsymmetric laminates is slightly different, the overall principle and procedure explained in this section remains the same for all those simulations.

Problem Formulation in FEA

The problem formulation consists of the following parts: the geometrical modeling of the laminate, lamina material assignment, laminate stacking sequence, meshing of the laminate, loading and boundary conditions. The overall simulation consists of three steps as follows,

1. Simulation of the cured shape / first stable shape by applying the necessary curing conditions.

2. Simulation of the snap through behavior or shape change from the first stable state to the second stable state.
3. Simulation of the snap back behavior or shape change from the second stable state back to the first stable state.

Except for the loading and boundary conditions, all other parts in the problem formulation remains constant for all the three steps. Finally, the post processing is done to interpret the results of the simulations.

Geometrical modeling of the laminate

Individual laminates as shown in Fig.3.1 (a) are directly modeled in FEA, whereas the multiple connected laminates as shown in Fig.3.1 (b), are modeled in Solidworks CAD software and imported into FEA. In Solidworks, the overall geometry is modeled first and then it is split into smaller geometries as per the required combination of geometries. This helps in assigning each of the smaller geometries with different laminate stacking sequence, once it is imported into FEA.

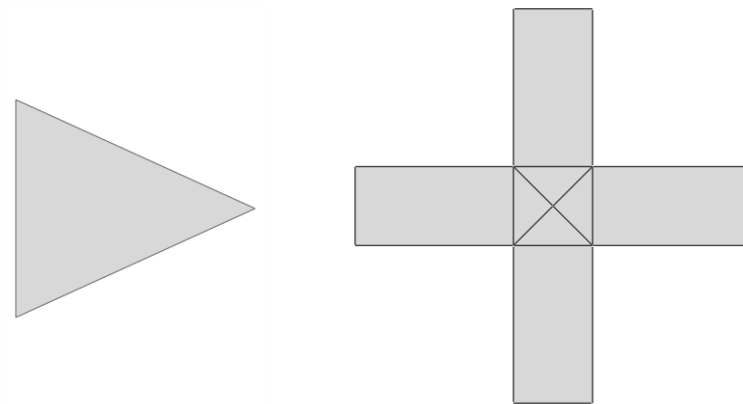


Figure 3.1: (a) Individual laminate, (b) Multiple connected laminates

Lamina material assignment

The material used in the experiment is DA 409U / G35-150 prepregs, purchased from Adhesive Prepregs for Composite Manufacturers LLC. The material properties needed for the simulation are modulus of elasticity (E_1, E_2), modulus of rigidity (G_{12}, G_{13}, G_{23}), Poisson's ratio (ν_{12}) and coefficient of thermal expansion (α_1, α_2). The supplier had only provided the tensile modulus (modulus of elasticity) and flexural modulus for this material. From the literature [13], it was found that AS4 – 8552 prepregs have the nearest tensile and flexural moduli as shown in Table 3.1. Hence, the material properties of AS4 – 8552 prepregs as given in Table 3.2 are considered for the simulation.

Property / Material	DA 409U / G35-150	AS4 – 8552
Tensile Modulus	18.8 msi	19.6 msi
Flexural Modulus	17.9 msi	18.4 msi

Table 3.1: Moduli comparison of two different prepregs

Property	Value
E_1	135 GPa
E_2	9.5 GPa
ν_{12}	0.3
G_{12}	5 GPa
G_{13}	7.17 GPa
G_{23}	3.97 GPa
α_1	$-2 \times 10^{-8} / ^\circ\text{C}$
α_2	$-3 \times 10^{-5} / ^\circ\text{C}$
Ply thickness	0.15 mm

Table 3.2: Material properties of the AS4 – 8552 prepregs [13]

Laminate stacking sequence

In general, the laminated FRP is modeled in FEA using the “Composite Section” option. In this option, the laminate stacking sequence is represented by, the angle of each lamina with respect to the x-axis of the global coordinates, the thickness of each lamina,

and the material properties of each lamina. FEA computes the A, B and D matrices (stiffness matrix of laminate) internally as per the data provided. In all the simulations, the thickness and the material properties of the lamina are maintained same and only the fibre orientation is altered. As per the angle convention in FEA, angle to the clockwise direction is considered positive. For example, four different angle 0° , 90° , 45° and -45° lamina are shown in Fig.3.2.

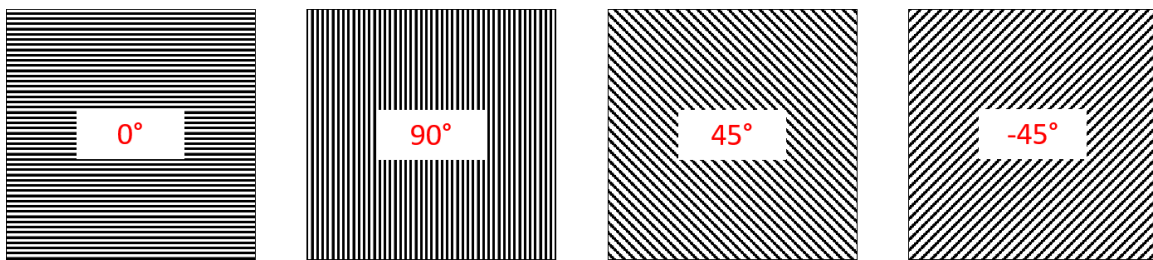


Figure 3.2: Angle convention in FEA simulations

Meshing of the laminate

A thick shell element S4R is used for meshing of the laminates. Composites are always modeled as thick shells even if they are geometrically thin because they have relatively low shear modulus, thus necessitating inclusion of their shear deformation in the same way as thick shells do. For each laminate (individual or multiple connected), mesh convergence is carried out separately to determine the optimum number of elements. In most cases, quadrilateral mesh is used, but in few instances a combination of triangular and quadrilateral mesh is used as shown in Fig.3.3 (a) & (b).

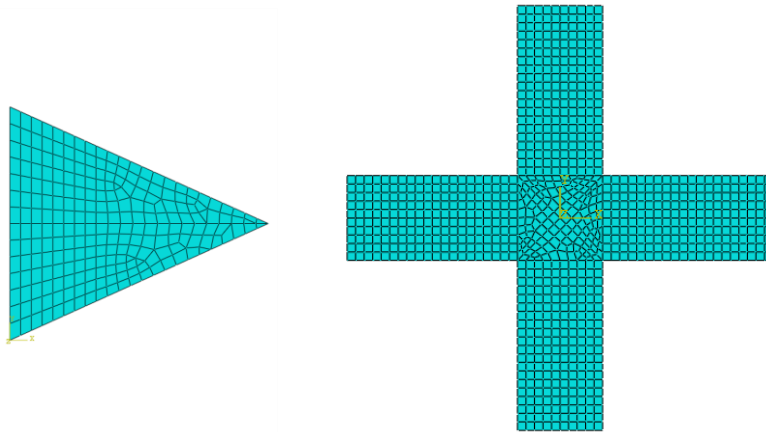


Figure 3.3: (a) Mesh of individual laminate, (b) Mesh of multiple connected laminate

Loading and boundary conditions

The loading and boundary conditions for each of the three steps is different. Since the first step is simulation of the curing process, the loading is provided by the “Predefined Field” option in FEA. In this option, if the temperature difference between a predefined temperature field and an initial temperature is provided, it creates thermal strains based on the thermal expansion coefficient given for the material. Therefore the curing temperature, in this case 121°C (250°F) is provided as the initial temperature and the room temperature 20°C is provided as the predefined field temperature to simulate the curing process. A simple boundary condition is applied in the first step, the node at the geometric center or centroid of the structure whichever is applicable is clamped. This is done to suppress rigid body motions and to reproduce the free-free boundary conditions. First step is a *STATIC step where large deformation theory (NLGEOM) is used to perform a non-linear static analysis.

Before proceeding to the loading and boundary conditions of the second and third step, it is necessary to relook at Fig.2.1 presented again as Fig 3.4 and note few key points.

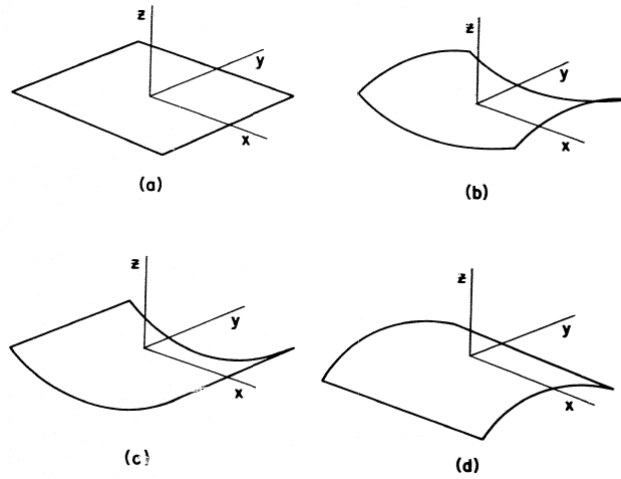


Figure 3.4: Laminate shapes (a) at elevated curing temperature, and at room temperature, (b) saddle shape, (c) first cylindrical shape, (d) second cylindrical shape [4]

Fig 3.4 (c) shows the first cylindrical shape / post fabrication (post fab) shape, in this the curvature is about the y-axis and the shape is concave looking from the top. Fig. 3.4 (d) shows the second cylindrical shape / post load shape, in this the curvature is about the x-axis and the shape is convex looking from the top. The loading of the second and third steps are dependent on the concave / convex curvature and the boundary conditions are dependent on the axis about which the curvature is present. The loading and boundary conditions for both the steps can be represented pictorially as shown in Fig. 3.5.

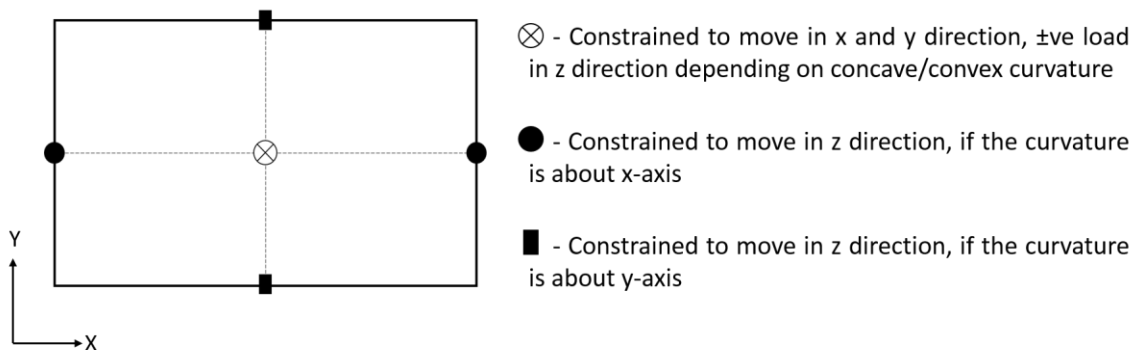


Figure 3.5: Loading and boundary conditions for snap through and snap back simulations

For example, the loading and boundary conditions for simulating the snap through behavior of a laminate shown in Fig.3.4 is by constraining its geometric center to move in x and y directions, applying load in its geometric center in +z direction, and constraining its mid-points of the two horizontal edges to move in z direction. Second and third steps are *STATIC STABILIZE steps, where the automatic stabilization taken care by the damping factors is used to perform a pseudo-dynamic non-linear analysis.

Post processing

Post processing is done to find out the snap through and snap back loads. By using the post processing options in FEA, the load vs displacement plot at the load application point is generated as shown in Fig.3.6. This plot gives the critical load (snap through / snap back) at which the shape change happens. During the shape change, a huge change in displacement happens at a constant load, which implies that the flat portion of the plot gives the critical load at which it happens. For load values less than the critical load, the shape change does not happen, so the load values are gradually increased till it crosses the critical load and the shape changes. Even after the shape changes, the laminate still takes more load and displaces beyond the stable shape, which is the reason for the extended portion of the plot after the critical load is crossed.

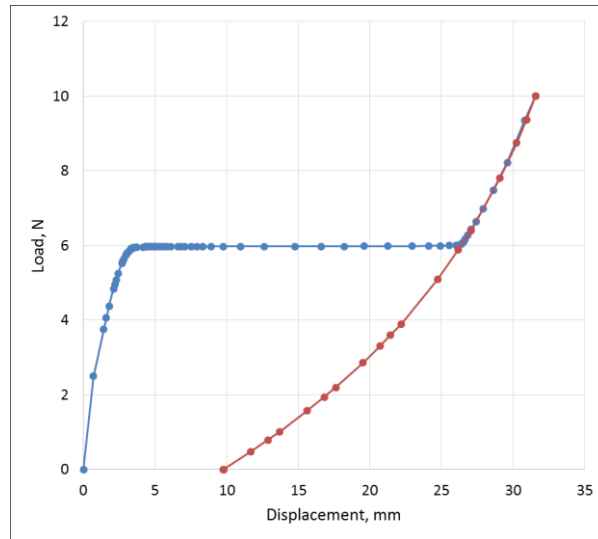


Figure 3.6: Load vs displacement plot at the load application point

Once the load is released, the excess displacement goes off and the laminate comes back to the stable shape, as indicated by the red curve in Fig.3.6. Therefore, both the second and third steps has one more sub-step each, which is the unloading step. The critical load of the second and third steps gives the snap through and snap back loads respectively.

Preliminary Simulation and Inference

A preliminary simulation of the bistable behavior of an individual rectangular unsymmetric laminate was carried out and the critical load values were found. Also, from the results obtained, major inferences were made, which were helpful for all other simulations in this research.

Preliminary simulation

Since it is an individual laminate of a simple rectangular geometry, the modeling is done in FEA itself as shown in Fig.3.7 (a). The dimensions of the rectangle considered is 120 x 100 mm (length x breadth). The material assigned to the lamina is AS4 – 8552 and

the properties which are given in Table 3.1 are used. It is considered to be a cross-ply laminate with laminate stacking sequence $[0/90]_T$ and a lamina thickness of 0.15 mm. The meshing is done with S4R elements, the mesh consisted of 480 elements and 525 nodes as shown in Fig.3.7 (b).

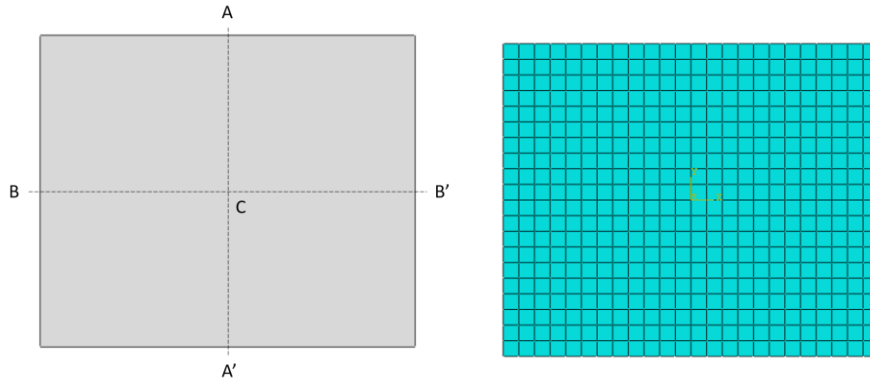


Figure 3.7: Rectangular laminate (a) Geometrical model, (b) Quadrilateral mesh

To simulate the overall behavior of the unsymmetric laminate, the following three steps were followed,

1. To obtain the first shape, the node at the geometric center C was clamped and the curing process was implemented by using the predefined field option in FEA (Curing temperature - 121°C (250°F); Room temperature - 20°C).
2. To obtain the second shape, a two-step process was followed:
 - a. Nodes at both the points A and A' were constrained to move in the z direction, node at the geometric center C was constrained to move in the x and y direction and a suitable load above the snap through load was applied at the same node.
 - b. All the boundary conditions were held the same and the load was released.

3. To obtain back the first shape, again a two-step process was followed:
 - a. Nodes at both the points B and B' were constrained to move in the z direction, node at the geometric center C was constrained to move in the x and y direction and a load above the snap back load was applied at the same node.
 - b. All the boundary conditions were held the same and the load was released.

The first and second stable shapes of the laminate obtained from the preliminary simulation are as shown in Fig.3.8 (a) & (b).

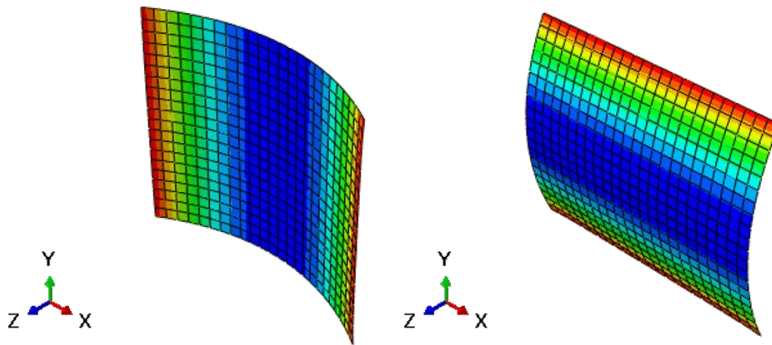


Figure 3.8: (a) First stable shape, (b) Second stable shape

If both the load vs displacement plots of snap through and snap back behavior are combined together, it forms a closed loop as shown in Fig.3.9.

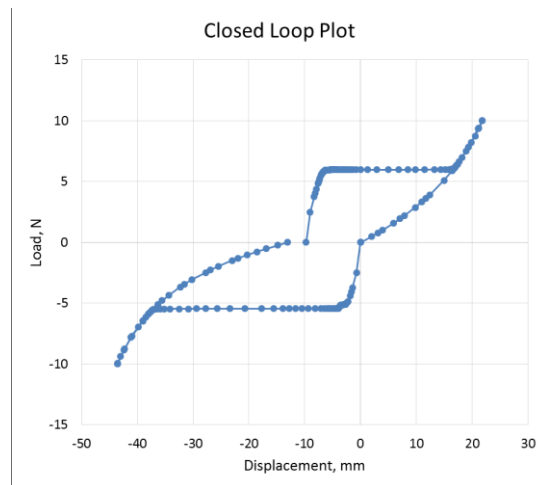


Figure 3.9: Combined load vs displacement plot of snap through and snap back

Inference

As seen from Fig.3.8 (a) & (b), both the shapes obtained are similar to the shapes in Fig.3.4 (c) & (d), which validates the simulation. The laminate stacking sequence consists of two fibre orientations, 0° fibres oriented along x-axis (along length) and 90° fibres oriented along y-axis (along breadth). Out of these two, 0° fibres are longer in length, since the length of the rectangle is more than its breadth. In this way, if we consider laminates with only two fibre orientations, in most of the geometries except for squares and few other cases, fibres oriented in one of the directions (long fibres) will be longer than the fibres oriented in the other direction (short fibres). The three major inferences from the preliminary simulation are,

1. The reason for the first shape / post fab shape to be curved about y-axis and not about x-axis is, the first shape is always determined by the orientation of the long fibres and the second shape is determined by the orientation of the short fibres. Since in this case, the long fibres are the 0° fibres and they are oriented along the x-axis, the curvature is along x-axis / about y-axis, otherwise it would have been the other way around.
2. The reason for the first shape /post fab shape to have a concave curvature looking from the top rather than a convex curvature is, the concave / convex curvature is always determined by the location of the long fibre in the laminate stacking sequence. Since in this case, the long fibres are present in the bottom of the laminate stacking sequence, the curvature is concave from the top, otherwise it would have been the other way around.

3. The reason for the snap through load to be always higher than the snap back load is, snap through load is always dependent on the long fibre and snap back load is dependent on the short fibre. A more pronounced reason for this inference is provided in the next chapter.

PART-II: EXPERIMENTS

The first part of the experiments is fabrication of the unsymmetric laminate and the second part is the measurement of snap through and snap back loads of the unsymmetric laminate. There are many types of laminated FRP fabrication, in this research the unsymmetric laminates are fabricated using compression molding of prepregs. The description of the mold, prepreg and the fabrication process are explained. An entirely new experimental setup was developed to measure the critical loads. The description of the experimental setup, the working principle and the operating procedure are also explained.

Fabrication of the Unsymmetric Laminates

The unsymmetric laminates were fabricated from the unidirectional prepreg DA 409U / G35 150 material using an aluminum mold in a WABASH PC hot press.

Mold and Prepreg

Initially, the older mold from the previous research by Murray [29] was used for the fabrication. The mold consisted of a top plate, a bottom plate and four side plates, assembled together by using ten hex head bolts and nuts. The exploded view of the older mold assembly is as shown in Fig.3.10. The mold dimension is 7 in x 4 in and the maximum dimension of a laminate that can be fabricated using this mold is 5 in x 2.5 in (approx. 126

mm x 63 mm). In the previous research, the bolt heads and nuts were not concealed in the top and bottom plates respectively, they were protruding outside as shown in Fig. 3.11. Since a conventional oven was used for the fabrication process, the heat transfer was through convection, hence the protrusions did not cause any issues.

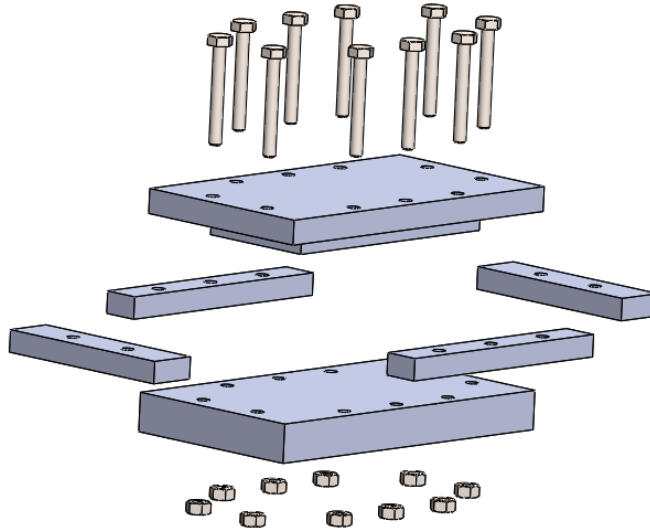


Figure 3.10: Exploded view of the older mold

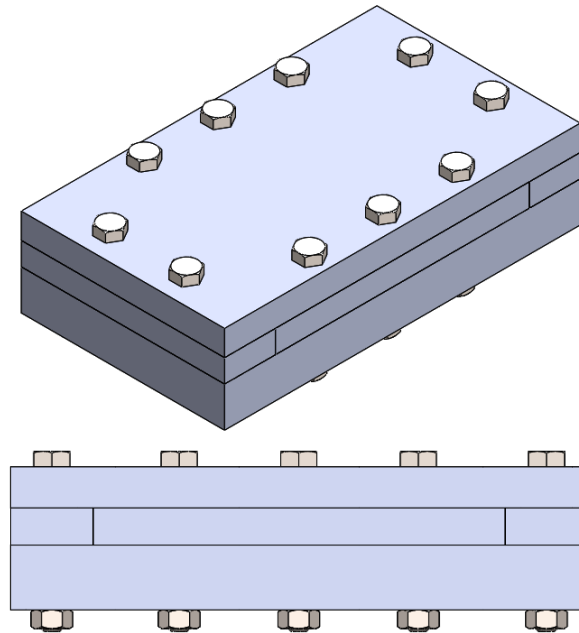


Figure 3.11: Isometric and front view of the older mold

In the current research, a hot press is used for the fabrication, the heat transfer is through conduction. In this case, if the bolt heads and nuts are protruding outside, then those will come in direct contact with the platens of the press, which would cause the bolts to bend because of the high temperature and applied pressure. To prevent the bolts from bending and to prevent it from becoming non-reusable, the top and bottom plates are slightly modified such that the two plate surfaces comes in direct contact with the platens. The modifications done are, tapping the bottom plate holes, making countersunk in the top plate holes and changing the bolts from hex head bolts to countersunk bolts. This removes the usage of nuts, and makes the countersunk bolt heads to flush with the top plate surface as shown in Fig.3.12, thereby avoiding the protrusions on either side.

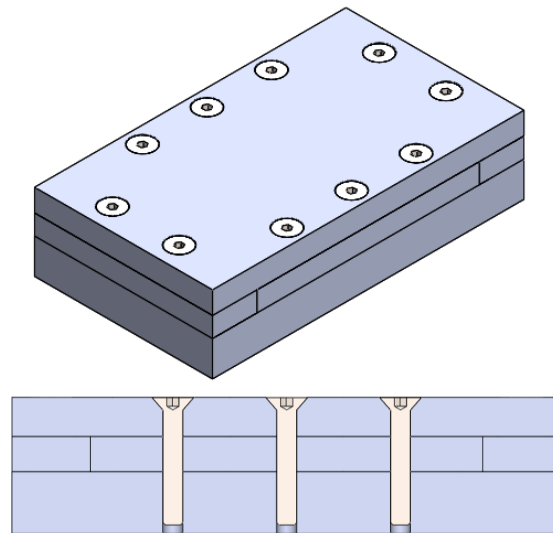


Figure 3.12: Isometric and sectional front view of the corrected mold

Prepregs are pre-impregnated fibres, where the matrix material is already present. Prepregs generally comes in the form of unidirectional fibres, and the matrix generally epoxy resin is present in the B stage condition. Using prepregs is one of the fastest way of

composite fabrication and is also costlier than other methods. The prepreg used in this research is made of unidirectional carbon fibres and epoxy matrix.

Fabrication process

The first step in the fabrication process is the mold preparation. The mold is prepared by applying three different coatings namely, sealant, mold release agent and quick skin agent. Sealant is applied to prevent the epoxy from flowing outside of the mold, as the epoxy becomes liquid, when it is raised to the curing temperature. The mold release agent is applied for easy removal of the laminate from the mold, once the fabrication process is done. The quick skin agent is applied to improve the surface finish of the laminate.

The second step is cutting the prepreg for required dimensions and orientation of fibres. Since it is a unidirectional prepreg, by default all the fibres are oriented in a single direction. Appropriate cutting needs to be done, to obtain fibres oriented in other directions as needed in the laminate stacking sequence.

The third step is laying up each individual prepreg, one above the other in the mold bottom plate, according to the laminate stacking sequence. Since epoxy has a very good adhesive property, all layers stick to each other firmly.

The fourth step is closing the mold. All the side plates are kept in place, the top plate is closed and all the ten bolts are fastened. Since hardened steel fasteners are screwed into aluminum threads (comparatively softer material), proper anti-seize is used to prevent threads from getting worn out.

The fifth step is the curing process, where the closed mold with the prepreg inside, is kept in a hot press and cured as per the conditions provided by the prepreg supplier. For

the prepreg used in this research, the curing conditions are 250°F temperature and 80 psi pressure for 1 hour duration.

The final step is removing the cured laminate from the mold. Once the curing process is done, the mold is allowed to cool down to the room temperature, the mold is opened and the cured laminate is taken out.

Experimental Setup

A simple experimental setup based on the conventional load measurement technique is developed. That is, the basic concept of applying load by means of adding physical weights is used in this experimental setup. The boundary conditions used in the simulations are replicated. Also the setup is designed in such a way that, both the snap through and snap back loads can be measured just by changing the location of the weights and not disturbing the laminate.

Description of the experimental setup

The 3D CAD model of the experimental setup is as shown in Fig.3.13. The main framework is a simple construction that consists of a top plate, bottom plate and four columns, the overall dimension of the setup is 1ft x 1ft x 2 ft. The laminate is held in the middle of the framework, by means of strings attached to 2 eyebolts in the top plate and 2 eyebolts in the bottom plate. The setup also has a three pulley arrangement on the bottom side to pull the laminate downwards and a two pulley arrangement on the top side to pull the laminate upwards. The weights are added by using a slotted weight hanger system as shown in Fig.3.14, hence the weights can only be increased in discrete steps.

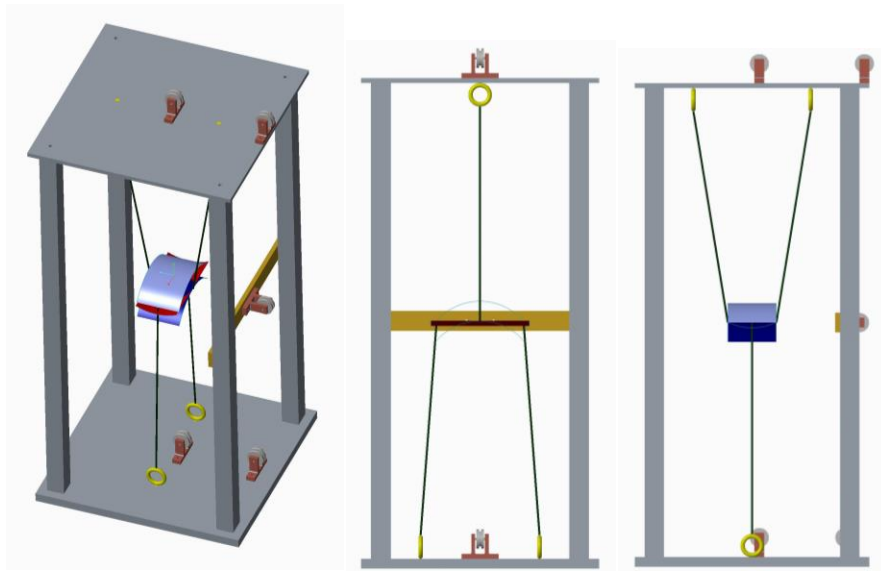


Figure 3.13: Isometric, front and side views of the experimental setup



Figure 3.14: Slotted weight hanger system (image courtesy – science lab supplies)

Working principle

The enlarged image of the laminate portion in Fig.3.13 is as shown in Fig.3.15. It appears, as if there are three different laminates present, but they are actually the three different positions of a single laminate. Dark blue is the first position, red is the second position and light blue is the third position.

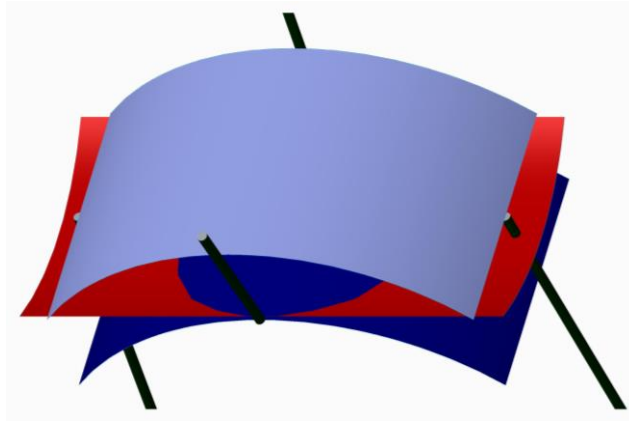


Figure 3.15: Laminate portion in the experimental setup

The natural gravity pull and replication of the boundary conditions used in the simulations helps in the working of this experimental setup. The working principle is as follows,

1. In the first position, the laminate is in its post fab shape. The top two strings are in their fully extended position, and the bottom two strings are loose. When the load is applied in the geometric center of the laminate in such a manner that the laminate is pulled downwards, the top two strings constrains the mid-point of the two horizontal edges from moving in the z direction, and all four strings restricts the load application point to move only in the z direction. Once the critical load is reached, the shape changes and the laminate goes to the second position. After this, when the load is removed, the laminate retains the post load shape and remains in the second position.
2. In the second position, the laminate is in its post load shape. The top two strings and the bottom two strings are in their fully extended position. When the load is applied in the geometric center of the laminate in such a manner that the laminate is pulled upwards, the bottom two strings constrains the mid-point of the two vertical edges from

moving in the z direction, and all four strings restricts the load application point to move only in the z direction. Once the critical load is reached, the shape changes and the laminate goes to the third position.

3. In the third position, the laminate is back in its post fab shape. The bottom two strings are in their fully extended position, and the top two strings are loose. This is an intermediate position because only till the load is present, the laminate stays in this position. Once the load is removed, the laminate goes back to the first position.

Operating procedure

When the laminate is in its post fab shape (first position), the weights are added in the location as shown in Fig.3.16 (a). This pulls the laminate downwards and the weight at which the shape changes to the post load shape (second position), gives the measure of the snap through load of the laminate. After measurement, when the weights are removed, the post load shape is retained as per the bistable characteristics. When the laminate is in its post load shape (second position), the weights are added in the location as shown in Fig.3.16 (b). This pulls the laminate upwards and the weight at which the shape goes back to the post fab shape (third position), gives the measure of the snap back load of the laminate. After measurement, when the weights are removed, the post fab shape is retained but the laminate goes back to the first position.

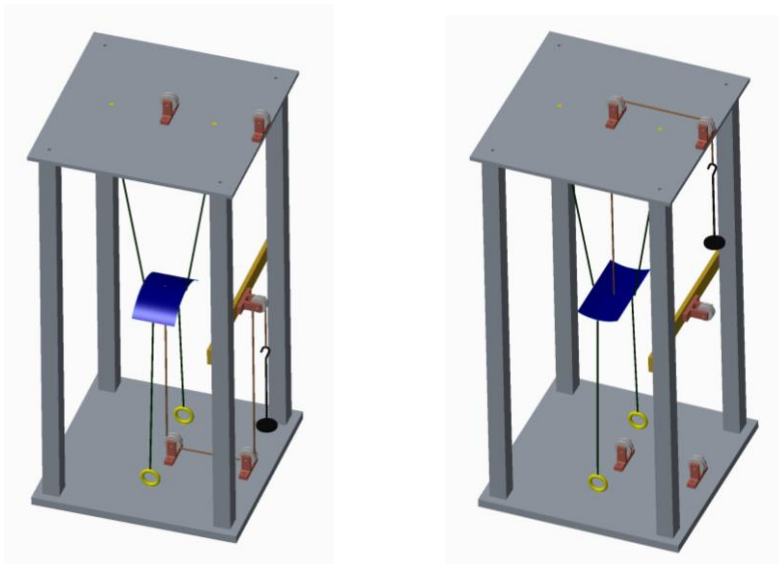


Figure 3.16: (a) Snap through loading position, (b) Snap back loading position

CHAPTER FOUR

RESULTS AND DISCUSSION

Both the simulation and experimental results are discussed in this chapter. In accordance with the research objectives, the simulation results are discussed in two parts: Study of individual unsymmetric laminates and study of combination of symmetric & unsymmetric laminates. The experimental results are discussed in the third part.

PART-I: STUDY OF INDIVIDUAL UNSYMMETRIC LAMINATES

There was a lot of work done in the literature on the unsymmetric laminates in its individual form, but one of the major gap identified was the study on the factors affecting the snap through & snap back loads of these laminates. The advantage of studying this topic in detail is, it helps in understanding which parameters need to be varied, in order to alter the critical loads at which shape change occurs in any given structure. This forms the main concentration of the first part of the research. The two major factors considered are,

- i. Effect of Geometry
- ii. Effect of Fibre Orientation

Effect of Geometry on the Snap Through and Snap Back Loads of an Individual Unsymmetric Laminate

In literature, the major geometries of individual unsymmetric laminates studied so far were either rectangle or square. Whereas isosceles trapezoid and isosceles triangle geometries are also included in this study. As shown in Fig.4.1, a rectangle or square can

be converted into both isosceles trapezoid and isosceles triangle (special case - equilateral triangle) just by reducing one of the side dimension 'c', keeping the base 'b' and height 'a' dimensions constant. This is the reason behind adding only these two shapes in the study and not any other standard shapes.

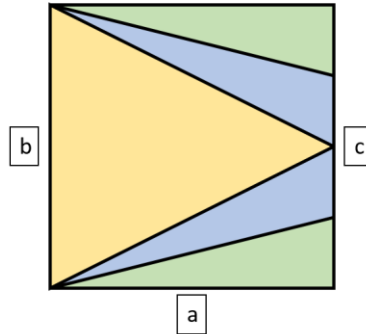


Figure 4.1: Variation in geometry based on 'c' dimension

For example, if the side length 'c' is continuously reduced i.e., with continuous reduction in the ratio 'c/b', any rectangle or square becomes an isosceles trapezoid at first and when the ratio reaches zero, it becomes an isosceles triangle. Also, since square is a special case of a rectangle with all 4 side lengths equal, that is brought under the rectangle classification; effectively left with three major geometries: Rectangle, Isosceles Trapezoid & Isosceles Triangle. All these geometries were studied, each in 2 different ways: first the height dimension 'a' was increased, and the base dimension 'b' was kept constant; second 'b' was increased and 'a' was kept constant. This gave 6 variations as follows, Rectangle – I & II, Trapezoid – I & II and Triangle – I & II.

In case of unsymmetric laminate with only two fibre orientations, whenever the dimensions were altered, there was a change in geometry, which in turn changed two internal parameters, namely, Average Fibre Length (AFL) and Number of Fibres (Count) in the two fibre directions (Longer & Shorter fibre direction). It has been noticed, the

change in snap through and snap back loads of an individual unsymmetric laminate were mostly affected by these parameters, more than the geometry itself (as geometry is nothing but a name given to different shapes formed by different combination of these two parameters). Considering both parameters in each of the fibre direction, gave a total of 4 factors - AFL_{long} and $Count_{long}$; AFL_{short} and $Count_{short}$. These were considered as the major factors in this study of the effect of geometry. Also as stated earlier in Chapter 3, snap through load and snap back load are associated with the longer fibre direction and shorter fibre direction respectively. Based on the simulations of various geometries with same AFL_{long} to AFL_{short} ratio, it was found even though the ratio might remain same, the snap through and snap back loads varied based on the variation of individual AFL_{long} and AFL_{short} values proving the above statement. Also the simulations carried out, with different laminate sizes within a same geometry with the same AFL_{long} to AFL_{short} ratio, for example in case of rectangle 120 X 60 mm and 240 X 120 mm, validated this inference.

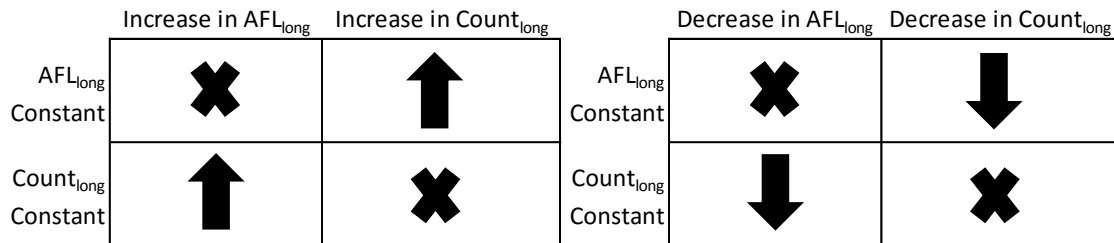


Figure 4.2: Snap through / longer fibre interaction chart

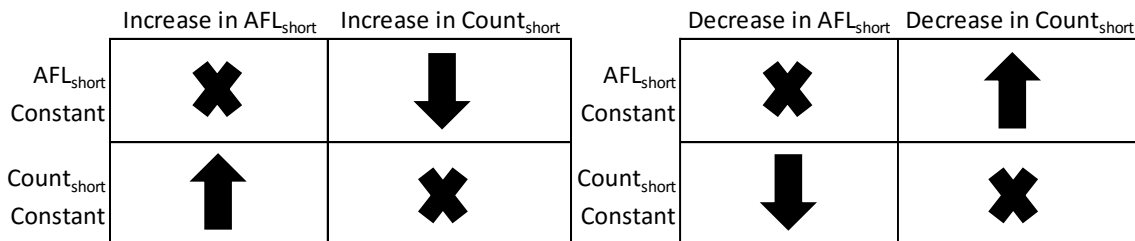


Figure 4.3: Snap back / shorter fibre interaction chart

As shown in the above Fig.4.2 and 4.3, the way in which the AFL and Count interacts varies between snap through / longer fibres and snap back / shorter fibres. For snap through, if either AFL_{long} or $Count_{long}$ increases with the other remaining constant, the load increases. But for snap back, if AFL_{short} increases with $Count_{short}$ remaining constant, the load increases and if $Count_{short}$ increases with AFL_{short} remaining constant, the load decreases. These relations can also be stated in a simplified form as follows,

$$\text{Snap Through Load} = f(AFL_{long}, Count_{long})$$

$$\text{Snap Back Load} = f(AFL_{short}, -Count_{short})$$

As either ‘a’ or ‘b’ was varied, one at a time and the other was kept constant, all the plots had been made with respect to the ‘a/b’ ratio. This ratio is a non-dimensional quantity which relates these two dimensions and is also shape independent. Also, throughout this entire study, the prepreg material (DA409U – G35/150), lamina thickness (0.15 mm) and laminate stacking sequence ([0/90]) was maintained constant.

Rectangle - I

In this case, as shown in Fig.4.4 the height ‘a’ was increased and base ‘b’ was kept constant, thus increasing the ‘a/b’ ratio. In rectangular geometry, both AFL_{long} and AFL_{short} are the same as the respective dimensions itself, for e.g. In the first rectangle 60 X 100 mm, the longer fibres are in the 90° direction (along Y-axis) and its length AFL_{long} is 100 mm, the shorter fibres are in the 0° direction (along X-axis) and its length AFL_{short} is 60 mm. As ‘a’ was kept on increasing, it went towards ‘b’ and as soon as it crossed ‘b’, longer fibres shifted to 0° direction and shorter fibres shifted to 90° direction.

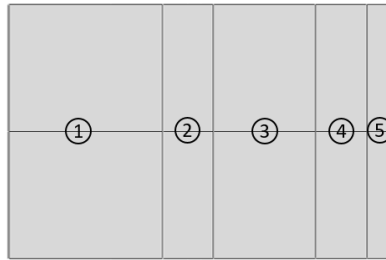


Figure 4.4: Rectangle – I (Increasing ‘a’, keeping ‘b’ constant)

Until ‘a’ was lesser than ‘b’ (i.e., ‘a/b’ < 1), the AFL_{long} remained constant at 100 mm and only $Count_{long}$ increased, whereas once ‘a’ became greater than ‘b’ (i.e., ‘a/b’ > 1), the AFL_{long} started to increase (120,140 and 150 mm) and $Count_{long}$ remained constant. Also until ‘a’ was lesser than ‘b’ (i.e., ‘a/b’ < 1), the AFL_{short} increased (60 and 80 mm) and $Count_{short}$ remained constant, whereas once ‘a’ became greater than ‘b’ (i.e., ‘a/b’ > 1), the AFL_{short} remained constant at 100 mm and $Count_{short}$ started to increase. The increase or decrease of snap through load, as ‘a/b’ ratio increased was dependent on the way the AFL_{long} and $Count_{long}$ varied and interacted with each other, while increase or decrease of snap back load was dependent on the way the AFL_{short} and $Count_{short}$ varied and interacted with each other. Thus based on the interaction charts (Fig.4.2 & 4.3), the final outcomes are as shown in Table 4.1.

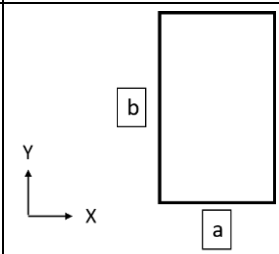
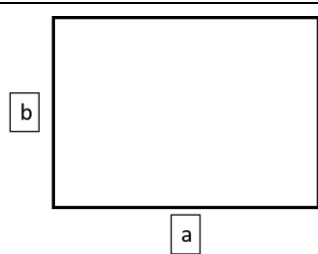
Condition	$a < b$	$a > b$
Geometry		
Dimension a X b mm	60 X 100, 80 X 100	120 X 100, 140 X 100, 150 X 100
Snap Through Load	Increases with 'a/b' increase (AFL _{long} Constant, Count _{long} Increases)	Increases with 'a/b' increase (AFL _{long} Increases, Count _{long} Constant)
Snap Back Load	Increases with 'a/b' increase (AFL _{short} Increases, Count _{short} Constant)	Decreases with 'a/b' increase (AFL _{short} Constant, Count _{short} Increases)

Table 4.1: Rectangle – I snap through and snap back load trend

Results from FEA are plotted in Fig.4.5 and these matched well with the results from the table. From the plots, it can be seen as 'a/b' ratio increases, the snap through load in both conditions "a < b" and "a > b" showed an increasing trend, whereas snap back load increased when "a < b" and started to decrease when "a > b".

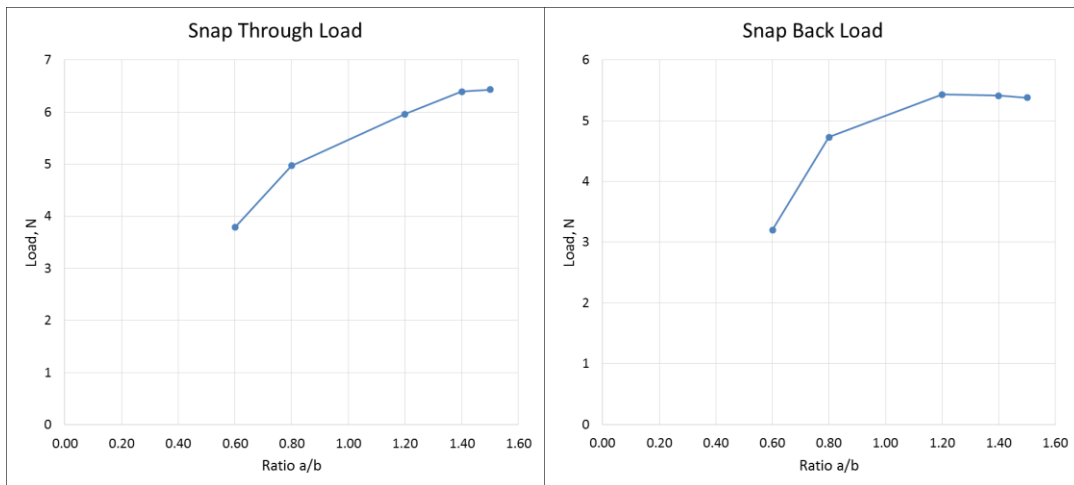


Figure 4.5: Rectangle – I FEA plots

Rectangle - II

In this case, as shown in Fig.4.6 the base 'b' was increased and height 'a' was kept constant, thus reducing the 'a/b' ratio. Initially, the longer fibres were in 0° direction and shorter fibres were in 90° direction, which got interchanged after 'b' crossed 'a'. In the previous case, we have considered the trend with respect to increasing 'a/b' ratio, so to obtain results in similar lines, the trends need to be observed moving from Rectangle 5 to Rectangle 1 in Fig.4.6 rather than moving from Rectangle 1 to Rectangle 5 as done in the previous case. Until 'b' was lesser than 'a', the AFL_{long} remained constant at 100 mm and only $Count_{long}$ decreased, whereas once 'b' became greater than 'a', the AFL_{long} started to decrease (150,140 and 120 mm) and $Count_{long}$ remained constant. Also until 'b' was lesser than 'a', the AFL_{short} decreased (80 and 60 mm) and $Count_{short}$ remained constant, whereas once 'b' became greater than 'a', the AFL_{short} remained constant at 100 mm and $Count_{short}$ started to decrease. Even though these many differences were present between Rectangle – I & II, physically an orientation change only has happened. The distribution of fibres remained exactly the same in both cases, leading to a mere interchange of the axis about which the curvature happened in the two shapes. The curvature values and load required to change shapes remained constant.



Figure 4.6: Rectangle – II (Increasing 'b', keeping 'a' constant)

After considering the interactions between the parameters of the longer fibres for snap through load and shorter fibres for snap back load, the final outcomes are as shown in Table 4.2. Results from FEA are plotted in Fig.4.7, and it matched the trend from the table. The snap back load trend changed from Decreasing to Increasing at the same point where it changed from Increasing to Decreasing in the case of Rectangle – I.

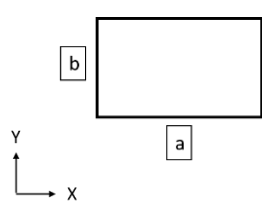
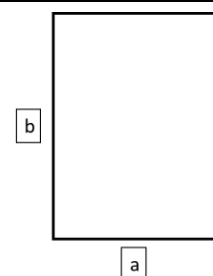
Condition	$b < a$	$b > a$
Geometry		
Dimension a X b mm	100 X 60, 100 X 80	100 X 120, 100 X 140, 100 X 150
Snap Through Load	Decreases with 'a/b' increase (AFL _{long} Constant, Count _{long} Decreases)	Decreases with 'a/b' increase (AFL _{long} Decreases, Count _{long} Constant)
Snap Back Load	Decreases with 'a/b' increase (AFL _{short} Decreases, Count _{short} Constant)	Increases with 'a/b' increase (AFL _{short} Constant, Count _{short} Decreases)

Table 4.2: Rectangle – II snap through and snap back load trend

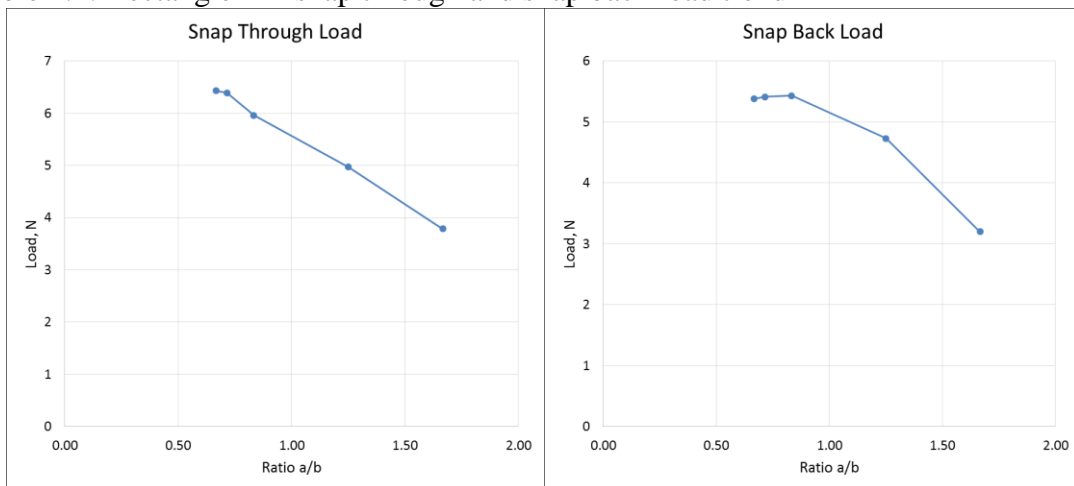


Figure 4.7: Rectangle – II FEA plots

Trapezoid - I

An isosceles trapezoid with 'c' dimension equal to half of 'b' dimension was considered for the detailed study. In this case, as shown in Fig.4.8 the height 'a' was increased and base 'b' was kept constant, thus increasing the 'a/b' ratio. In this specific trapezoidal geometry, the AFL of the 90° fibres remained constant at 75 mm and Count of the 0° fibres remained constant, irrespective of 'a' dimension and whether 90° or 0° is the longer / shorter fibre direction. Initially, the longer fibres were in 90° direction and the shorter fibres were in 0° direction, the reversing of the longer and shorter fibre directions did not happen exactly when 'a' crossed 'b' but even before that, as soon as 'a' crossed 95 mm the direction shift occurred.

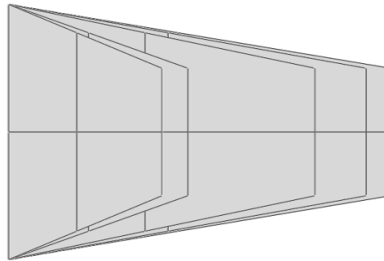


Figure 4.8: Trapezoid – I (Increasing 'a', keeping 'b' constant)

When the trend of snap through and snap back loads is observed based on AFL_{long} , AFL_{short} , $Count_{long}$ and $Count_{short}$ values, it remained exactly the same as that of Rectangle – I as shown in Table 4.3. Also it matched well with the FEA results plotted in Fig.4.9.

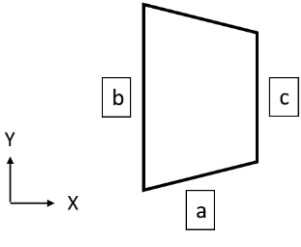
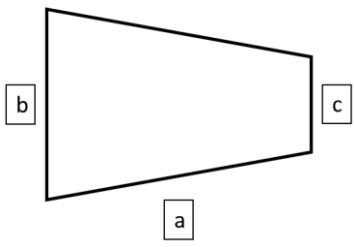
Condition	$a < b$	$a > b$
Geometry		
Dimension a X b mm	60 X 100, 70 X 100	120 X 100, 140 X 100, 150 X 100
Snap Through Load	Increases with 'a/b' increase (AFL _{long} Constant, Count _{long} Increases)	Increases with 'a/b' increase (AFL _{long} Increases, Count _{long} Constant)
Snap Back Load	Increases with 'a/b' increase (AFL _{short} Increases, Count _{short} Constant)	Decreases with 'a/b' increase (AFL _{short} Constant, Count _{short} Increases)

Table 4.3: Trapezoid – I snap through and snap back load trend

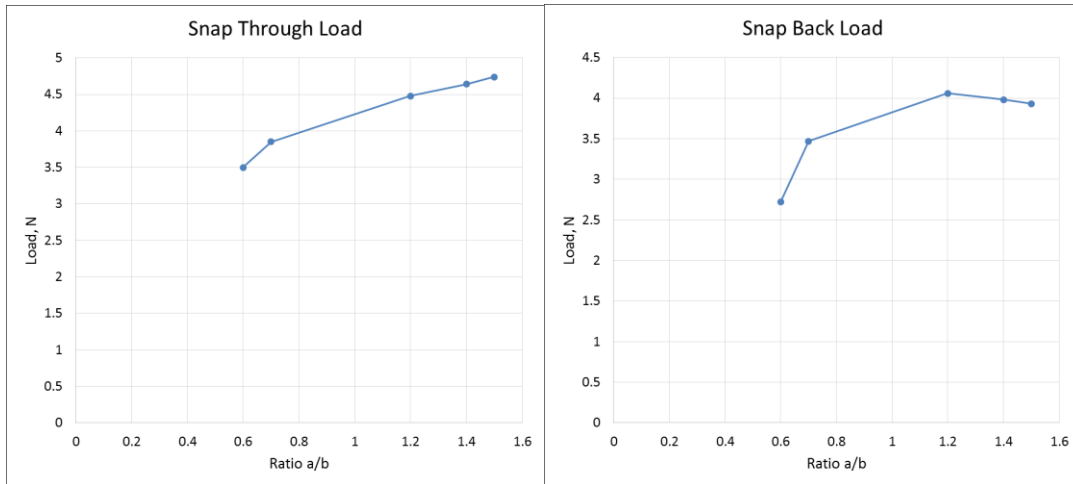


Figure 4.9: Trapezoid – I FEA plots

Trapezoid - II

In this case, as shown in Fig.4.10 the base 'b' was increased and height 'a' was kept constant, thus reducing the 'a/b' ratio. Here the only thing which remained constant was the Count of the 90° direction fibres; all other parameters were varying. The AFL in the 0° direction can be considered as constant because the increase of it was very less in

magnitude compared to the decrease of AFL in the 90° direction. In this way we can still use the interaction charts (Fig.4.2 & 4.3) formulated previously. Initially, the longer fibres were in 0° direction and the shorter fibres were in 90° direction, which got interchanged somewhere between $b = 80$ and 120 mm. Since both the AFL were continuously varying it was difficult to find the exact transition point. Again as the ‘a/b’ ratio was reducing when we increased ‘b’, the trends were identified appropriately, to be inline with other cases and shown in Table 4.4.

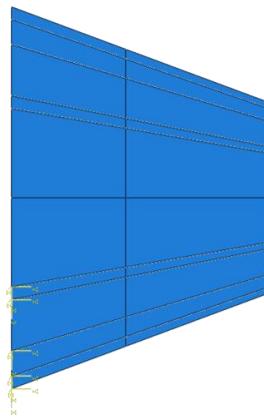


Figure 4.10: Trapezoid – II (Increasing ‘b’, keeping ‘a’ constant)

Results from FEA are plotted in Fig.4.11, and it matched the trend from the table. Unlike Rectangle – I & II, the snap back load trend did not change from Decreasing to Increasing exactly at the same point where it changed from Increasing to Decreasing in case of Trapezoid – I. It changed at a slightly shifted point when $b = 140$ mm instead of 120 mm.

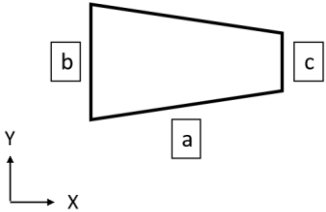
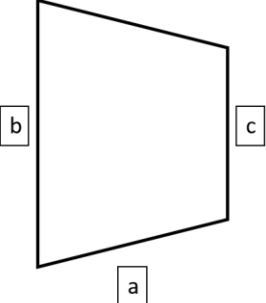
Condition	$b < a$	$b > a$
Geometry		
Dimension a X b mm	100 X 70, 100 X 80	100 X 120, 100 X 140, 100 X 150
Snap Through Load	Decreases with 'a/b' increase (AFL_{long} minor Increase, $Count_{long}$ Decreases)	Decreases with 'a/b' increase (AFL_{long} Decreases, $Count_{long}$ Constant)
Snap Back Load	Decreases with 'a/b' increase (AFL_{short} Decreases, $Count_{short}$ Constant)	Increases with 'a/b' increase (AFL_{short} minor Increase, $Count_{short}$ Decreases)

Table 4.4: Trapezoid – II snap through and snap back load trend

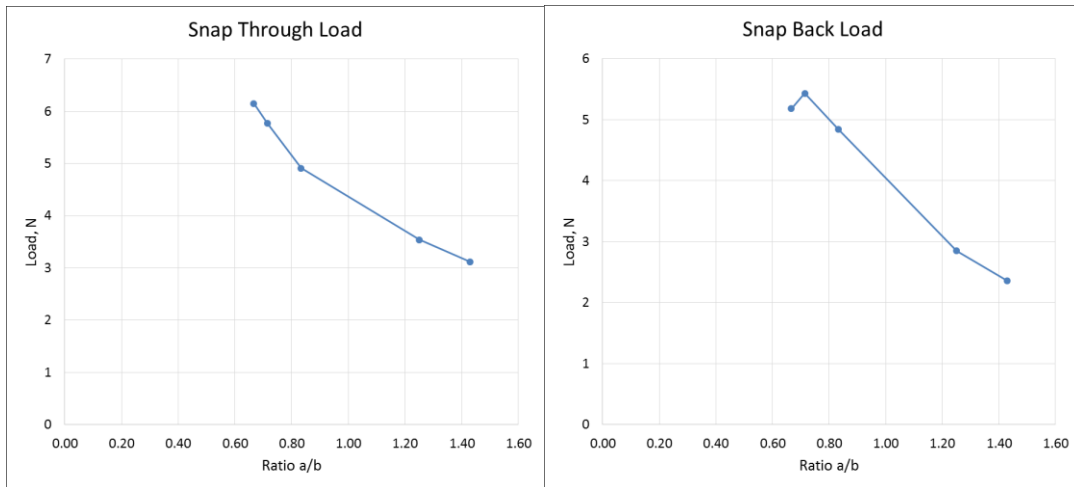


Figure 4.11: Trapezoid – II FEA plots

Triangle - I

In this case, as shown in Fig.4.12 the height 'a' was increased and base 'b' was kept constant, thus increasing the 'a/b' ratio. In this triangular geometry, the AFL of the 90° fibres remained constant at 50 mm and Count of the 0° fibres remained constant,

irrespective of ‘a’ dimension and whether 90° or 0° is the longer / shorter fibre direction. Initially, the longer fibres were in 90° direction and the shorter fibres were in 0° direction, the reversing of the longer and shorter fibre directions did not happen exactly when ‘a’ crossed ‘b’, but as soon as ‘a’ crossed 95 mm the direction shift occurred same as Trapezoid - I.

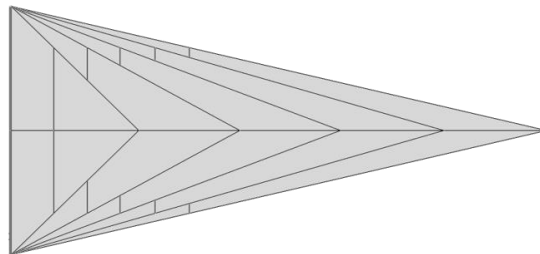


Figure 4.12: Triangle – I (Increasing ‘a’, keeping ‘b’ constant)

When the trend of the snap through load is observed it remained exactly the same as that of Trapezoid – I but the snap back load started decreasing from 70 mm onward rather than 120 mm (where it started decreasing in Trapezoid – I) as shown in Table 4.5. Also it matched well with the FEA results plotted in Fig.4.13.

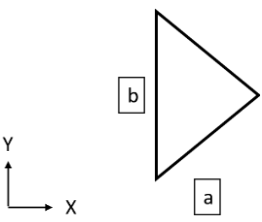
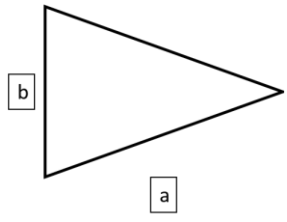
Condition	a < b	a > b
Geometry		
Dimension a X b mm	50 X 100, 70 X 100	110 X 100, 130 X 100, 150 X 100
Snap Through Load	Increases with ‘a/b’ increase (AFL _{long} Constant, Count _{long} Increases)	Increases with ‘a/b’ increase (AFL _{long} Increases, Count _{long} Constant)
Snap Back Load	Increases with ‘a/b’ increase (AFL _{short} Increases, Count _{short} Constant)	Decreases with ‘a/b’ increase (AFL _{short} Constant, Count _{short} Increases)

Table 4.5: Triangle – I snap through and snap back load trend

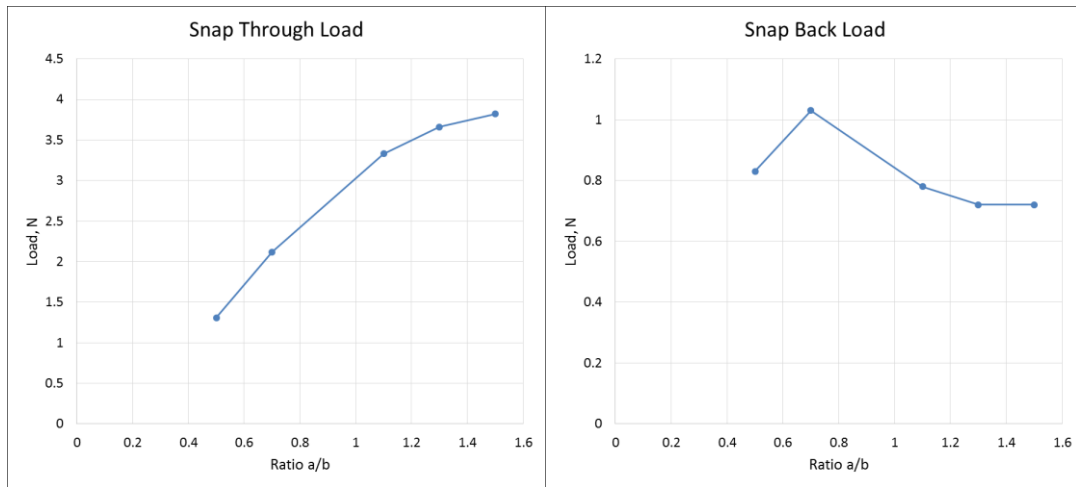


Figure 4.13: Triangle – I FEA plots

Triangle - II

In this case, as shown in Fig.4.14 the base ‘b’ was increased and height ‘a’ was kept constant, thus reducing the ‘a/b’ ratio. Here the only thing which remained constant was the Count of the 90° direction fibres; all other parameters were varying. The AFL in the 0° direction can be considered as constant because the increase of it was very less in magnitude compared to the decrease of AFL in the 90° direction. In this way we can still use the interaction charts (Fig.4.2 & 4.3) formulated previously. Initially, the longer fibres were in 0° direction and the shorter fibres were in 90° direction, which got interchanged somewhere between a = 90 and 110 mm. Since both the AFL were continuously varying it was difficult to find the exact transition point.

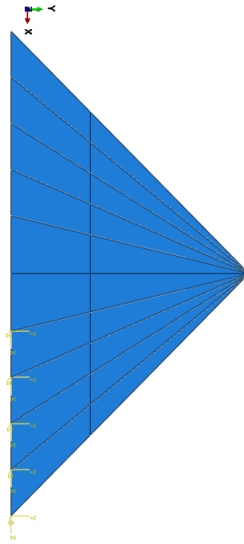


Figure 4.14: Triangle – II (Increasing ‘b’, keeping ‘a’ constant)

Results from FEA are plotted in Fig.4.15, and it matched well with the trends shown in Table 4.6. Similar to Trapezoid – I & II, the snap back load trend changed from Decreasing to Increasing at a shifted point when $b = 130$ mm instead of 70 mm, where it changed from Increasing to Decreasing in the case of Triangle - I.

Condition	$b < a$	$b > a$
Geometry		
Dimension a X b mm	100 X 70, 100 X 90	100 X 110, 100 X 130, 100 X 150
Snap Through Load	Decreases with ‘a/b’ increase (AFL_{long} minor Increase, $Count_{long}$ Decreases)	Decreases with ‘a/b’ increase (AFL_{long} Decreases, $Count_{long}$ Constant)
Snap Back Load	Decreases with ‘a/b’ increase (AFL_{short} Decreases, $Count_{short}$ Constant)	Increases with ‘a/b’ increase (AFL_{short} minor Increase, $Count_{short}$ Decreases)

Table 4.6: Triangle – II snap through and snap back load trend

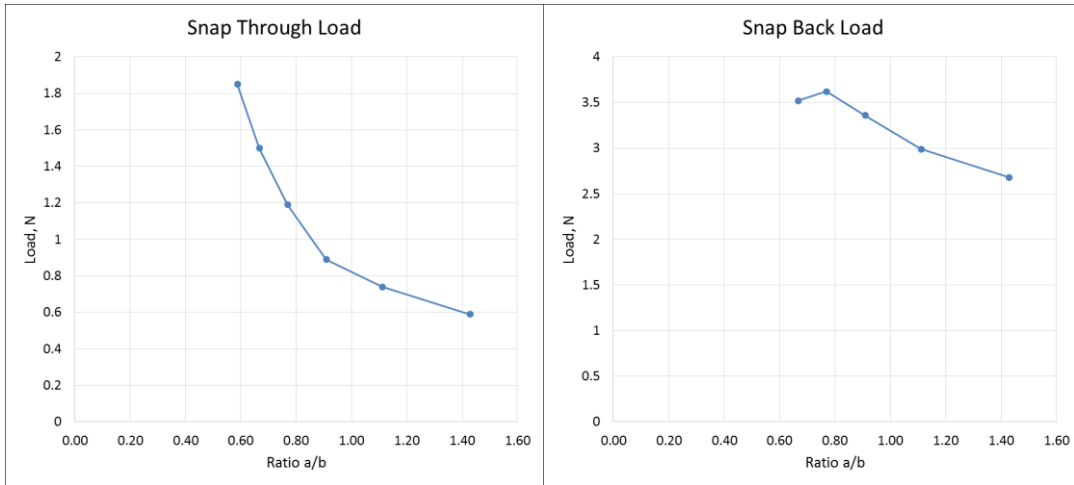


Figure 4.15: Triangle – II FEA plots

Types of Triangle

Since the main concentration is on Triangle geometry and in Triangle – I & II cases, it was only possible to analyse isosceles triangles, one more study was conducted to specifically look at different types of triangle. Keeping the base & height dimensions constant and just by changing the three internal angles of a triangle, different types of triangle can be formed. In Fig.4.16 (a), if α or β or γ is kept at 90° and the sum of the other 2 angles is kept at 90° , it becomes a right angle triangle; if α , β & γ are kept less than 90° , it becomes an acute triangle and if any two of α , β & γ are made equal and the third angle is kept less than 90° , it becomes an isosceles triangle. Obtuse triangles were not considered, as the centroid of those triangles moves outside the geometry. For example, keeping $b = 100$ mm & $a = 140$ mm, considering three cases where (1) $\beta = 90^\circ$ & $\alpha + \gamma = 90^\circ$, (2) $\beta = 79.875^\circ$, $\alpha = 61.821^\circ$ & $\gamma = 38.304^\circ$ and (3) $\beta = \alpha = 70.346^\circ$ & $\gamma = 39.308^\circ$ gives all three types as shown in Fig.4.16 (b). Also, triangles 4 & 5 can be formed just by reversing the angles α and β of triangles 1 & 2.

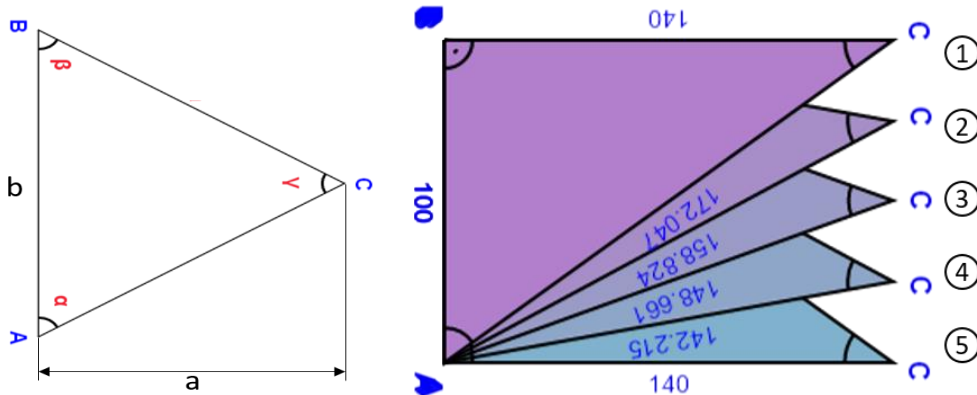


Figure 4.16: (a) Triangle notation, (b) Representation of triangle types

Instead of changing the angles, all these types of triangle can also be formed just by altering the vertical distance of edge 'C' from the center point of the baseline 'A-B' while maintaining the horizontal distance of edge 'C' from baseline 'A-B' constant. For example, if the vertical distance is half of the baseline length, it forms a right angle triangle; if it is zero, it forms an isosceles triangle and if it is anywhere between half of the baseline length and zero, it forms an acute triangle.

Triangle Geometry	Post Fab Shape	Post Load Shape

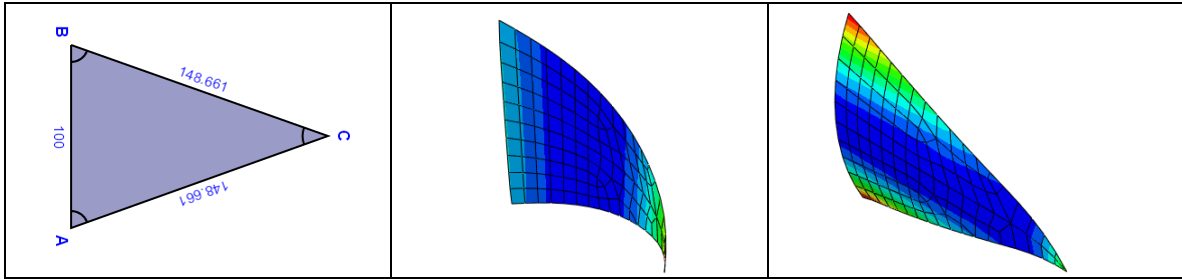


Table 4.7: Post fab and post load shapes of different types of triangle

As shown in Table 4.7, all three triangles had a similar post fab and post load shapes. As far as the loads were concerned, when the geometry moved towards isosceles triangle from right angle triangle, snap through load increased and snap back load decreased as shown in Fig. 4.17.

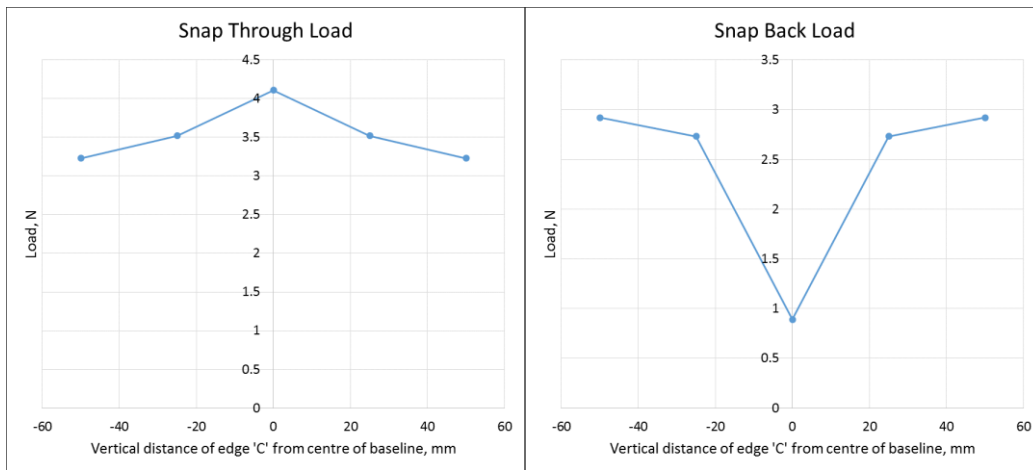


Figure 4.17: Types of triangle FEA plots

There was no change in the longer fibre and shorter fibre directions, as the shape changed from right angle triangle to isosceles triangle. The longer fibres were in the 0° direction and shorter fibres were in the 90° direction for all three types of triangle. AFL_{long} increased as the shape changed from right angle to isosceles and $Count_{long}$ remained constant, which means from the interaction charts, the snap through load increases. Both the AFL_{short} and $Count_{short}$ remained constant, as the shape changed from

right angle to isosceles, but still there was a decrease in the snap back load, this was attributed to the distribution of fibres. Because in right angle triangle, along one of the edges 'B-C' all the 90° fibre (shorter fibre) ends were aligned and as the shape changed, the alignment was lost along that edge and in case of an isosceles triangle the edge did not have any of the 90° fibre ends aligned. This caused a decrease in snap back load as the shape changed.

Effect of Fibre Orientation on the Snap Through and Snap Back Loads of an Individual Unsymmetric Laminate

The effect of fibre orientation was studied for both rectangular and triangular geometries. As this gave a better understanding, and a possibility to generalize the effects irrespective of the geometry.

Rectangle Geometry

To understand the influence of fibre orientation in rectangle, the geometry was maintained constant and the angle of 2 ply's were changed from [0/90] to [90/0] in steps of 15° i.e., [-15/75], [-30/60], [-45/45], [-60/30] and [-75/15]. The difference in angle between the 2 ply's was maintained at 90°, to have a uniform comparison. This was carried out for the different rectangle dimensions considered earlier in the study of effect of geometry and the same trend was observed throughout. The major observations are,

- The inverse angle combinations [0/90] & [90/0], [-15/75] & [-75/15] and so forth, had same snap through & snap back load values, only the concave / convex shape in the post fab & post load states were reversed.

- $[-45/45]$ had a saddle shape and did not exhibit snap through or snap back phenomenon.
- Both the load values went on decreasing as the first ply angle was increased from 0° till 45° , and then started increasing from 45° till 90° .

For one of the rectangular dimensions (60 X 100 mm), the post fab and post load shapes obtained by varying the ply angles are as shown in Table 4.8. The plot of snap through and snap back loads for the same set of rectangles are as shown in Fig. 4.18.

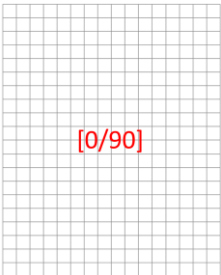
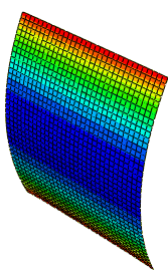
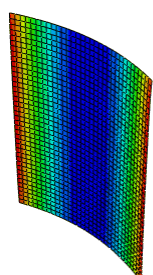
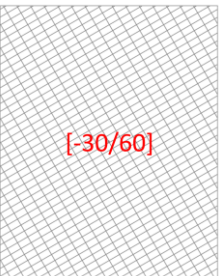
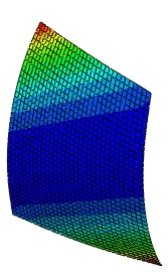
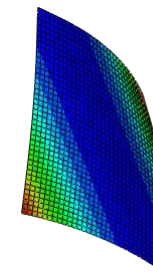
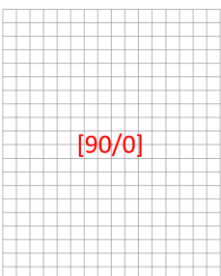
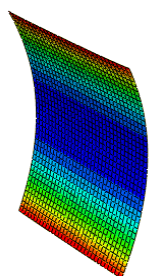
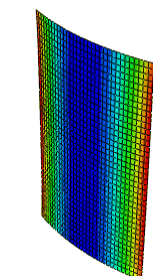
Laminate Structure	Post Fab Shape	Post Load Shape
 <p style="text-align: center;">$[0/90]$</p>		
 <p style="text-align: center;">$[-30/60]$</p>		
 <p style="text-align: center;">$[90/0]$</p>		

Table 4.8: Post fab and post load shapes of different fibre orientation in rectangles

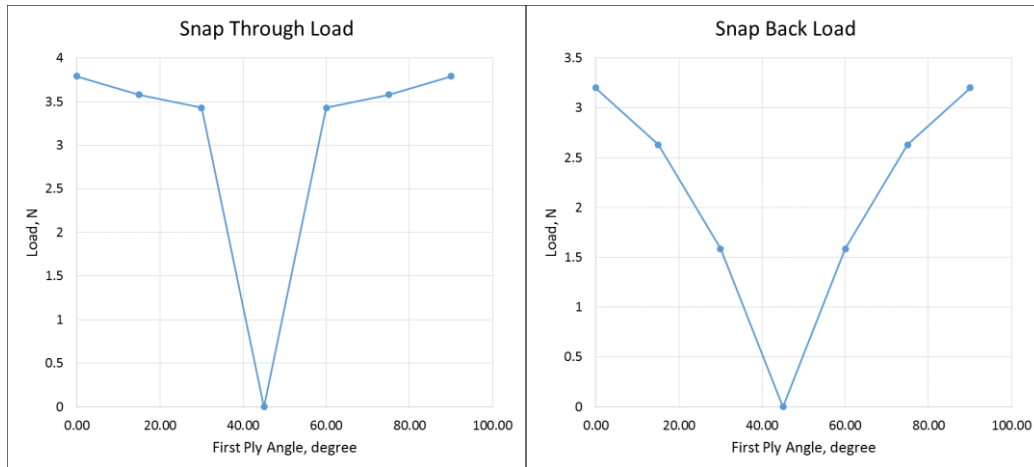


Figure 4.18: Rectangle – fibre orientation FEA plots

From the table it is clearly seen, as the ply angle changes from 0° and 90° , the curvatures are no longer about the global coordinates, but about the local coordinates of the fibres. As stated earlier in Chapter 3, the concave / convex shape is dependent on the position of the longer fibres in the laminate stacking sequence, whether it is on the top side or the bottom side of the midplane. That is the reason when the ply angles were inverted, there was just a reversal of concave / convex shapes, whereas the curvature and load values remained exactly the same. As far as load values are concerned, although both $\text{Count}_{\text{long}}$ and $\text{Count}_{\text{short}}$ vary randomly as the first ply angle was increased, the decrease of AFL_{long} and $\text{AFL}_{\text{short}}$ resulted in the decrease of snap through and snap back loads respectively. In the case of $[-45/45]$, the AFL_{long} and $\text{AFL}_{\text{short}}$, $\text{Count}_{\text{long}}$ and $\text{Count}_{\text{short}}$ were equal, which led to a saddle shape and these laminates did not have the bistable feature.

Triangle Geometry

To understand the influence of fibre orientation in triangle, a specific triangle was selected where the 3 internal angles of the triangle were 40° , 60° and 80° as shown in Fig.

4.19. Such a triangle was selected because it would be easy to change the ply angles and see the effect clearly. To maintain the difference in angle between the 2 ply's at 90° throughout, the first ply was selected perpendicular to each of the three edges and second ply parallel to the same edge. Thus the three laminate stacking sequence chosen for the study were $[0/90]$ (Edge 1), $[60/-30]$ (Edge 2) and $[-80/10]$ (Edge 3).

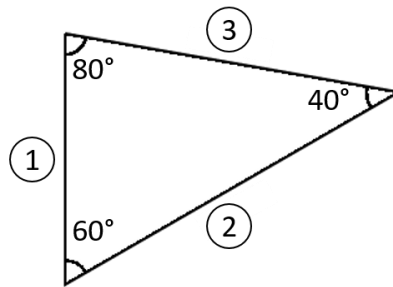


Figure 4.19: 40° - 60° - 80° triangle

Laminate Structure	Post Fab Shape	Post Load Shape

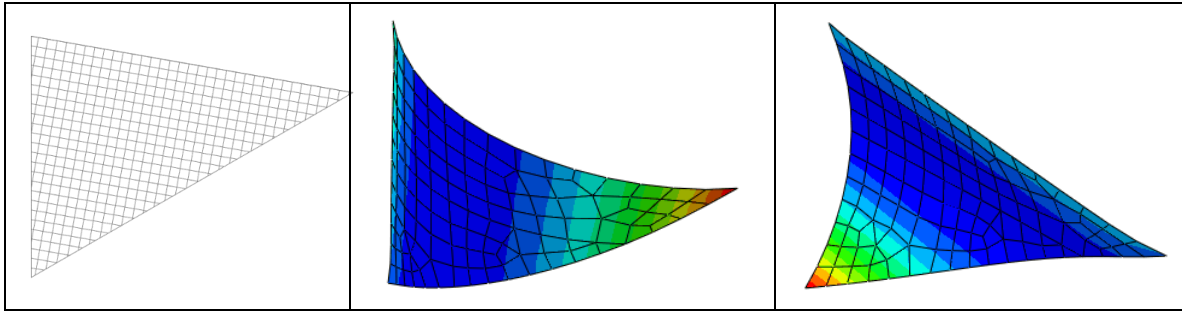


Table 4.9: Post fab and post load shapes of different fibre orientation in triangles

Similar to the rectangles, as the fibre orientation changed, the local coordinate about which the curvature occurs also changed, and in this case, it changed from one edge to the other. As seen from Table 4.9, in the first laminate stacking sequence $[0/90]$, the 0° fibres (perpendicular direction to the edge) were the longer fibres and it was present on the bottom side of the mid plane, making the post fab state to have a concave shape. For the other two laminate stacking sequences, the longer fibres were in the parallel direction to the respective edges i.e., on top side of the midplane, making the post fab state to have a convex shape. There was not any clear pattern noticed in the change of snap through and snap back load values when the fibre orientation was changed, as all the four factors AFL_{long} and $Count_{long}$; AFL_{short} and $Count_{short}$ varied randomly because of the variation in each of the edge lengths.

PART-II: STUDY OF COMBINATION OF SYMMETRIC AND UNSYMMETRIC LAMINATES

There was only a limited amount of work done in literature on the behaviour of different combinations of symmetric and unsymmetric laminates connected to each other. In this research, to get a basic understanding of these kinds of connected laminates, various standard geometries were split into smaller geometries (mainly square, rectangle

and triangle), each of those smaller geometries were made into symmetric / unsymmetric laminates and all different combinations of those laminates were studied. It was possible to achieve many different shapes from any of the standard geometries based on the split up and the laminate stacking sequence (LSS) of the connected symmetric and unsymmetric laminates. The four standard geometries considered are,

- i. Square
- ii. Rectangle
- iii. Circle
- iv. Ellipse

Also two shape morphing applications in an automobile were identified and the laminate configurations needed to achieve the desired bistable shapes in those two applications were determined. The applications considered are,

- i. Headrest
- ii. Spoiler

Square Geometry

The square geometry was split in two different ways, first it was split into four equal smaller squares as shown in Fig. 4.20 (a) and second it was split into nine smaller squares as shown in Fig. 4.20 (b).

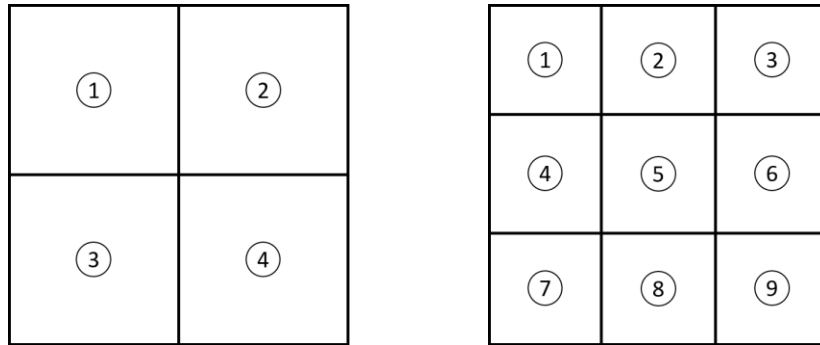


Figure 4.20: (a) Four squares split-up (b) Nine squares split-up

Four Squares

The LSS of all the four squares were altered such that it formed all possible combinations of symmetric and unsymmetric laminates. ‘S’ denotes symmetric laminate with $[0/90]_S$ LSS and ‘U’ denotes unsymmetric laminate with $[0_2/90_2]_T$ LSS. The four unique combinations formed were SUUS, SUSU, SUSS and UUSU in the numbering order shown in Fig.4.21 (a). For example, in the first case the squares 1 & 4 were made as symmetric laminates and the squares 2 & 3 were made as unsymmetric laminates. Even though, there are $4^2 = 16$ combinations possible, this being a bisymmetric structure, there are only four unique combinations and all others are repetitions. All four of these combinations exhibited bistability, their post fab and post load shapes are as shown in Table. 4.10.

Laminate Structure	Post Fab Shape	Post Load Shape				
<table border="1" style="width: 100%; text-align: center;"> <tr> <td style="width: 50%;">Symmetric 0/90/90/0</td> <td style="width: 50%;">Unsymmetric 0/0/90/90</td> </tr> <tr> <td>Unsymmetric 0/0/90/90</td> <td>Symmetric 0/90/90/0</td> </tr> </table>	Symmetric 0/90/90/0	Unsymmetric 0/0/90/90	Unsymmetric 0/0/90/90	Symmetric 0/90/90/0	<p style="text-align: right;">N 0 0 N</p>	<p style="text-align: right;">N 1 1 N</p>
Symmetric 0/90/90/0	Unsymmetric 0/0/90/90					
Unsymmetric 0/0/90/90	Symmetric 0/90/90/0					

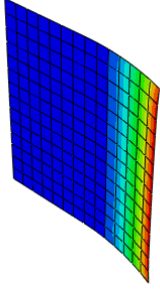
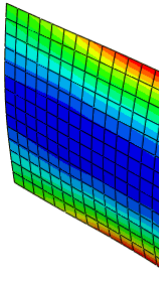
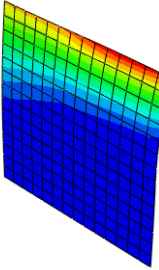
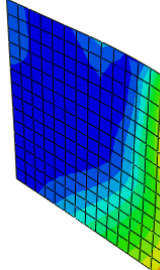
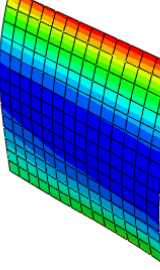
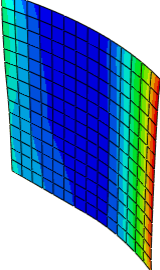
<table border="1"> <tbody> <tr> <td data-bbox="277 268 418 409">Symmetric 0/90/90/0</td> <td data-bbox="423 268 565 409">Unsymmetric 0/0/90/90</td> </tr> <tr> <td data-bbox="277 415 418 556">Symmetric 0/90/90/0</td> <td data-bbox="423 415 565 556">Unsymmetric 0/0/90/90</td> </tr> </tbody> </table>	Symmetric 0/90/90/0	Unsymmetric 0/0/90/90	Symmetric 0/90/90/0	Unsymmetric 0/0/90/90	 N 0 N 0	 N 1 N 1
Symmetric 0/90/90/0	Unsymmetric 0/0/90/90					
Symmetric 0/90/90/0	Unsymmetric 0/0/90/90					
<table border="1"> <tbody> <tr> <td data-bbox="277 617 418 758">Symmetric 0/90/90/0</td> <td data-bbox="423 617 565 758">Unsymmetric 0/0/90/90</td> </tr> <tr> <td data-bbox="277 764 418 905">Symmetric 0/90/90/0</td> <td data-bbox="423 764 565 905">Symmetric 0/90/90/0</td> </tr> </tbody> </table>	Symmetric 0/90/90/0	Unsymmetric 0/0/90/90	Symmetric 0/90/90/0	Symmetric 0/90/90/0	 N 0 N N	 N 1 N N
Symmetric 0/90/90/0	Unsymmetric 0/0/90/90					
Symmetric 0/90/90/0	Symmetric 0/90/90/0					
<table border="1"> <tbody> <tr> <td data-bbox="277 966 418 1106">Unsymmetric 0/0/90/90</td> <td data-bbox="423 966 565 1106">Unsymmetric 0/0/90/90</td> </tr> <tr> <td data-bbox="277 1113 418 1253">Symmetric 0/90/90/0</td> <td data-bbox="423 1113 565 1253">Unsymmetric 0/0/90/90</td> </tr> </tbody> </table>	Unsymmetric 0/0/90/90	Unsymmetric 0/0/90/90	Symmetric 0/90/90/0	Unsymmetric 0/0/90/90	 0 0 N 0	 1 1 N 1
Unsymmetric 0/0/90/90	Unsymmetric 0/0/90/90					
Symmetric 0/90/90/0	Unsymmetric 0/0/90/90					

Table 4.10: Post fab and post load shapes of different combination of four squares

In Table 4.10, the curvature about x-axis is marked as ‘0’, curvature about y-axis is marked as ‘1’ and no curvature is marked as ‘N’. In all four combinations, the symmetric laminates remained flat without any curvature in both the post fab and post load shapes. And the unsymmetric laminates had curvature about x-axis in the post fab shape and curvature about y-axis in the post load shape.

Nine Squares

Two different sets of symmetric / unsymmetric laminate arrangement is formed with the nine squares. In the first set, the square 5 in Fig. 4.20 (b) alone was made as unsymmetric laminate, and all other squares were made as symmetric laminates. The second set is the reverse of the first set i.e., square 5 alone was made as symmetric laminate and all other squares were made as unsymmetric laminates. The study is conducted by increasing the size of square 5 in both sets while maintaining the overall size to be constant. Thus the squares 2, 4, 6 & 8 will no longer be squares and will change to rectangles whereas squares 1, 3, 7 & 9 will become much smaller squares.

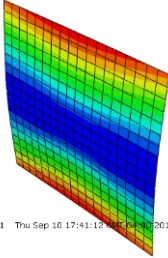
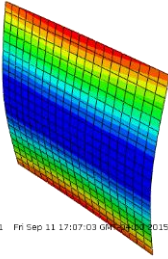
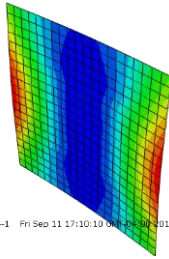
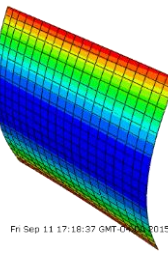
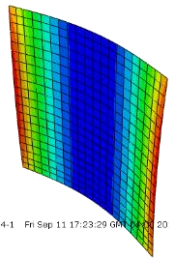
Laminate Structure	Post Fab Shape	Post Load Shape									
<table border="1" style="width: 100%; text-align: center;"> <tr> <td>0/90/90/0</td> <td>0/90/90/0</td> <td>0/90/90/0</td> </tr> <tr> <td>0/90/90/0</td> <td style="color: red;">0/0/90/90</td> <td>0/90/90/0</td> </tr> <tr> <td>0/90/90/0</td> <td>0/90/90/0</td> <td>0/90/90/0</td> </tr> </table>	0/90/90/0	0/90/90/0	0/90/90/0	0/90/90/0	0/0/90/90	0/90/90/0	0/90/90/0	0/90/90/0	0/90/90/0	 <p style="text-align: center; font-size: small;">4-1 Thu Sep 10 17:41:12 GMT+05:30 2015</p>	
0/90/90/0	0/90/90/0	0/90/90/0									
0/90/90/0	0/0/90/90	0/90/90/0									
0/90/90/0	0/90/90/0	0/90/90/0									
<table border="1" style="width: 100%; text-align: center;"> <tr> <td>0/90/90/0</td> <td>0/90/90/0</td> <td>0/90/90/0</td> </tr> <tr> <td>0/90/90/0</td> <td style="color: red;">0/0/90/90</td> <td>0/90/90/0</td> </tr> <tr> <td>0/90/90/0</td> <td>0/90/90/0</td> <td>0/90/90/0</td> </tr> </table>	0/90/90/0	0/90/90/0	0/90/90/0	0/90/90/0	0/0/90/90	0/90/90/0	0/90/90/0	0/90/90/0	0/90/90/0	 <p style="text-align: center; font-size: small;">4-1 Fri Sep 11 17:07:03 GMT+05:30 2015</p>	 <p style="text-align: center; font-size: small;">4-1 Fri Sep 11 17:10:10 GMT+05:30 2015</p>
0/90/90/0	0/90/90/0	0/90/90/0									
0/90/90/0	0/0/90/90	0/90/90/0									
0/90/90/0	0/90/90/0	0/90/90/0									
<table border="1" style="width: 100%; text-align: center;"> <tr> <td>0/90/90/0</td> <td>0/90/90/0</td> <td>0/90/90/0</td> </tr> <tr> <td>0/90/90/0</td> <td style="color: red;">0/0/90/90</td> <td>0/90/90/0</td> </tr> <tr> <td>0/90/90/0</td> <td>0/90/90/0</td> <td>0/90/90/0</td> </tr> </table>	0/90/90/0	0/90/90/0	0/90/90/0	0/90/90/0	0/0/90/90	0/90/90/0	0/90/90/0	0/90/90/0	0/90/90/0	 <p style="text-align: center; font-size: small;">4-1 Fri Sep 11 17:18:37 GMT+05:30 2015</p>	 <p style="text-align: center; font-size: small;">4-1 Fri Sep 11 17:23:29 GMT+05:30 2015</p>
0/90/90/0	0/90/90/0	0/90/90/0									
0/90/90/0	0/0/90/90	0/90/90/0									
0/90/90/0	0/90/90/0	0/90/90/0									

Table 4.11: Post fab and post load shapes of different combination of nine squares - I

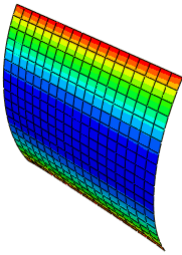
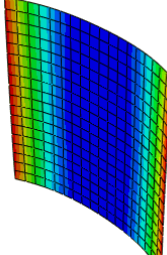
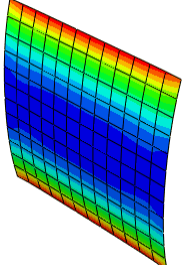
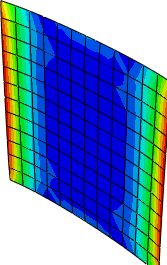
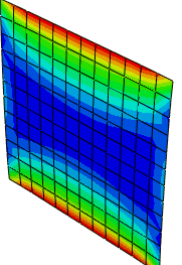
Laminate Structure	Post Fab Shape	Post Load Shape															
<table border="1"> <tr> <td>0/0/90/90</td> <td>0/0/90/90</td> <td>0/0/90/90</td> </tr> <tr> <td>0/0/90/90</td> <td>0/90/90/0</td> <td>0/0/90/90</td> </tr> <tr> <td>0/0/90/90</td> <td>0/0/90/90</td> <td>0/0/90/90</td> </tr> </table>	0/0/90/90	0/0/90/90	0/0/90/90	0/0/90/90	0/90/90/0	0/0/90/90	0/0/90/90	0/0/90/90	0/0/90/90								
0/0/90/90	0/0/90/90	0/0/90/90															
0/0/90/90	0/90/90/0	0/0/90/90															
0/0/90/90	0/0/90/90	0/0/90/90															
<table border="1"> <tr> <td>0/0/90/90</td> <td>0/0/90/90</td> <td>0/0/90/90</td> </tr> <tr> <td></td> <td></td> <td></td> </tr> <tr> <td>0/0/90/90</td> <td>0/90/90/0</td> <td>0/0/90/90</td> </tr> <tr> <td></td> <td></td> <td></td> </tr> <tr> <td>0/0/90/90</td> <td>0/0/90/90</td> <td>0/0/90/90</td> </tr> </table>	0/0/90/90	0/0/90/90	0/0/90/90				0/0/90/90	0/90/90/0	0/0/90/90				0/0/90/90	0/0/90/90	0/0/90/90		
0/0/90/90	0/0/90/90	0/0/90/90															
0/0/90/90	0/90/90/0	0/0/90/90															
0/0/90/90	0/0/90/90	0/0/90/90															
<table border="1"> <tr> <td>0/0/90/90</td> <td>0/0/90/90</td> <td>0/0/90/90</td> </tr> <tr> <td></td> <td></td> <td></td> </tr> <tr> <td>0/90/90/0</td> <td>0/90/90/0</td> <td>0/90/90/0</td> </tr> <tr> <td></td> <td></td> <td></td> </tr> <tr> <td>0/0/90/90</td> <td>0/0/90/90</td> <td>0/0/90/90</td> </tr> </table>	0/0/90/90	0/0/90/90	0/0/90/90				0/90/90/0	0/90/90/0	0/90/90/0				0/0/90/90	0/0/90/90	0/0/90/90		
0/0/90/90	0/0/90/90	0/0/90/90															
0/90/90/0	0/90/90/0	0/90/90/0															
0/0/90/90	0/0/90/90	0/0/90/90															

Table 4.12: Post fab and post load shapes of different combination of nine squares – II

The various bistable shapes obtained for three different sizes of square 5 in first set are shown in Table 4.11 and in second set are shown in Table 4.12. In the first set, initially when the size of square 5 was same as all the other squares, it was not bistable and had only post fab shape, that too almost flat without any curvature. But as the size started increasing, the bistable feature was observed and also the curvature in both shapes were increasing in a directly proportional manner. The second set had the reverse case, the curvature started decreasing with the increase in size of square 5 and after a specific point, it lost bistability as the unsymmetric laminates were comparatively very small in size and it almost behaved like a symmetric laminate.

Rectangle Geometry

The rectangle geometry was split into three triangles (two right angle triangle and one acute triangle). The main advantage of splitting geometries using triangles is that, each geometry can be split into how many ever triangles needed and whatever may be the number of triangles chosen to split the geometry, each of those triangle sizes can be altered in many different ways to approximate the given geometry. In this case, the sizes of the three triangles chosen are altered in the specific way as shown in Fig. 4.21.

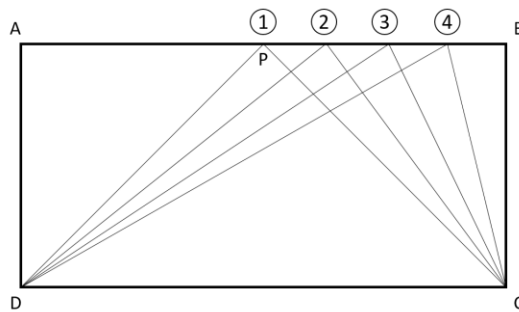


Figure 4.21: Split-up of rectangle geometry into three triangles

The point 'P' is moved along the edge 'A-B' from its initial point (the midpoint of edge 'A-B') towards the corner 'B'. In each position of 'P' marked as 1, 2, 3 & 4, the line joining the corners 'C' and 'D' to the point 'P' splits the rectangle into two right angle triangles and one acute triangle. Even if the point 'P' is moved towards the corner 'A', same set of triangles only will be formed, so to avoid repetition, the four sets of triangles shown in Fig.4.21 alone are considered for the study. Since there are three triangular laminates forming the rectangle geometry and each can be made either symmetric or unsymmetric, there are 6 possible combinations and along with the four sets of different size triangles, a total of 24 variations are considered for the study. The post fab and post load shapes of all these variations are shown in Table 4.13.

	Post Fab	Post Load	Post Fab	Post Load	Post Fab	Post Load	Post Fab	Post Load
USS								
UUS								
USU								
SUS								
SUU								
SSU								

Table 4.13: Post fab and post load shapes of different combination of three triangles forming rectangle

The arrangements SUU & SSU for the first set of triangles are left blank because they are the same as UUS & USS, as point 'P' lies on the midpoint of edge 'A-B' making both the right triangles to be of the same size. Wherever the post load shape is left blank, those variations did not have the bistable feature, the main reason being in all those cases the symmetric laminate sizes was comparatively larger than the unsymmetric laminate sizes. If the triangle ADP was considered specifically, it can be seen from the post fab shape of the first three arrangements, moving from triangle sets 1 to 4, the curvature increase as the edge length of the triangle increases. It is the exact opposite for the triangle BCP, the curvature decreases as its edge length decreases. In the post load shape of the arrangements UUS & SUS, it might look like the symmetric laminates are having curvature, but it is seen that way only because of the application of fixed boundary conditions in the center point of the overall geometry as explained in Chapter 3.

Circle Geometry

A circular geometry with two concentric circles was considered, where the inner circle had a radius equal to one third of the outer circle. The inner circle splits the overall geometry into two portions. The outer circle was approximated with three different polygons in an ascending order of the number of sides such as 10-, 12- and 16-sided. Each of those polygons were split into equally sized triangles, the number of triangles being the same as the number of sides of the polygon. For example, a 10-sided polygon, was split into 10 triangles as shown in Fig.4.22 (a).

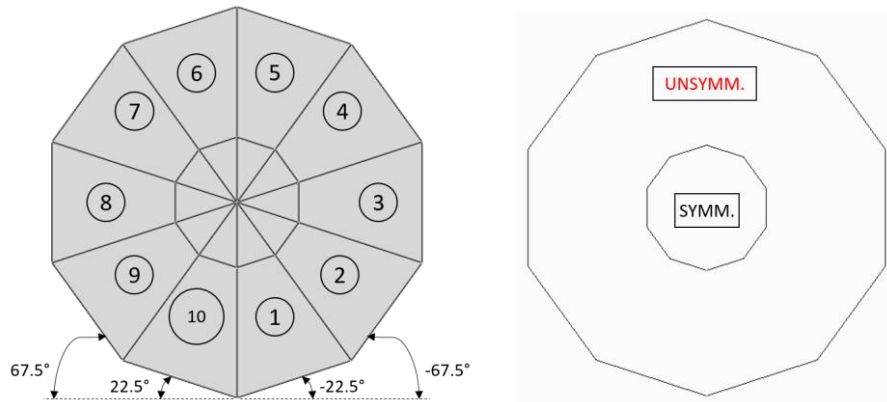


Figure 4.22: (a) Circle approximation – 10 sided polygon, (b) LSS representation

Since the inner circle was also approximated, all the triangles were divided into smaller triangles in the inner portion and trapezoids in the outer portion. The inner portion triangles were made as symmetric laminates and the outer portion trapezoids were made as unsymmetric laminates as shown in Fig.4.22 (b). The LSS selected for the unsymmetric laminates were such that, the fibre orientation in the first & second layers were parallel to the outer edge of the trapezoids (along the circle periphery) and third & fourth layers were perpendicular to it. In Fig.4.22 (a), the LSS of the unsymmetric trapezoidal laminates 1, 2 and 3 were selected as $[-22.5_2/67.5_2]_T$, $[-67.5_2/22.5_2]_T$ and $[90_2/0_2]_T$ respectively and the LSS of their corresponding symmetric triangular laminates were selected as $[-22.5/67.5]_S$, $[-67.5/22.5]_S$ and $[90/0]_S$. Thus the LSS of the symmetric laminates were realized by just rearranging the layers of the respective unsymmetric laminates and keeping the fibre angles unchanged.

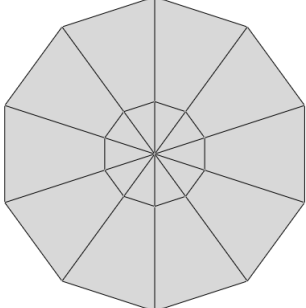
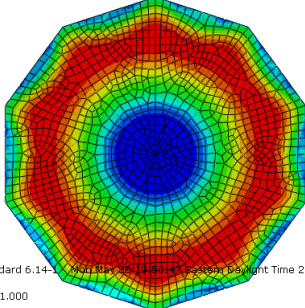
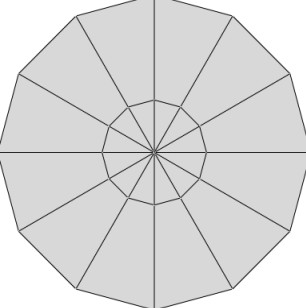
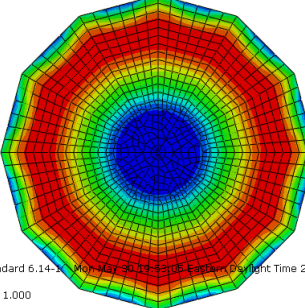
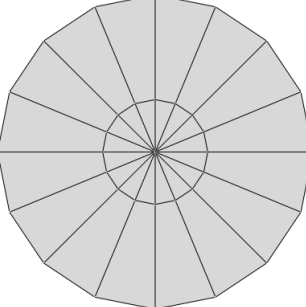
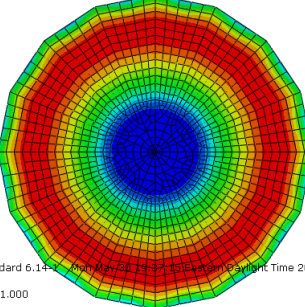
Laminate Structure	Post Fab Shape
	 <p data-bbox="933 546 1274 598">Standard 6.14-1 - 2016 May 21 13:52:05 Eastern Daylight Time 2016 = 1.000 See Scale Factor: +1.000e+00</p>
	 <p data-bbox="933 871 1274 924">Standard 6.14-1 - 2016 May 21 13:52:05 Eastern Daylight Time 2016 = 1.000 See Scale Factor: +1.000e+00</p>
	 <p data-bbox="933 1201 1274 1253">Standard 6.14-1 - 2016 May 21 13:52:05 Eastern Daylight Time 2016 = 1.000 See Scale Factor: +1.000e+00</p>

Table 4.14: Post fab shapes of different polygon approximations

As shown in Table 4.14, all the approximations gave similar results, the symmetric laminates remained flat and unsymmetric laminates had a curvature. These structures had only one stable shape and they did not have the bistable feature. Even though this research mainly concentrates on shape morphing bistable laminates, these kind of structures can find applications in the manufacturing field, where a plain mold can be used to form specified curvatures instead of using complex shaped molds.

Ellipse Geometry

One standard ellipse geometry and two variations of it have been studied. All three geometries and their tessellated versions are as shown in Fig.4.23.

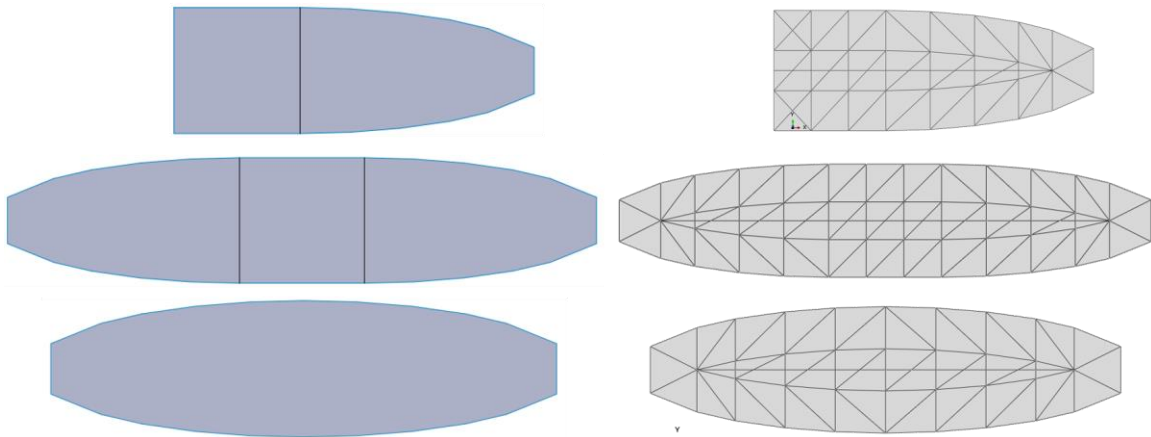


Figure 4.23: Tessellation of ellipse and its two variations

In the first variation, only one half of the ellipse was attached to a square geometry and in the second variation both halves of the ellipse were attached to either side of the square geometry. The tessellation was done in a specific manner, such that whatever angle the outer edge of the triangles (along the periphery of the ellipse) makes with the horizontal base line is a whole number. Also the triangles were grouped together based on their LSS. The LSS of each of those groups in all three structures and their respective post fab shapes are shown in Table 4.15.

Laminate Structure	Post Fab Shape

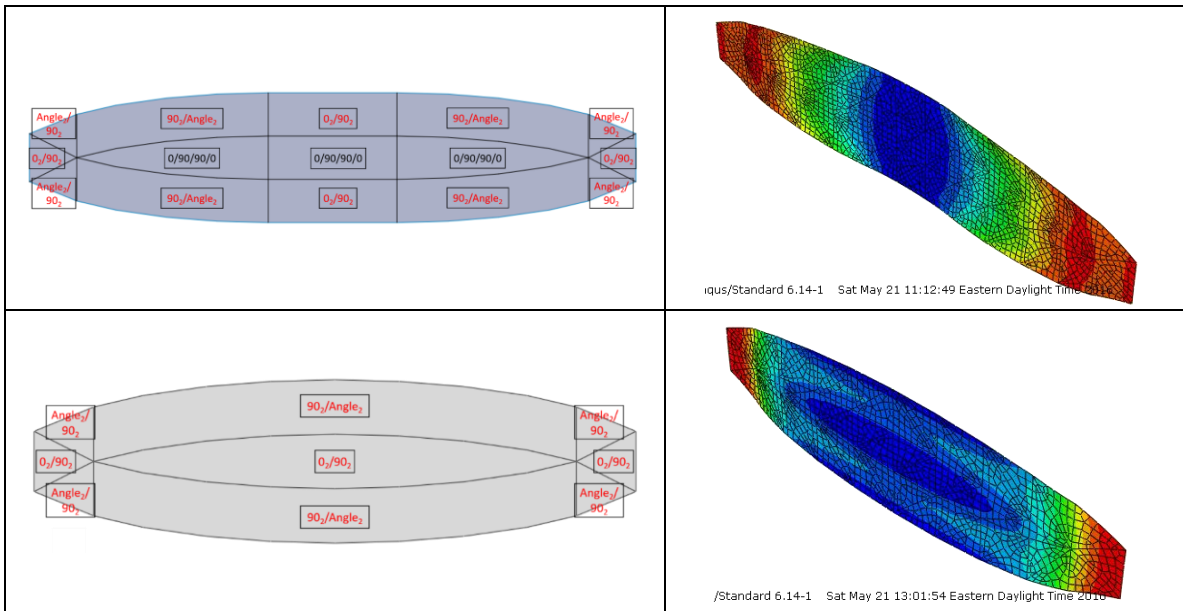


Table 4.15: LSS and post fab shapes of ellipse and its variations

The main objective was to make the entire outer edge curved towards either the top side or the bottom side. To attain this objective, the LSS of each and every group of triangles was altered. After many iterations, it has been achieved in all three structures as can be seen in Table 4.15. The exaggerated view of the lower portion of the first structure is shown in Fig.4.24, to provide a better explanation of the LSS selected for these structures. The LSS of the triangles 1 & 2 - $[0_2/90_2]_T$, 3 & 4 - $[90_2/-1.5_2]_T$, 5 & 6 - $[90_2/-4.5_2]_T$ and 7 & 8 - $[90_2/-8_2]_T$. The triangles 3 to 8 has been grouped into $[90_2/Angle_2]_T$ for easier representation in the table, all other regions are also grouped in similar lines.

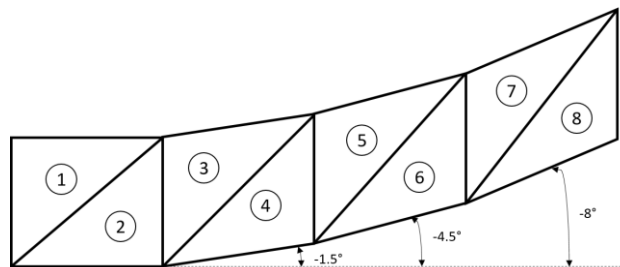
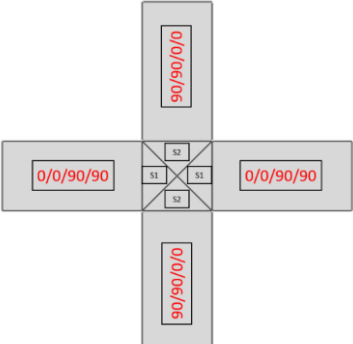
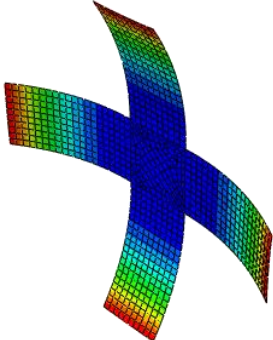
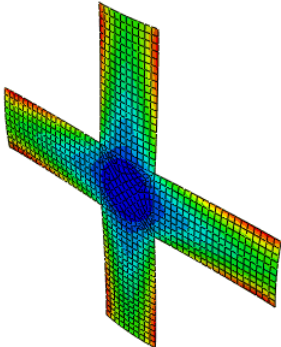


Figure 4.24: Blown up view of the tessellated lower portion of first ellipse variation

There was one major difference between the ellipse geometry and the circle geometry, the difference in angle between the layers about the midplane was not maintained at 90° in the ellipse geometry. The fibres in the bottom side of the midplane was oriented parallel to the outer edge of the triangles (along the periphery) and top side of the midplane was 90° irrespective of the angle of the bottom side, also for few triangles the top and bottom sides were reversed. Similar to circle geometry, here again none of the three structures exhibited bistability and had only one stable shape.

Headrest Application

Head rest in an automobile comes in 2 different types, the flat type headrest and the protruded type headrest. Using bistable composites, it is possible to combine both these types in a single structure and also interchange between the two types, as per the user comfort. To attain this objective, a plus shaped laminate structure was selected. The plus shape was split into four rectangles on the four legs and four triangles on the middle square portion. All the rectangles were made as unsymmetric laminates and all the triangles were made as symmetric laminates.

Laminate Structure	Post Fab Shape	Post Load Shape
		

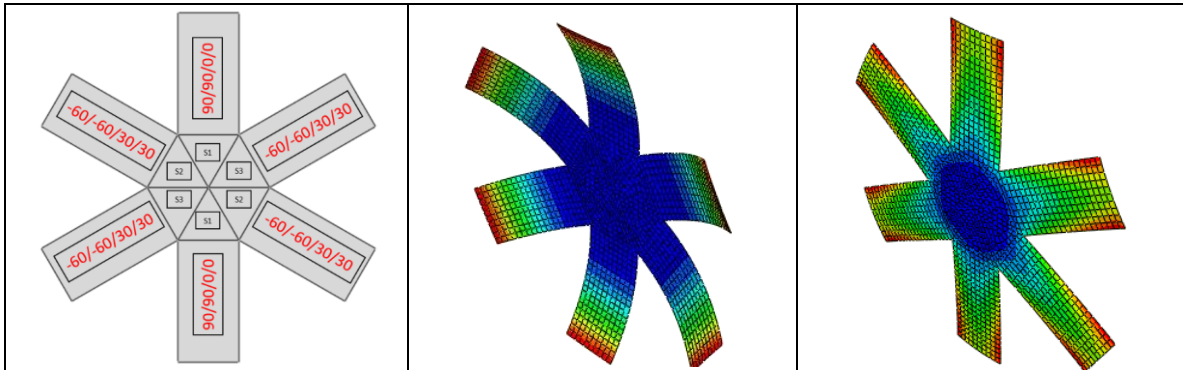


Table 4.16: Post fab and post load shapes of two variations of plus structure

The LSS, the post fab and post load shapes are as shown in Table 4.16. There were two types of unsymmetric LSS – $[0_2/90_2]_T$ (Horizontal legs) & $[90_2/0_2]_T$ (Vertical legs) and two types of symmetric LSS – $[0/90]_S$ (S1) & $[90/0]_S$ (S2) used in the plus shape to achieve the desired shapes. Also this kind of a structure is not only restricted to the plus shape, if the middle square is replaced by a hexagon or any other polygon with increased number of legs and the LSS are changed accordingly, this would still work. The way in which the two shapes of this plus structure can be used for the headrest application is as shown in Fig.4.25. If all the four legs are connected using a curtain spring and the overall structure is covered by a fabric material which can stretch, then just by applying a load in the middle of the structure, the two shapes can be interchanged.

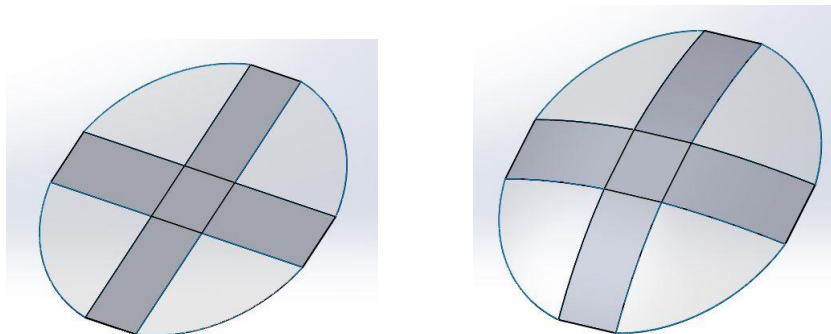


Figure 4.25: Flat type and protruded type headrest with plus shaped understructure

Spoiler Application

Spoilers are generally used as extra attachment in an automobile in its rear end, to change the air flow across the body to improve its aerodynamics. So it needs to be separately assembled whenever it is required and then dismantled, depending on the desired performance. By making the body component in the rear end of the automobile out of bistable composites, the spoiler arrangement can be added as an in-built feature. One of the two stable shapes can simulate the condition with spoiler and the other without spoiler. The laminate structure selected for this purpose, the LSS and the two stable shapes are as shown in Table 4.17. Three structures were considered. The first and second structures were the same, only difference being the radii added in the joining locations. This is because straight edges that are present in the first structure cannot be fabricated. The third structure had a slightly different LSS, which would be more suitable for the spoiler application. In all three structures, the LSS of the unsymmetric laminates were $[0_2/90_2]_T$ and the LSS of the symmetric laminates were $[0/90]_S$. In the first two structures, the middle two laminates were made unsymmetric and rest all were made symmetric. In the third structure, one more symmetric laminate was added between the middle two unsymmetric laminates, and all other symmetric laminates remained the same.

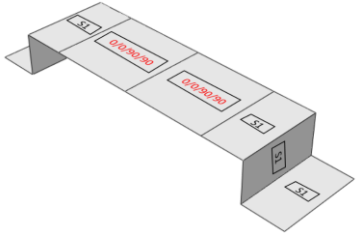
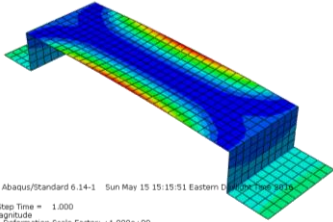
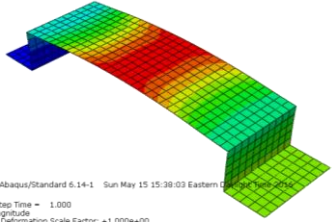
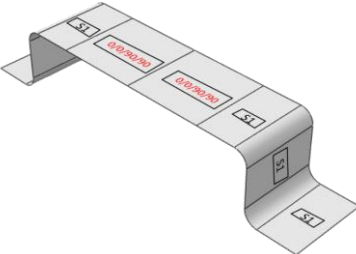
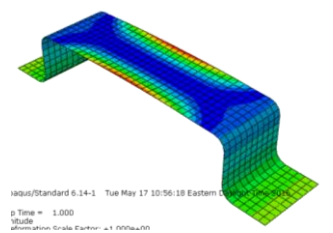
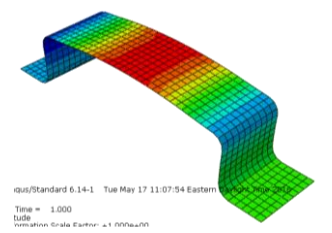
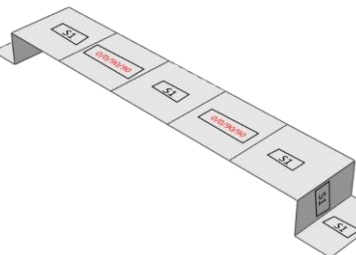
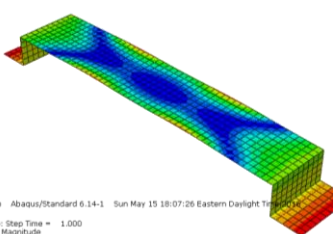
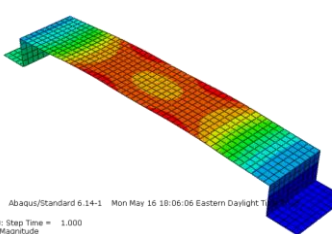
Laminate Structure	Post Fab Shape	Post Load Shape
	 <p data-bbox="662 506 971 548">Abaqus/Standard 6.14-1 Sun May 15 15:15:51 Eastern D Step Time = 1.000 Magnitude Postimulation: Grabs: Extern = 1.000e+00</p>	 <p data-bbox="1040 506 1349 548">Abaqus/Standard 6.14-1 Sun May 15 15:38:03 Eastern D Step Time = 1.000 Magnitude Postimulation: Grabs: Extern = 1.000e+00</p>
	 <p data-bbox="662 800 971 842">Abaqus/Standard 6.14-1 Tue May 17 10:56:18 Eastern D Step Time = 1.000 Magnitude Postimulation: Grabs: Extern = 1.000e+00</p>	 <p data-bbox="1040 800 1349 842">Abaqus/Standard 6.14-1 Tue May 17 11:07:54 Eastern D Step Time = 1.000 Magnitude Postimulation: Grabs: Extern = 1.000e+00</p>
	 <p data-bbox="662 1094 971 1136">Abaqus/Standard 6.14-1 Sun May 15 18:07:26 Eastern Daylight T Step Time = 1.000 Magnitude Postimulation: Grabs: Extern = 1.000e+00</p>	 <p data-bbox="1040 1094 1349 1136">Abaqus/Standard 6.14-1 Mon May 16 18:06:06 Eastern Daylight T Step Time = 1.000 Magnitude Postimulation: Grabs: Extern = 1.000e+00</p>

Table 4.17: Post fab and Post load shapes of three structures for spoiler application

As shown in Table 4.17, all three structures had two stable shapes, the post fab shape in which the upper part remained flat and the post load shape in which it was protruded upwards. The first two structures have protrusions in the middle of the upper part, whereas in the third structure the middle portion remains flat but overall the upper part is projected upwards which simulates the spoiler application. The shape change can be achieved by applying a load in the center of the upper part of the structure. In this way, the third structure can be actuated whenever the spoiler is needed and brought back to the flat shape for normal running condition.

PART-III: EXPERIMENT RESULTS

Fabrication Results

Observation

The two stable shapes of the unsymmetric laminate fabricated using the fabrication process explained in Chapter 3 is as shown in Fig.4.26 (a) & (b). It is a rectangular laminate of dimension 120 X 60 mm, the unidirectional prepreg used is DA 409U / G35 150, the laminate stacking sequence is $[0/90]_T$ and the lamina thickness is 0.15 mm. The first stable shape has a curvature about y-axis and the second stable shape has a curvature about x-axis.



(a) First stable shape



(b) Second stable shape

Figure 4.26: Rectangular unsymmetric laminate $[0/90]_T$

Trimming after Curing

When the cured laminate is removed from the mold, it has a built-up of material around all four edges of the rectangle as shown in Fig.4.27 (a). Due to the pressure applied, the fibres along the edges gets displaced and along with the over flown epoxy, this takes the shape of the mold and forms the built-up material along the edges. This acts like an imposed boundary condition and does not allow the laminate to go to its post fab

shape and also restricts the bistable behavior. The built-up boundary needs to be trimmed as shown in Fig.4.27 (b) to get rid of these issues.



Figure 4.27: After curing (a) without trimming edges, (b) with trimmed edges

Effect of Changes in Number of Plies

S. No.	LSS	Temperature (°F)	Time (hours)	Working Condition			
				Day 1	Day 2	Day 3	Current
1	[0/90]	250	1	Working	Working	Not Working	Not Working
2	[0/90]	250	1	Working	Working	Working	Not Working
3	[0/90]	250	1	Working	Working	Working	Not Working
4	[0 ₂ /90 ₂]	250	1	Not Working	Not Working	Not Working	Not Working
5	[0 ₃ /90 ₃]	250	1	Not Working	Not Working	Not Working	Not Working
6	[0/90]	250	1	Working	Working	Working	Not Working
7	[0 ₂ /90 ₂]	250	1	Not Working	Not Working	Not Working	Not Working
8	[0/90]	250	1	Working	Working	Not Working	Not Working
9	[0 ₂ /90 ₂]	250	1	Not Working	Not Working	Not Working	Not Working

Table 4.18: Changes in number of plies

The pressure is maintained constant at 80 psi for all the samples. Working – Sample stays in the second shape, even after the load is removed. Not Working – Sample comes back to the first shape, once the load is removed. As can be seen from Table 4.18,

a total of nine samples are fabricated among which only the two ply samples (1-3, 6, 8) worked, whereas the four ply (4, 7, 9) and six ply (5) samples did not work. For this laminate size, the simulation did not show bistability for the 6 ply LSS and it is the same with fabrication as well. For the 4 ply LSS, the simulation showed bistability, but none of the three samples fabricated are bistable. In the 2 ply LSS, three samples are working, out of the five samples fabricated. Among the three samples, one of the sample (6) is working perfectly fine, whereas in the other two samples (2 & 3) only half the geometry is working as shown in Fig. 4.28.



Figure 4.28: Two ply samples (a) sample 2, (b) sample 3

In both sample 2 and sample 3, half of the geometry always stays in any one of the shape (Sample 2 – first shape; Sample 3 – second shape) and does not change shape even when the load is applied. Except for samples 1 & 8 which stopped working on day 3 itself, all other two ply samples worked for 10 to 15 days from the time of fabrication before it ceased to work. To make the four ply samples to work and to prevent the two ply samples from losing its bistability, suitable corrections need to be carried out in the fabrication process.

Experimental Setup Results

Observation

The snap through and snap back loads measured using the experimental setup for three samples 2, 3 and 6 are as given in Table 4.19.

S. No.	Laminate sample	Description	Snap through load range	Snap back load range
1	Sample 2	Half geometry working	240 to 250 g (2.35 to 2.45 N)	20 to 30 g (0.20 to 0.29 N)
2	Sample 3	Half geometry working	210 to 220 g (2.06 to 2.16 N)	30 to 40 g (0.29 to 0.39 N)
3	Sample 6	Full geometry working	390 to 400 g (3.82 to 3.93 N)	15 to 20 g (0.15 to 0.20 N)

Table 4.19: Snap through and snap back loads from experiments

Since only half of the geometry is working in the first two samples, there is a reduction in snap through load compared to the third sample. Among the first two samples, sample 2 has higher snap through load and lower snap back load compared to the loads of sample 3. In sample 2, half of the geometry which does not has bistability stays in the first shape, and during load application for snap through, since the entire geometry is in the first shape, it provides more resistance for shape change, thereby the snap through load is higher. In sample 3, the half of the geometry which does not has bistability stays in the second shape, and during load application for snap through, since only half of the geometry is in the second shape, it provides comparatively less resistance for shape change, thereby the snap through load is lower. The same explanations would hold good for the opposite effect on snap back loads.

Comparison of Simulation and Experiment Results

The snap through and snap back loads for the same laminate from FEA simulations are as given in Table 4.20.

S. No.	Laminate sample	Snap through load	Snap back load
1	Simulation sample	4.57 N	3.32 N

Table 4.20: Snap through and snap back loads from simulation

In all three samples of the experiments, the snap back load is much lower than the snap through load. In sample 6, the snap back load is only 5% of the snap through load. In simulation, both the snap through and snap back loads are very close to each other, the snap back load is almost 73% of the snap through load. Curvature wise the results were consistent qualitatively for all the fabricated samples. There is a curvature reduction as the number of plies increases which matches with the simulation results. To correct the snap back loads discrepancy, suitable corrections need to be carried out in the simulation as well as the experimental setup.

CHAPTER FIVE

CONCLUSION AND FUTURE WORK

In the first part of this chapter, the brief summary of the procedure followed, results obtained in each and every step of this research and the specific contributions towards this research are provided. In the second part, the recommendations for future work are provided.

Conclusion

This thesis addressed three areas namely simulation process, fabrication of unsymmetric laminates and experimental setup for critical load measurement.

Simulation process

The simulation process was standardized in finite element analysis software. To understand the overall behavior of the unsymmetric laminates, all three stages such as curing, snap through and snap back were simulated. The “Composite Section” module in FEA was used for the laminated FRP modeling; the material properties of AS4 -8552 prepreg was assigned for the lamina; LSS was selected as per the requirement; S4R element was used for meshing; loading and boundary conditions were altered for each of the three stages; and post processing was done to compute the snap through and snap back loads.

Result: A preliminary simulation was conducted and the process was validated based on the existing literature.

Fabrication of unsymmetric laminates

The unsymmetric laminates were fabricated using the compression molding of prepregs fabrication method. The mold used in one of the previous research, where they used a conventional oven for the fabrication was modified, in order to be used in a hot press as per the fabrication process proposed in the current research. DA 409U / G35 150 unidirectional prepreg was used for the fabrication. The three major steps in the fabrication process are mold preparation, laying up the prepregs as per the LSS, and curing in the hot press as per the curing conditions provided by the prepreg supplier.

Result: The fabricated unsymmetric laminates had two stable shapes and exhibited snap through / snap back phenomenon.

Experimental setup for critical load measurement

The experimental setup was developed to measure the snap through and snap back loads. The loading and boundary conditions used in the simulation were replicated. The laminate was loaded in discrete steps by adding physical weights in a slotted weight hanger, and the load at which the laminate changed shape gave the measure of the critical load. An operating procedure was established for the load measurement.

Result: Both the snap through and snap back loads were measured in a single setup, just by changing the location where the weights were hanged and not disturbing the laminate.

The actual research objectives were divided into two major parts, behavior of individual unsymmetric laminates and behavior of combination of symmetric and unsymmetric laminates.

Individual unsymmetric laminates

The effect of geometry and fibre orientation on the snap through and snap back loads of the individual unsymmetric laminates were studied.

The effect of geometry was studied by looking at the change in snap through and snap back loads based on the geometrical change (shape and size) of the laminate. In this study, except for the geometry, all other properties like the prepreg material, lamina thickness and LSS were maintained constant. It was found, as far as unsymmetric laminates with only two fibre orientations were concerned, the geometry of the laminate can be characterized by the average fibre length and the number of fibres in the longer (AFL_{long} and $Count_{long}$) and shorter (AFL_{short} and $Count_{short}$) fibre directions. Also, the snap through loads and snap back loads are always dependent on the parameters in the longer fibre direction and shorter fibre direction respectively. Therefore, two separate interaction charts were prepared to show the effect of the interaction of the longer fibre direction parameters on the snap through loads and the interaction of the shorter fibre direction parameters on the snap back loads. Apart from these, simulations were conducted on different types of triangles (Right angle and Acute triangles) as well, which helped in identifying the fifth parameter, the distribution of fibres that affects the snap through and snap back loads.

Result: Both charts were validated by conducting simulations on three different geometries, each with two variations such as Rectangle – I & II, Isosceles Trapezoid – I & II and Isosceles Triangle – I & II. In few cases, even though the AFL and Count remained the same for different geometries, the difference in loads was caused by the change in the distribution of fibres.

The effect of fibre orientation was studied by looking at the change in snap through and snap back loads based on the change of lamina fibre orientations. In this study, except for the lamina fibre orientations, all other properties like the geometry, prepreg material, and lamina thickness were maintained constant. Two different geometries such as Rectangle and Triangle were studied. Here again, unsymmetric laminates with only two fibre orientations were considered. Both the fibre orientations were varied for the study, but still to have a uniform comparison, the difference in angle between them was always maintained at 90°.

Result: The same interaction charts prepared earlier holds good for this case too, the only difference being the curvatures were not with respect to the global coordinates anymore, but with respect to the local coordinates of the fibres.

Combination of symmetric and unsymmetric laminates

The possibility of obtaining different pairs of stable shapes from standard geometries like square, rectangle, circle and ellipse were explored. Each of these standard geometry laminates were divided into many smaller geometry laminates. The smaller geometry laminates were made into symmetric or unsymmetric laminates. Simulations were carried out for various combinations of these symmetric and unsymmetric laminates, to find out all the different pairs of stable shapes that were possible from the same standard geometry laminates. Also based on this approach, two shape morphing applications in the automobile field such as the headrest and spoiler were developed.

The square geometry was split into four equal smaller squares. Each of the smaller squares were made into either symmetric or unsymmetric laminates. A total of four unique

combinations of symmetric $[0/90]_S$ and unsymmetric $[0_2/90_2]_T$ laminates were possible. From the simulation of these combinations, four sets of bistable shapes were obtained, this proved that from a same standard geometry it is possible to obtain different sets of bistable shapes.

Result: All the symmetric laminates in any of the different combinations remained flat in both post fab and post load shapes. All the unsymmetric laminates in any of the different combinations had curvature about the same axis (for e.g., x-axis) in the post fab shape and had curvature about the other axis (for e.g., y-axis) in the post load shape.

The square geometry was split into nine smaller squares. First, the middle square alone was made into unsymmetric laminate $[0_2/90_2]_T$, and rest all were made into symmetric laminates $[0/90]_S$. When the size of the middle square was same as the other squares, the square geometry had only one shape and did not exhibit bistability. But as the size of the middle square was increased keeping the overall dimension constant, the square geometry became bistable and the curvatures in both shapes started increasing. Second, the middle square alone was made into symmetric laminate, and rest all were made into unsymmetric laminates. Here it was the opposite case, when the size of the middle square was same as the other squares, the square geometry had two shapes and exhibited bistability. But as the size of the middle square was increased keeping the overall dimension constant, the curvatures in both shapes started decreasing and eventually the square geometry lost bistability after a point and had only one shape.

Result: This provided a method to increase / decrease the curvature of both post fab and post load shapes, maintaining the overall geometry.

The rectangle geometry was split into two right angle triangles and one acute triangle. The size of all three triangles were varied, keeping the overall rectangle dimension constant and also different combinations of symmetric $[0/90]_S$ and unsymmetric $[0_2/90_2]_T$ laminates in each of the triangles were considered. A shape chart was created with 24 possible variations by considering four sets of triangle sizes and six arrangements of symmetric and unsymmetric combinations. Out of the 24, only 12 variations were bistable. The reason for this is, in the remaining 12 variations, the symmetric laminate sizes were comparatively larger than the unsymmetric laminate sizes. Thus, in a combination of symmetric and unsymmetric laminates, whenever the symmetric laminates occupies a larger portion compared to the unsymmetric laminates, then those combination of laminates will have only one stable shape. Just by splitting a rectangle into three triangles, where each of the triangle were made size alterable and by assigning different combination of symmetric and unsymmetric laminates to the three triangles, it was possible to obtain so many different sets of bistable shapes.

Result: This showed the capability of the bistable laminates that it can be used to create various bistable shapes from any given geometry, by splitting it into smaller geometries and iterating with different combinations of symmetric and unsymmetric laminates.

The circle geometry was split into two portions, by a concentric inner circle with radius equal to one third of the outer circle. Also the geometry was approximated into three different polygons such as decagon (10 sided), dodecagon (12 sided) and hexadecagon (16 sided) to get straight edges along which the fibres can be oriented. The polygons were split

into triangles, where the number of triangles were same as the number of sides of the polygon. Since the geometry was divided into two portions, the triangles were also split into smaller triangles in the inner portion and trapezoids in the outer portion. The smaller triangles were made into symmetric laminates and trapezoids were made into unsymmetric laminates. For all three approximations, the results were similar; the geometry had only one stable shape, the inner portion remained flat and the outer portion was curved. Though shape morphing is not possible with these kind of laminates, they can be used to obtain desired curvatures by using plain molds instead of complex shaped molds.

Result: The understanding of the method of orienting the fibres parallel and perpendicular to the straight edges of the triangles to achieve the desired curvatures.

The ellipse geometry along with two of its variations (a square with half ellipse and a square with two half ellipses) was also considered. All three geometries were tessellated into many smaller triangles. The target was to make the entire outer edge of all the three geometries, to curve inwards in either top or bottom direction. After performing many iterations, the triangles were divided into four groups and each group was assigned a specific LSS such as $[0_2/90_2]_T$, $[90_2/0_2]_T$, $[\text{Angle}_2/90_2]_T$ and $[90_2/\text{Angle}_2]_T$ to achieve this target. The “Angle” in these groups denotes, the angle that the outer edge of the triangles (along the periphery of the ellipse) makes with the horizontal base line. Similar to the circle geometry, all these ellipse geometries also had only one stable shape.

Result: The understanding of the manner in which the tessellation of a geometry should be done and the way in which the triangles should be grouped, based on their LSS to achieve the desired curvatures.

Potential Applications

The following two applications were inspired from BMW Gina Concept car [30], where to achieve similar kind of shape changes, they have used a fabric cover and a steel understructure. The major advantage of using bistable composites in these applications is the strength of the composites compared to the fabric and reduction in the mechanisms used in the metal understructure.

The headrest in an automobile comes in two different types, the flat type and the protruded type. Using bistable composites, it is possible to build a headrest which can work in both ways i.e., as a flat type headrest as well as a protruded type headrest, and it can be switched between the two types as per the user requirement. To design such a headrest, a plus geometry was selected, which was divided into four rectangular legs and a middle square. The middle square was further divided into four equal triangles. The triangles were made into symmetric laminates and the rectangles were made into unsymmetric laminates. After many iterations, the LSS of all these rectangles and triangles were selected in such a way that, in the first shape all four legs were sprung up while the middle portion remained flat and in the second shape all four legs as well as the middle portion remained flat.

Result: If all the four legs are connected by a curtain spring and the entire geometry is covered by a stretchable fabric kind of a material, then the first shape would replicate the protruded type headrest and the second shape would replicate the flat type headrest.

The spoiler is an external attachment to the rear end of an automobile which helps in improving the automobiles aerodynamic performance. It is attached whenever it is required and removed afterwards. If the rear end of an automobile was fabricated using

bistable composites, the spoiler can be made as an integral feature rather than having it as a separate attachment. It can be activated whenever it is required and deactivated afterwards. To attain this feature, the design selected for the rear end of an automobile is a U-shaped rectangular clamp like structure. The two S-shaped end portions of the clamp were made into symmetric laminates and the middle portion of the clamp was made into unsymmetric/symmetric/unsymmetric laminate arrangement. In the first shape, the symmetric laminates remained flat whereas the two unsymmetric laminates had curvatures, which pushed the entire middle portion of the clamp upwards, thus activating the spoiler like structure. In the second shape, both the symmetric and unsymmetric laminates remained flat, which brought down the entire middle portion of the clamp, thus deactivating the spoiler like structure.

Result: Both the type of arrangements, with or without spoiler can be made possible in an automobile without having to attach any separate fittings.

Fabrication and Experimental Setup

With the modified mold, many samples of 120 X 60 mm laminates were fabricated by varying the number of plies. The 4 layered $[0_2/90_2]$ and 6 layered $[0_3/90_3]$ samples did not exhibit bistability, they had only the post fab shape to be stable. Out of the 2 layered $[0/90]$ samples fabricated, the three working samples were considered for measuring the snap through and snap back loads using the experimental setup developed. The loads of all three samples were measured and the possible reasons for the variation in results were identified. The experimental results were also compared with simulation results, the snap

through loads were almost the same in both cases, but there was a drastic difference in the snap back loads.

Specific contributions

1. Development of two interaction charts to show the effect of geometry parameters (AFL and Count of long and short fibres) on the snap through and snap back load values. This kind of a chart does not exist in the literature reviewed.
2. A new methodology has been proposed to obtain desired bistable shapes from any given geometry based on the concept of tessellation.
3. A detailed explanation on the impact of local and global coordinates and the impact of symmetric laminate and unsymmetric laminate LSS on the different shapes possible in any given geometry has been provided.
4. Design and development of a simple and cost effective experimental setup, in which both the critical loads can be measured in a single setup without disturbing the laminate. In all of the literature reviewed, two setups are required to find the two load values.
5. Two potential applications, the headrest and the spoiler has been developed based on the findings from this research.

Future Work

The actual lamina properties of the unidirectional prepreg DA 409U / G35 150 is not used in the simulations. The properties of this prepreg can be measured by fabricating specimens as per the standards and conducting tensile test on them. If these properties are given as input to the simulations, then it will help in getting more accurate results.

The individual rectangular unsymmetric laminates simulations should be done to closer replicate experiments to correct the differences in snap back load values. Experimentations on triangles and rectangle split into multiple triangles for post fab and post load shape determination should be done.

The current fabrication process is carried out in a hot press, in which the heat transfer is through conduction which affects the orientation of the fibres while curing, in turn affecting the bistability of the fabricated samples. Instead, an autoclave or a conventional oven can be used, in which the heat transfer is through convection which does not affect the orientation of the fibres, in turn the fabricated samples will have better bistable features.

In the current experimental setup, the unsymmetric laminate is held in the middle of the frame by four strings (two from the top and two from the bottom), and these strings are attached to the laminate by means of holes drilled at four locations in the laminate. This weakens the sample, therefore a better clamp can be designed to avoid drilling of the holes.

Also instead of just changing the clamping method, even a complete boundary of symmetric laminates can be fabricated around the unsymmetric laminate to be tested as shown in Fig.5.1. This would help in pushing the boundary conditions far away from the actual laminate, and even though the curvature could reduce and the load required to snap might slightly increase, it would still give a better result. To get more accurate results, digital load measurement techniques can be used.

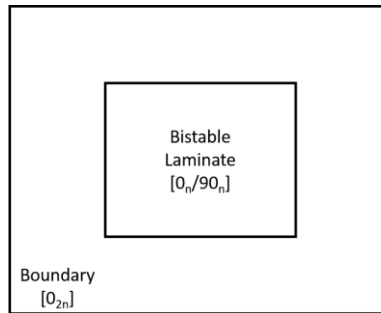


Figure 5.1: Bistable laminate with boundary symmetric laminate

The number of plies / laminate thickness can be investigated with respect to the laminate size (e.g. length and breadth in case of a rectangular laminate). This would help in making thicker laminates with 4 or more plies bistable. This is important because if these laminates are to be used in automobile and aircraft applications, two ply samples would not be sufficient. Also the effect of fibre and polymer material on higher number of plies can be studied.

From all the inferences obtained from the simulations of combination of symmetric and unsymmetric laminates, two different optimization problems can be formulated. First is a simplified optimization problem, in which the tessellation, the lamina material and the lamina thickness are kept constant; the fibre orientation is considered as the only design variable; and the objective is to find out the combination of LSS that can achieve the two desired shapes. Second is a complex optimization problem, in which only the lamina material and the lamina thickness are kept constant; both the tessellation and the fibre orientation are considered as the design variables; and the objective is still the same to find out the combination of LSS that can achieve the two desired shapes. Formulating and solving these two optimization problems will be the next major step, in order to attain the ultimate objective of this research in a much better way.

APPENDICES

Appendix A

Simulation Procedure in ABAQUS

If it is a simple geometry like an individual rectangle, trapezoid, triangle etc., it can be directly modeled in ABAQUS itself in the part module using the Part > Create: 3D, Deformable, Shell option. If it is a connected geometry, then the outer sketch is modeled in Solidworks 3D modeling software, saved as *.STP file and imported into ABAQUS using File > Import > Part> *.STP option. Once it is imported, using Tools > Partition option, the various individual geometries are created.

Once the part creation and partition are over, the lamina material properties and the stacking sequence assignments are made in the property module. First using the Material > Create option, the lamina properties provided in Chapter 3 are entered. Second using the Section > Create: Shell, Composite option, the required number of layers are created and the lamina material, thickness and orientation of fibres in each layer are entered. In this way, the required number of laminate stacking sequences are created. Third using the Assign > Section option and selecting individual geometry, the respective sections are assigned to each geometry. Once the section assignments are over, assembly is created in the assembly module using the Instance > Create: Independent (mesh on instance) option.

Once the assembly is created, the meshing is done in the mesh module. Using Seed > Instance or Edges option, the seeds are generated as per the mesh requirement, then the element type is assigned using Mesh > Element Type: Standard, Linear, Quad, Reduced integration option and finally meshing is done using Mesh > Instance option.

Once the meshing is done, the actual simulation starts, the simulation is done in three parts – curing process, snap through process and snap back process, each part has two steps, so a total of six steps are needed. In the first part, the first step is an initial step which is a default step in ABAQUS, in this step the curing temperature alone is entered in the load module, using the Predefined Field > Create: Other, Temperature option. The second step is created using the step module, Step > Create > Static, General > Nlgeom option, in this step the room temperature alone is entered in the load module, by using the Predefined Field > Edit: Predefined Field-1, Modified option. These two steps simulate the curing process. In both of these steps, the middle node of the overall geometry is assigned a fixed boundary condition.

In the second part, the first step is created in the step module, using the Step > Create > Static, General > Automatic Stabilization > Specify damping factor > 2.5E-7. Appropriate loading and boundary conditions provided in Chapter 3 are applied to simulate snap through loading process. Once a load above the critical load is applied and the shape change has happened, the second step is created in the step module, using the Step > Create > Static, General option. This step is used to simulate the snap through unloading process, so the loading and boundary conditions provided in the previous step are removed and again the fixed boundary condition on the middle node is applied. These two steps together simulate the overall snap through process.

Again these last two steps are repeated with different set of loading and boundary conditions to simulate the snap back process. Post processing is done to find the snap through and snap back load values from the simulations.

Appendix B

Part Drawings and Bill of Material of the Experimental Setup

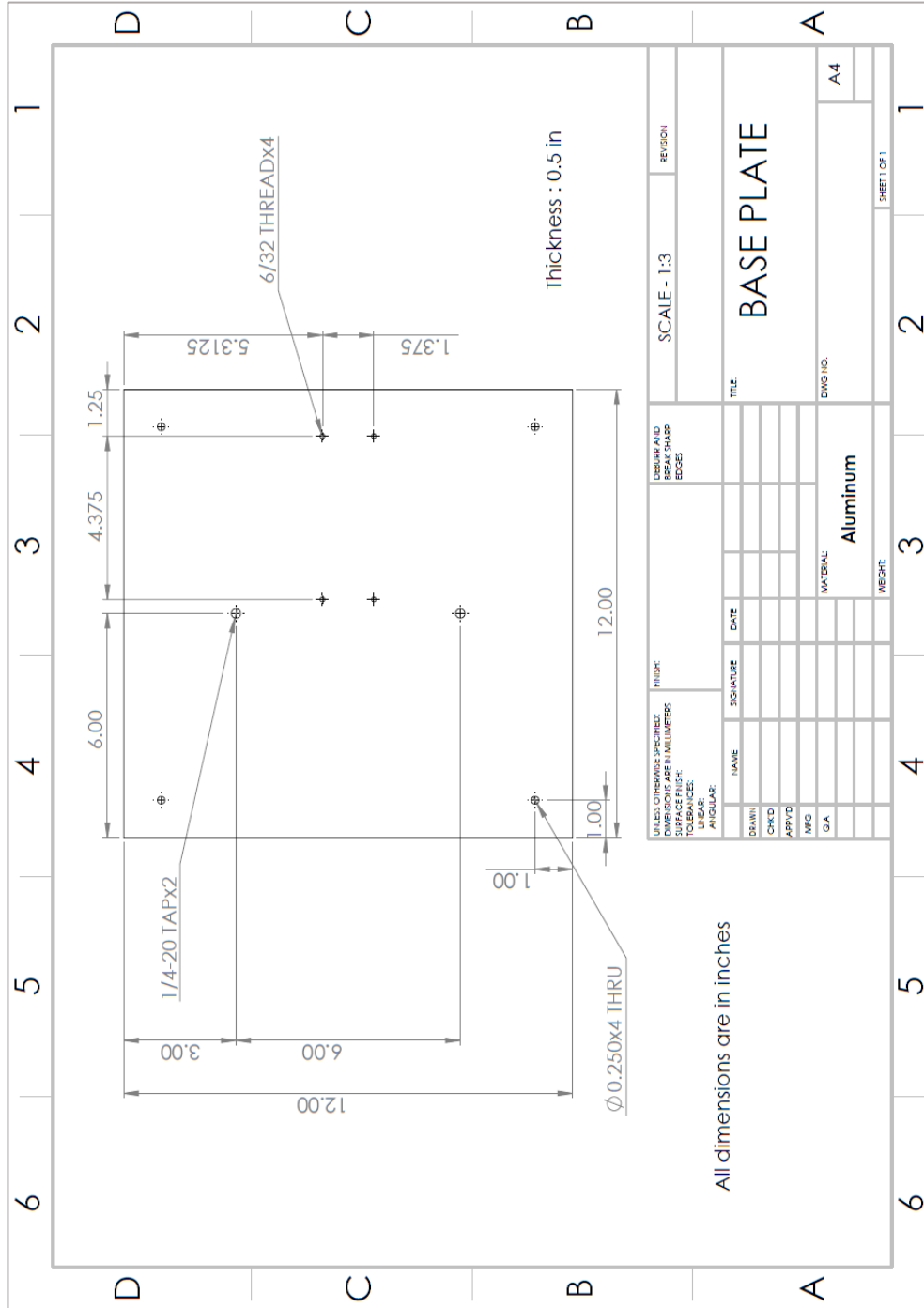


Figure B-1: Base plate drawing

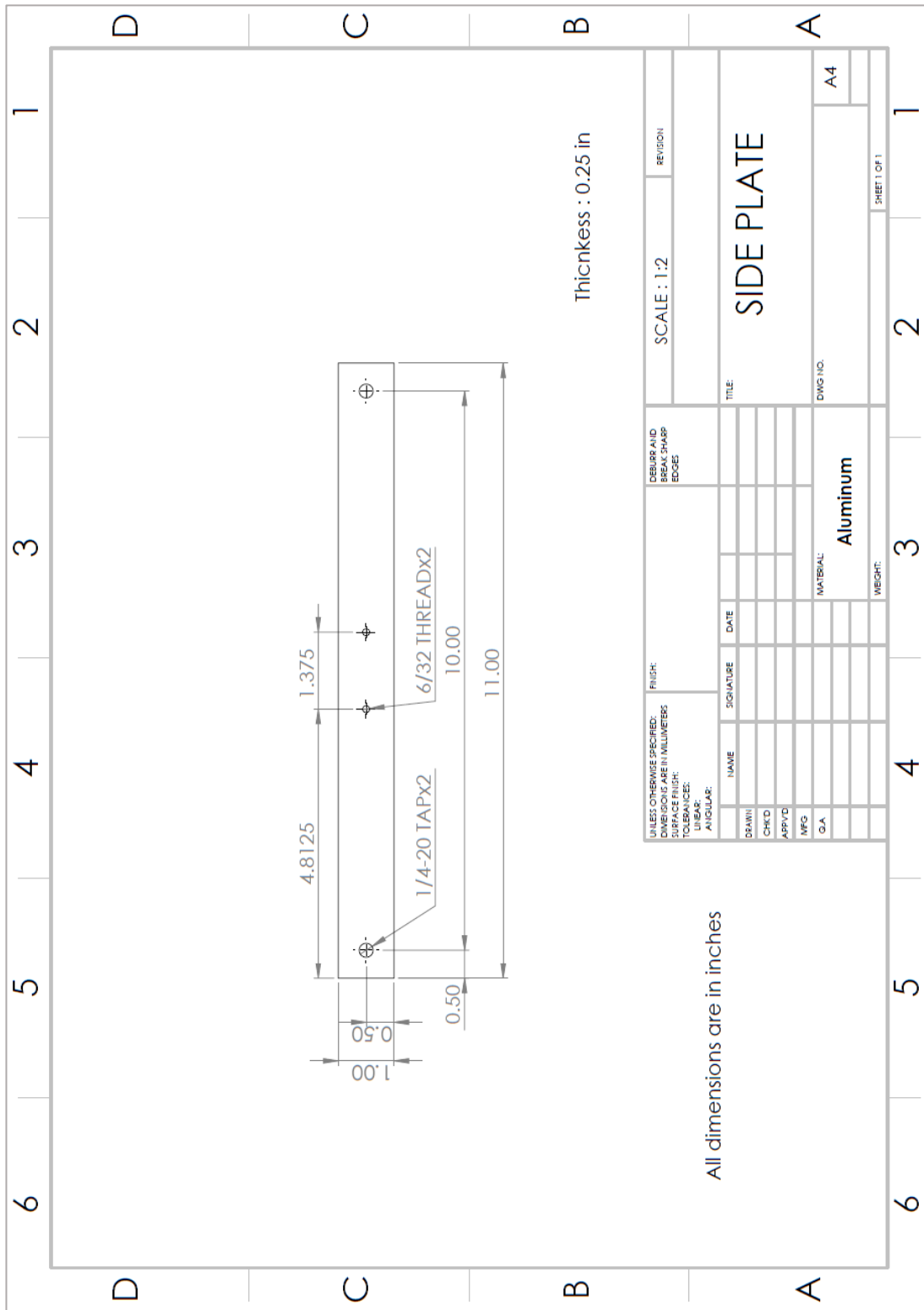


Figure B-3: Side plate drawing

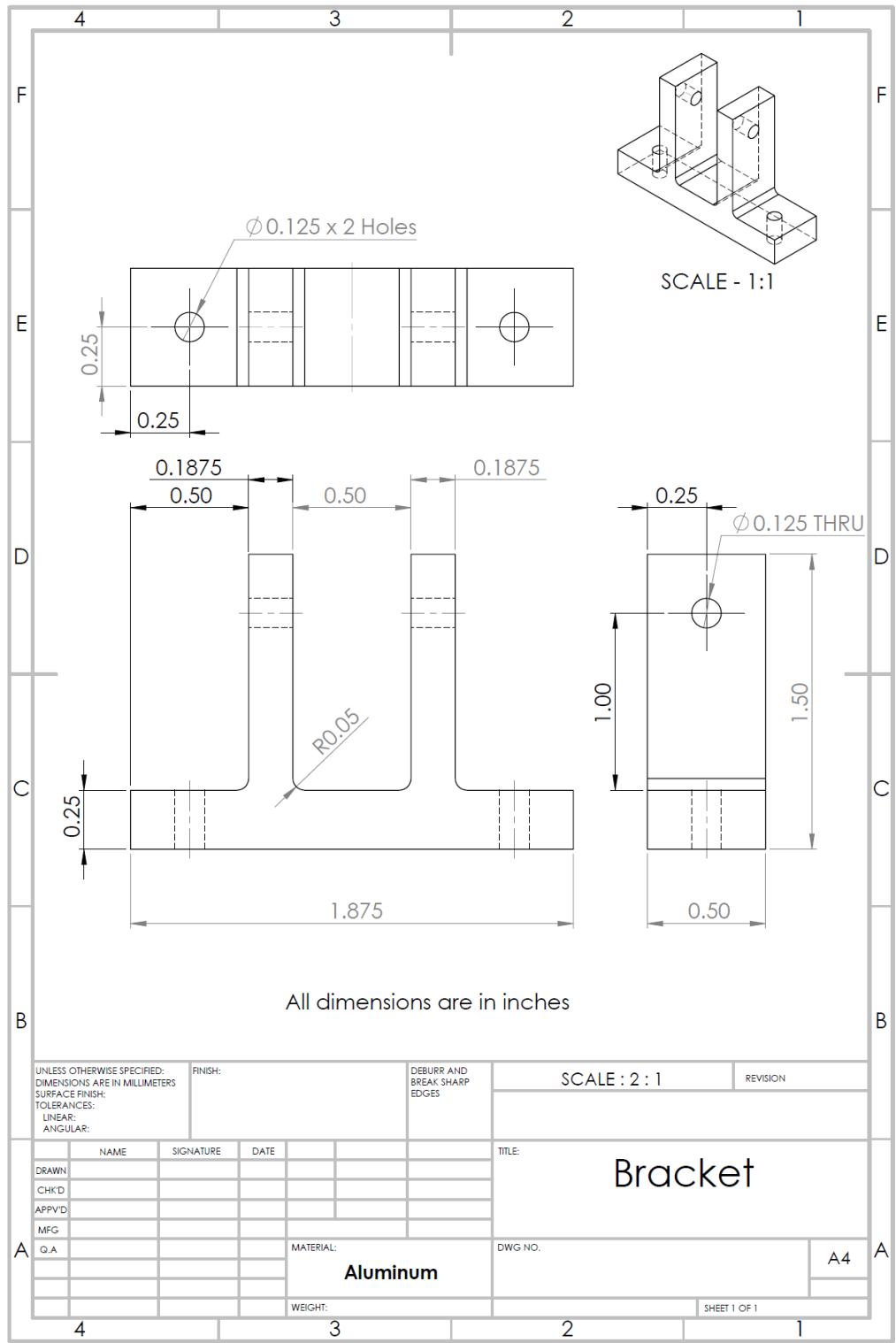


Figure B-4: Pulley bracket drawing

S. No	Item	Item description	Qty
1	Eyebolt	Steel Eyebolt without Shoulder - for Lifting, 1/4"-20 Thread Size, 1" Thread Length	4
2	Pulley	Fixed Pulley, for mounting on a plane surface	5
3	Bottom Plate	Aluminum 6061, 1/2" Thick, 12" x 12"	1
4	Top Plate	Aluminum 6061, 1/4" Thick, 12" x 12"	1
5	Side Plate	Aluminum 6061, Rectangular Bar, 1/4" x 1"	1
6	Frame	Aluminum T-Slotted Framing Extrusion, Single Profile, 1" Size, Solid	1
7	T-bolt	Steel End-Feed Fastener for 1" Single & 2" Quad Aluminum T-Slotted Framing Extrusion	2
8	1 X 7 Strand Wire	American Fishing Wire B090-4 90 Surfstrand Steel Leader Wire Brown 300' Spool	1
9	Thimble	Stainless Steel Thimbles, Teardrop-Shape, .063 in (1.59 mm) cable diameter max, Bright, 10 pc	1
10	Crimp	American Fishing Wire J03B-B #3 Single Barrel Sleeves Black 100pc	1
11	Split Shot	Water Gremlin Removable Split Shot Packs - Size B or BB	1
12	Slotted Weights	Slotted Weight Set of 14 Brass with Stand and Hanger	1

Table B-1: Bill of Material

REFERENCES

- [1] Carman, G. & Garcia, E., Eds., 1993, Adaptive Structures and Material Systems, American Society of Mechanical Engineers.
- [2] Guran, A. & Inman, D., Eds., 1995, Wave Motion, Intelligent Structures and Nonlinear Mechanics, World Scientific.
- [3] Srinivasan, A.V., 2000, Smart Structures: Analysis and Design, Cambridge University Press.
- [4] Campanile, L. F., 2007, Adaptive Structures: Engineering Applications, Wiley, Chichester, England, U.K.
- [5] Barbero, E. J., 2010, Introduction to Composite Materials Design, Second Edition, Taylor & Francis.
- [6] Dietz, A. G. H., 1965, Composite materials, by Albert G.H. Dietz, Philadelphia, American Society for Testing and Materials.
- [7] Pilla, S. and Schmueser, D., 2016, Advanced Mechanics of Composite Materials & Structures, Lecture Notes – CUICAR.
- [8] Jones, R. M., 1998, Mechanics of Composite Materials, Taylor & Francis.
- [9] Hyer, M.W., 1981, “Calculations of the Room-Temperature Shapes of Unsymmetric Laminates”, *J. Compos. Mater.*, **15**, pp. 296-310.
- [10] Dano, M.-L., and Hyer, M. W., 1998, “Thermally-induced deformation behavior of unsymmetric laminates,” *Int. J. Solids Struct.*, **35**(17), pp. 2101–2120.
- [11] Jun, W. J., and Hong, C. S., 1990, “Effect of residual shear strain on the cured shape of unsymmetric cross-ply thin laminates,” *Compos. Sci. Technol.*, **38**(1), pp. 55–67.
- [12] Gigliotti, M., Wisnom, M. R., and Potter, K. D., 2004, “Loss of bifurcation and multiple shapes of thin [0/90] unsymmetric composite plates subject to thermal stress,” *Compos. Sci. Technol.*, **64**(1), pp. 109–128.
- [13] Portela, P., Camanho, P., Weaver, P., and Bond, I., 2008, “Analysis of morphing, multi stable structures actuated by piezoelectric patches,” *Comput. Struct.*, **86**(3-5), pp. 347–356.

- [14] Tawfik, S., Tan, X., Ozbay, S., and Armanios, E., 2006, “Anticlastic Stability Modeling for Cross-ply Composites,” *J. Compos. Mater.*, **41**(11), pp. 1325–1338.
- [15] Hyer, M. W., 1981, “Some Observations on the Cured Shape of Thin Unsymmetric Laminates,” *J. Compos. Mater.*, **15** (2), pp. 175–194.
- [16] Mattioni, F., Weaver, P. M., Potter, K. D., and Friswell, M. I., 2008, “Analysis of thermally induced multistable composites,” *Int. J. Solids Struct.*, **45**(2), pp. 657–675.
- [17] Mattioni, F., Weaver, P. M., and Friswell, M. I., 2009, “Multistable composite plates with piecewise variation of lay-up in the planform,” *Int. J. Solids Struct.*, **46**(1), pp. 151–164.
- [18] Dano, M. L., and Hyer, M. W., 2001, “Snap-through of unsymmetric fiber-reinforced composite laminates,” *Int. J. Solids Struct.*, **39**(1), pp. 175–198.
- [19] Tawfik, S. a., Stefan Dancila, D., & Armanios, E. (2011). Planform effects upon the bistable response of cross-ply composite shells. *Composites Part A: Applied Science and Manufacturing*, **42**(7), 825–833.
- [20] Potter, K. D., and Weaver, P. M., 2004, “A concept for the generation of out-of-plane distortion from tailored frp laminates,” *Compos. Part A Appl. Sci. Manuf.*, **35**, pp. 1353–1361.
- [21] Daynes, S., and Weaver, P., 2010, “Analysis of unsymmetric CFRP-metal hybrid laminates for use in adaptive structures,” *Compos. Part A Appl. Sci. Manuf.*, **41**(11), pp. 1712–1718.
- [22] Mattioni, F., Gatto, A., Weaver, P., Friswell, M., and Potter, K., 2006, “The application of residual stress tailoring of snap-through composites for variable sweep wings,” 47th AIAA/ASME/ASCE/AHS/ASC Struct. Struct. Dyn. Mater. Conf. 14th AIAA/ASME/AHS Adapt. Struct. Conf. 7th, (May), pp. 1–12.
- [23] Diaconu, C. G., Weaver, P. M., and Mattioni, F., 2008, “Concepts for morphing airfoil sections using bi-stable laminated composite structures,” *Thin-Walled Struct.*, **46**(6), pp. 689–701.
- [24] Arrieta, a. F., Hagedorn, P., Erturk, a., and Inman, D. J., 2010, “A piezoelectric bistable plate for nonlinear broadband energy harvesting,” *Appl. Phys. Lett.*, **97**(10), pp. 1–3.
- [25] Hufenbach, W., and Gude, M., 2002, “Analysis and optimisation of multistable composites under residual stresses,” *Compos. Struct.*, **55**(3), pp. 319–327.

- [26] Hufenbach, W., Gude, M., Kroll, L., Sokolowski, A., and Werdermann, B., “Adjustment of residual stresses in unsymmetric fiber-reinforced composites using genetic algorithms,” *Mech. Compos. Mater.*, **37**(1), pp. 71–78.
- [27] Betts, D. N., Kim, H. A., and Bowen, C. R., 2012, “Optimization of Stiffness Characteristics for the Design of Bistable Composite Laminates,” *AIAA J.*, **50**(10), pp. 2211–2218.
- [28] Cui, Y., and Santer, M., 2015, “Highly multistable composite surfaces,” *Compos. Struct.*, **124**, pp. 44–54.
- [29] Murray, D. V, and Myers, O. J., 2013, “Modeling bistable composite laminates for piezoelectric morphing structures,” *ISRN Mater. Sci.*, **2013**, pp. 1–12.
- [30] BMW Media Information, 2008, The BMW GINA Light Visionary Model - Innovative approach and optical expression of creative freedom.